Manipulation and Imaging of Interactions Between Layer-by-layer Capsules and Live Cells Using Nanopipettes and SICM

Submitted in partial fulfillment of the requirements of the Degree of Doctor of Philosophy

Yuxiu Chen

Supervisors:
Dr. Pavel Novak
Prof. Gleb Sukhorukov

School of Engineering and Materials Science
Queen Mary, University of London
2018

Declaration

I, Yuxiu Chen, confirm that the research included within this thesis is my own work or that where it has been carried out in collaboration with, or supported by others, that this is duly acknowledged below and my contribution indicated. Previously published material is also acknowledged below.

I attest that I have exercised reasonable care to ensure that the work is original and does not to the best of my knowledge break any UK law, infringe any third party's copyright or other Intellectual Property Right, or contain any confidential material.

I accept that the College has the right to use plagiarism detection software to check the electronic version of the thesis.

I confirm that this thesis has not been previously submitted for the award of a degree by this or any other university.

Signature:
Date:

Details of collaboration and publications:

CHEN, Y., SUKHORUKOV, G. B. & NOVAK, P. 2018. Visualising nanoscale restructuring of a cellular membrane triggered by polyelectrolyte microcapsules. *Nanoscale,* 10, 16902-16910.

Abstract

Polymer-based multilayer microencapsulation technology represents one of the promising strategies for intracellular drug delivery, however, the membrane processes involved in vehicle internalisation are not fully understood. Here we employed scanning probe microscopy technique called Scanning Ion Conductance Microscopy (SICM) to study these complex processes at nanoscale resolution in real time. We were able to image topography simultaneously with local elastic modulus throughout the whole course of microcapsule internalisation in A549 cell culture without disrupting the internalisation process. The imaging revealed that capsules triggered formation of membrane protrusions in their vicinity which designated important but not sufficient step towards full capsule internalisation. The crucial aspect appeared to be nanoscale restructuring of these protrusions into smooth thin layers extending over the surface of capsules. Simultaneous mapping of elastic modulus during capsule internalisation allowed monitoring the structural changes during extension of the membrane sheets over the surface of capsule and subsequent post-internalisation phenomenon of capsule buckling. To our knowledge these are the first experimental data capturing the interactions between cellular membrane and microcapsules in its whole complexity with nanoscale resolution. The methodology established here has a potential to provide new insights into interactions at the interface between nanostructured materials and cellular membrane under physiological conditions.

Acknowledgement

First of all, I would like to thank my PhD supervisor, Dr Pavel Novak, who offered me the opportunity to study at QMUL, and was always there throughout my four years of PhD, providing constant guidance and encouragement.

I am also grateful to my second supervisor, Prof. Gleb Sukhorukov and his group. It was my pleasure to be part of Gleb's group and I really enjoyed that friendly and inspiring atmosphere of the group.

I would like to thank my colleagues at SEMS, Gudhit P. Singh, Xinru Deng, Jose Perez-Tores and other PhD fellows for sharing precious memories during my PhD. I would like to thank Alex Wibawa especially, for he is more than a colleague to me, but also a dear friend.

I would like to thank Shafir Iqbar, who taught me the cell culture and provided me a welcoming environment in the Cell and Tissue Lab.

I dedicate this thesis to my family.

Contents

List of figures

List of symbols and abbreviations

CellMask™, CellMask™ Orange Plasma Membrane Stain

$CaCl_2$, Calcium chloride

Na_2CO_3, Sodium carbonate

AFM, Atomic force microscopy

CLSM, Confocal laser scanning microscopy

DMEM, Dulbecco's modified eagle medium

EDTA, Ethylenediaminetetraacetic acid

FCS, Fetal calf serum

FITC, Fluorescein isothiocyanate isomer I

HPICM, Hopping mode ion conductance microscopy

L-15, Leibovitz's L-15 Medium

MF, Formaldehyde particles

PAH, Poly(allylamine hydrochloride)

PBS, Phosphate buffered Saline

PSS, Poly(sodium 4-styrenesulfonate

SEM, Scanning electron microscopy

SICM, Scanning ion conductance microscopy

SSCM, Scanning surface confocal microscopy

TEM, Tunneling electron microscopy

1. Introduction

Usability of many chemical substances with significant potential for biomedical applications is limited by their poor solubility in water or limited stability in the physiological environment. One of promising strategies for therapeutic targeted delivery of these types of substances into cells and tissues is their encapsulation inside polyelectrolyte microcapsules (Volodkin et al., 2004b, Sukhorukov et al., 1998b). Successful internalisation of microcapsules loaded with various macromolecules have been observed in several types of living cells (Javier et al., 2008, Kastl et al., 2013), however the mechanisms of the uptake of capsules by living cells are not yet fully understood. Detailed understanding of physico-chemical and mechanical interactions between capsules and living cells is required for specific targeting, effective delivery, and elimination of any potential toxic side effects. This has been largely limited by capabilities of available imaging techniques and lack of specific fluorescent markers for certain types of cellular uptake. The rate of internalisation of microcapsules was primarily studied at the level of cell population using conventional optical/fluorescence microscopy, confocal microscopy, and flow cytometry (Gao et al., 2016, Ai et al., 2005, Sun et al., 2015). These conventional fluorescence methods are known to be prone to overestimating the number of internalised capsules due to their limited capability to exclude capsules which were not fully internalised and remained attached to the cell surface (Javier et al., 2006). Experimental evidence with resolution high enough to resolve the fine membrane processes interacting with microcapsules has been limited to fixed samples imaged by scanning electron microscopy and transmission electron microscopy (Kastl et al., 2013) capturing randomly timed “snapshots” of what is likely to be highly dynamic and complex interaction. Physical force interactions between cellular membrane and capsules during the internalisation were suggested to cause buckling of capsules based on indirect evidence obtained using fluorescence microscopy in live cells

(Palankar et al., 2013) and separate measurements of capsule deformation under colloidal probe atomic force microscopy (AFM) outside of the cellular environment (Delcea et al., 2010, Dubreuil et al., 2003). However, our knowledge of the mechanical properties of the fine membrane structures directly involved in the internalisation process or how these structures form during the internalisation is very limited, if non-existent.

Here we employ a different approach based on a high-resolution scanning probe technique called scanning ion conductance microscopy (SICM). SICM uses reduction in ionic current through the probe represented by an electrolyte-filled glass nanopipette immersed in saline solution to detect proximity of sample surface (Hansma et al., 1989, Korchev et al., 1997a). The technique has been previously used for high-resolution scanning of biological samples of complexity similar to what can be expected in case of microcapsules interacting with cells (Novak et al., 2014, Novak et al., 2009), and also for mapping mechanical properties at high resolution (Ossola et al., 2015, Rheinlaender and Schaffer, 2013). It has been proved to be able to visualise internalisation process of 200 nm carboxy-modified latex nanoparticles (Novak et al., 2014), however it is not clear whether it would be suitable for visualising internalisation of substantially larger, microscale-sized particles.

The aim of this research was to visualize the live internalisation process of microcapsules entering cells by using SICM. The first two chapters of this thesis are introduction and literature review, which summarise the current state of the art. Chapter 3 states the aim and objectives of this study. Chapter 4 introduces the materials and methods we used in our research. Chapter 5, 6, 7 present the main findings of our research. Chapter 5 states the challenges we met in visualising the live internalisation of microcapsule as well as our solution for overcoming those challenges. At the end of that chapter, we describe the detailed procedure we used for recording the live internalisation

of microcapsules. The results we got using this procedure are presented in chapter 6 and 7. In chapter 8, we discuss the results we found by comparing them to the results of previous research. In chapter 9, we summarise our study and give some suggestions on future work.

2. Literature review

2.1 Polyelectrolytes microcapsules

Polyelectrolytes microcapsules are hollow polymer-based microscale drug carriers synthesized using layer-by-layer assembly of the polyelectrolytes (Sukhorukov et al., 1998a). Polyelectrolyte is a group of polymers that consist of charged or ionizable monomers and the counterpart ions. The polyelectrolytes can be classified into polycations and polyanions according to their charges after dissolved in aqueous solution. The polyelectrolyte layer-by-layer assembly is a technique used to synthesize multilayers by alternately adsorbing oppositely charged electrolytes onto the surface of substrates. By repeating this, multilayers of desired thickness can be built. It was first introduced by Decher et al. (Decher et al., 1992) and its ability was at first demonstrated by building multilayer film on glass slides (Figure 2.1A). The electrostatic force between the polyanion and polycation plays a vital role in the adsorption of each layer. Another key element in the assembly of multilayers is called overcompensation, which is the reversal of surface charge after the deposition of each polyelectrolyte layer. This is realized by the coiled conformation of the polymeric chains as illustrated in Figure 2.1B (Decher, 1997).

As the layer-by-layer assembly rely purely on electrostatic interaction, there is no restriction with the size and shape of the substrate. In theory, all substrates could be used as the substrate for layer-by-layer assembly as long as they are charged. In 1998, Sukhorukov et al (Donath et al., 1998, Sukhorukov et al., 1998b, Sukhorukov et al., 1998a) successfully applied layer-by-layer technique to the synthesis of microcapsules by deposition on micro size beads followed by dissolution of the core. The process of microcapsule synthesis is similar to that of building multilayer films, which is illustrated in Figure 2.2.

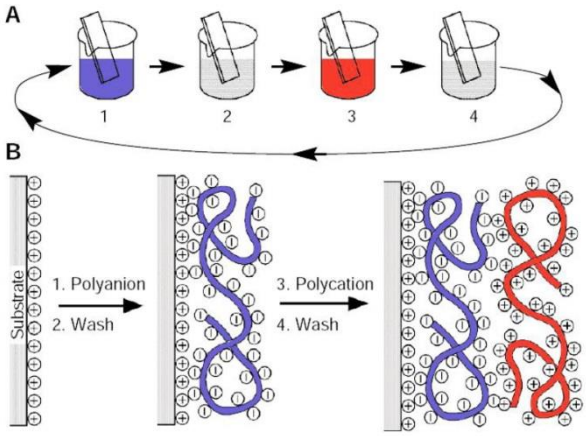

Figure 2.1 The principle of layer-by-layer assembly. (A) Schematic of building multilayers on glass slides by dipping the slide into beakers filled with polyanion (step 1) and polycation (step 3) solution respectively. The clear beakers in step 2 and 4 represent washing step. (B) Schematic of charge reversal after each deposition of polyelectrolyte layer (Decher, 1997)

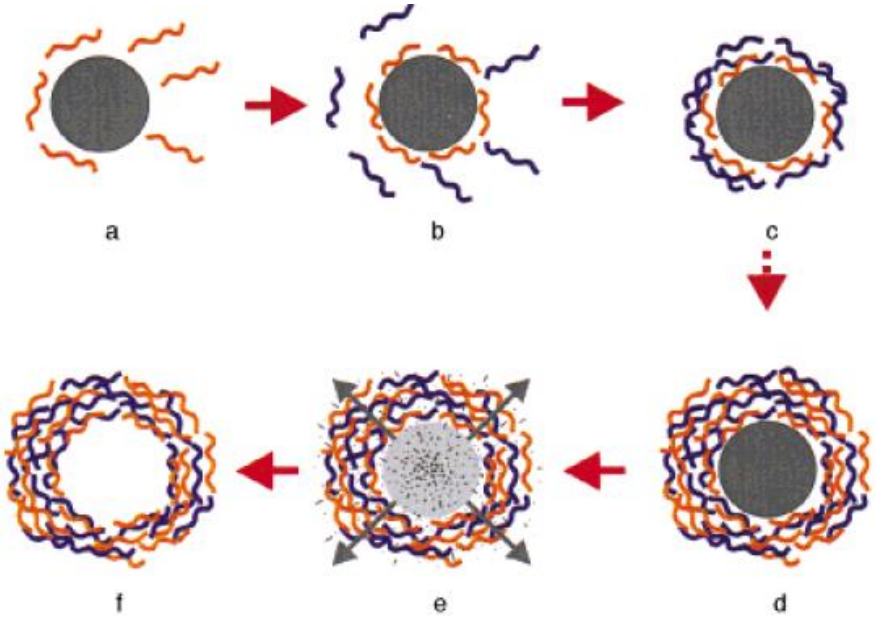

Figure 2.2 The synthesis of the microcapsule using layer-by-layer assembly. (a-d) layer by layer deposition of polyanion and polycation onto the sacrificial core, (e) the dissolution of sacrificial core, (f) obtained hollow polyelectrolyte multilayer capsule. (Donath et al., 1998).

Many particles could be used as the substrates for the synthesis of microcapsules. The most commonly used one is crosslinked melamine formaldehyde particles (MF) (Donath et al., 1998), which could be dissolved by 0.1 M HCl after the deposition of multilayers. The problem with using MF particles is that it is difficult to completely remove the core as the oligomers from dissolution have difficulty with diffusion out of the multilayers and the

extreme pH condition used for core removal is also not suitable for the encapsulation of those sensitive biomolecules (Volodkin et al., 2004a).

A common alternative to MF particles that avoids the problems mentioned above is $CaCO_3$ particles (Volodkin et al., 2004a). The $CaCO_3$ could be crystallized from supersaturated solutions. Facts that affect the quality of the resultant microcapsules includes concentration of the salts, pH, temperature, rate of the mixing and the additives added. Uniform and un-aggregated microcapsules homogeneous in size could be synthesized if the crystallization process was carefully controlled. A simple and reproducible procedure for the preparation of spherical and un-aggregated $CaCO_3$ microcapsules with a narrow size distribution around 5 μm was reported by Volodin et al. and widely practiced by other researchers (Volodkin et al., 2004a). These particle templates could be easily removed with EDTA at neutral pH after the deposition of polyelectrolyte multilayers. The end products of dissolution are calcium ions and CO_2 which could diffuse easily out the multilayers without leaving any residues. In addition, the porous structure of $CaCO_3$ offers large surface area for the encapsulation of drugs, such as large biomolecule, proteins and DNA. To conclude, $CaCO_3$ particle is a good overall template that meets most general requirements for the synthesis of polyelectrolyte microcapsules.

As for the component of the multilayers, the most commonly used polyelectrolytes for the deposition of multilayers are synthetic polymers, poly(allylamine hydrochloride) (PAH) and poly(sodium 4-styrenesulfonate) (PSS). Biodegradable polymers such as chitosan, poly-L-arginine, dextran sulfate sodium salts are also widely used as they could spontaneously decompose themselves inside the human body and are considered safe for pharmaceutical purposes. Apart from macromolecules, metal nanoparticles, such as gold, silver and magnetite nanoparticles, could be incorporated into

the polyelectrolyte multilayers by electrostatic interaction. The incorporated nanoparticles grant the microcapsules with additional functions such as triggered release, magnetic field responsive, etc.

Since the introduction of polyelectrolytes microcapsules in 1997 (Donath et al., 1998, Sukhorukov et al., 1998b, Sukhorukov et al., 1998a), they have been intensively studied for drug delivery applications (Sukhorukov et al., 2007, De Geest et al., 2009). Functionalized microcapsules were designed to encapsulate drugs (macromolecules, proteins, DNAs) (Sukhorukov et al., 2000, Sukhorukov et al., 2001, Shchukin et al., 2003, Volodkin et al., 2004a), to be biocompatible and biodegradable (Shenoy et al., 2003, De Geest et al., 2006) and to respond to the external stimuli, such as light irradiation or magnetic field, for controlled release (Stuart et al., 2010, Yi and Sukhorukov, 2013).

2.2 Cell culture and endocytic pathways

2.2.1 A549 cells

A549 cell is a human lung carcinoma epithelial cell line first developed by Giard in 1972 as an established cell line (Giard et al., 1973). This cell line has been used as a model for the study particle toxicity (Chang et al., 2011, Davoren et al., 2007, Gualtieri et al., 2009, Foster et al., 2001) and particle internalisation (Huang et al., 2002, Rejman et al., 2005). Lung epithelial cells are regarded as an attractive target for the study of drug delivery. The epithelial surface of lung is the largest surface area in human body that is in direct contact with the environment (Muhlfeld et al., 2008). Other advantages of targeting lung cells include non-invasive administration, avoidance of first pass metabolism and direct delivery to the site of action for respiratory diseases treatment (Mansour et al., 2009).

2.2.2 Characteristics of epithelial cells

Epithelial cells form firmly bounded cell layers that cover the internal and external surfaces of the organ. This interface between the internal and external environments of the body serves as the biological barrier for the substance coming in and out of human body (Muhlfeld et al., 2008).

As epithelial cells form a uniform monolayer, they are polarized and exhibit specific domains as illustrated in Figure 2.3. The surface of the cell membrane faces outside is called apical region. This region has membrane protrusions such as microvilli and cilia. Microvilli are tiny brush like plasma membrane structures that contribute to the adhesion and adsorption of the cell membrane (Takeuchi et al., 1994). Microvilli consist mainly of plasma membrane and actin filaments and are covered with glycocalyx that helps the binding of substances. There are thousands of microvilli on the apical surface of the epithelial cells that increase the surface area of the plasma membrane and as a result, the adhesion and adsorption of the membrane.

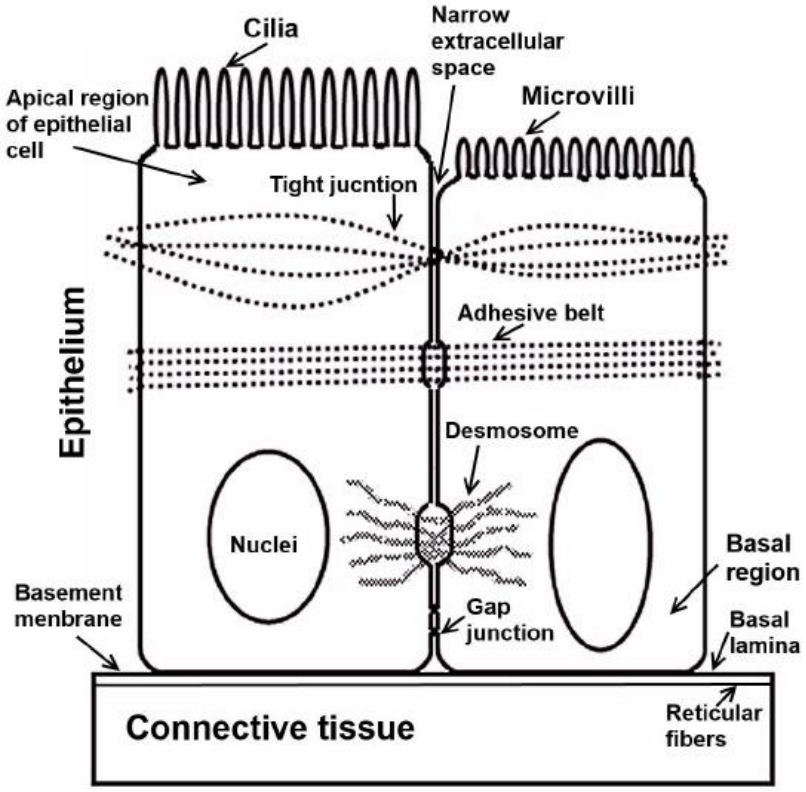

Figure 2.3 Schematic of epithelial cell junctions

Cilia are longer and thicker membrane protrusions that consists of two different forms, primary cilia and motile cilia (Satir, 2017). The primary cilia appear in almost all mammalian cells. However, each individual cell possesses only one primary cilium. The function of primary cilia had been neglected before for a long period of time. However, nowadays, more and more researches suggest their importance in cell signalling. On the other hand, motile cilia beat in coordinated waves and act as nanoscale mechanical devices that move liquid over the membrane surface (Satir, 2017).

2.2.3 Endocytic pathways

Endocytosis is a process in which cell internalise molecules or particles through its plasma membrane. This process is realised by the cell membrane via several different pathways. Depend on their mechanism, they could be categorised into two major mechanism: phagocytosis, which means "cell eating" (the uptake of large particles) and pinocytosis, which means "cell drinking" (the uptake of fluid and solutes) (Conner and Schmid, 2003). A schematic of different endocytic pathways is illustrated in Figure 2.4.

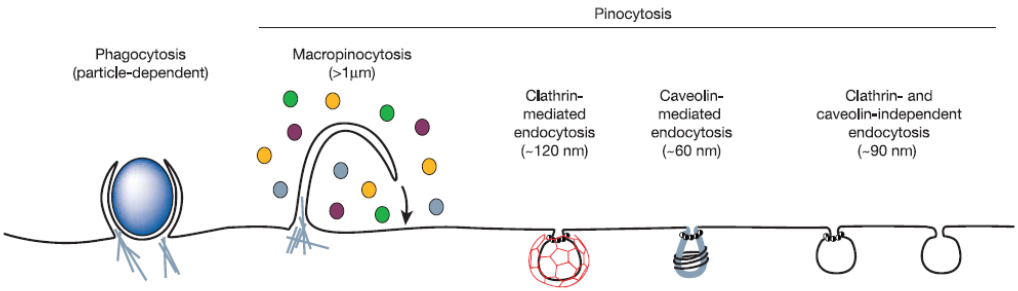

Figure 2.4 Endocytic pathways of mammalian cell. (Conner and Schmid, 2003)

Phagocytosis is a specialized mechanism which plays a crucial role in the immune system, made famous by the important macrophage cell. Not all cells have the ability to phagocyte, the phagocytosis only happened in special cells, namely, macrophages, monocytes, neutrophils and dendritic cells. Phagocytosis occurs in these cells is also called professional phagocytosis. It

is also reported that cells like fibroblasts, epithelial and endothelial, might also possess a certain degree of phagocytosis in their internalisation behaviour. However, phagocytosis in those cells usually happens in a much lower extent and is called unprofessional phagocytosis (Hillaireau and Couvreur, 2009). The phagocytosis follows these three steps: Firstly, the particles are recognized by opsonisation in the bloodstream. Secondly, the opsonised particles adhere onto the cell membrane. Thirdly, the particles are internalised by cells (Hillaireau and Couvreur, 2009).

While phagocytosis is believed to be limited to specific cell types, pinocytosis is a vital mechanism utilised by any cell type for uptake of nutrition and exchange signals, which could be further classified into clathrin-mediated endocytosis, caveolin-mediated endocytosis, macropinocytosis and other clathrin and caveolin independent pinocytosis, according to their mechanisms. In macropinocytosis, the cell membrane ruffles by actin driven formation of the membrane protrusions. This process is triggered by the signalling cascades mediated by Rho-family GTPases. Unlike phagocytosis, in which protrusions "zipper up" along the ligand coated particle, in macropinocytosis, the protrusions engulf a large volume of fluid and form endocytic vesicles, macropinosome (Conner and Schmid, 2003).

2.2.4 Chemical inhibitors

To date, the most reliable and efficient tool for studying the endocytic pathways is using chemical inhibitors (Nakase et al., 2004, Grimmer et al., 2002). Chemical inhibitors defunctionalise a specific type of protein or chemical that is essential to cells' internalisation process and thus block the involved internalisation pathway. However, the chemical inhibition is not designed to block one specific endocytic pathway. So usually, a combination of the results of several different chemical inhibitors should be collected and

a proper analysis is required. Kastl et al studied the inhibition rate of the internalisation of PSS/PAH microcapsules by breast cancer cells with different inhibitors (Kastl et al., 2013). The inhibitors and concentrations used and the degree of inhibition on cell endocytosis were listed in a detailed and comprehensive table (Table 1). The concentrations were chosen to ensure that under that concentration the inhibitors are still active and the concentration is not too high so that it would not damage the viability of the cell.

pharmacological/chemical inhibitor or alteration of the cellular environment	concentration	associated pathway	quantification of inhibition
cell incubation at 4 °C		all	100%
methyl-beta-cyclodextrin	2000 μM	lipid rafts and lipid-raft-mediated macropinocytosis	93%
bafilomycin A_1	1 μM	phagocytosis	84%
concanamycin A	0.5 μM	phagocytosis	63%
cytochalasin D	20 μM	phagocytosis	49%[a]
amiloride	500 μM	macropinocytosis	38%
nocodazole	1 μM	endocytosis	23%
heparinases	5 U	adsortive mechanisms	17%
chlorpromazine	15 μM	clathrin-mediated endocytosis	16%
dynasore	80 μM	clathrin- and lipid rafts/caveolae-mediated endocytosis	14%
potassium depletion		clathrin-mediated endocytosis	→0%
nystatin	10 μg/mL	lipid rafts/caveolae	1%
cell incubation in serum-free medium		determined by the adsorbed proteins	−26%

Table 1 The influence of inhibitor on the internalisation of microcapsules (Kastl et al., 2013)

Cytochalasin D is a fungal metabolite that inhibits actin polymerization by binding to F-actin filaments preventing their growth (Vieira et al., 2002). F-actin is well known for being responsible for the rearrangement of the plasma membrane during processes such as ruffling, migration and phagocytosis. Actin polymerization around the nascent phagosome is a feature of all types of phagocytosis. Nevertheless, a functional actin cytoskeleton plays also a role on the micropinocytosis (Kruth et al., 2005).

Methyl-beta-cyclodextrin (MβCD) is an inhibitor frequently studied to investigate the mechanism of micropinocytosis (Edidin, 2003, Grimmer et al., 2002). MβCD depletes cholesterol from plasma membrane and the

removal of cholesterol from the plasma membrane disrupts lipid raft mediated endocytic pathways, including caveolae and macropinocytosis. MβCD is a polysaccharide containing a hydrophobic core with high affinity for cholesterol. MβCD has a significant effect on altering the structure of cholesterol-rich domains such as the lipid rafts (caveolae dependent and independent) and the lipid raft-mediated macropinocytosis, a lipid raft-dependent and receptor-independent form of endocytosis that requires actin membrane protrusions.

2.3 Cellular uptake of microcapsules

2.3.1 Effect of particle properties on the internalisation

The internalisation of the nanomaterials depends on the structure and the chemical properties of the nanomaterials, namely the size (Albanese et al., 2012, Foster et al., 2001), shape (Sahay et al., 2010, Champion et al., 2007), stiffness (Liu et al., 2012, Sun et al., 2015, Hartmann et al., 2015), and surface charge (Javier et al., 2006).

Particles of different sizes and shapes have been reported to be internalised by the cells, such as gold nanoparticles (Shukla et al., 2005), carbon nanotube (Kam et al., 2004), etc. For particles larger than 500 nm, they are likely to be internalised by micropinocytosis and phagocytosis (Best et al., 2012). Generally speaking, smaller particles have a faster internalisation rate (Foster et al., 2001, Foged et al., 2005). The influence of the particle shape on the process of the phagocytosis was revealed by Champion et al (Champion et al., 2007). In that study, polymeric microparticles of complex shapes were used and the results showed it was the curvature at the point of contact with the macrophage rather than shape or the size of the particle that was crucial to the internalisation (Figure 2.5). For instance, an ellipse shaped particle could be internalised in a few minutes if the narrower and sharper side of the particle makes the first contact. However, if it is the elongated side that makes

the first contact, no internalisation would happen.

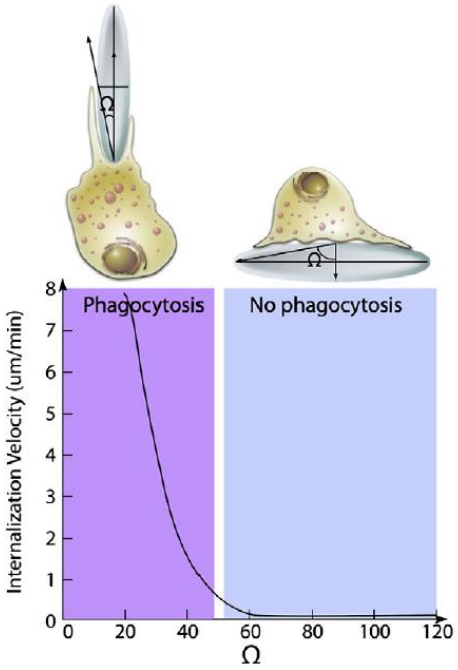

Figure 2.5 Effect of the curvature at the point of contact on the rate of phagocytosis. Ω is the angle between the membrane normal at the point of initial contact and the line defining the particle curvature at this point. (Champion et al., 2007)

The stiffness is an important parameter that decide the percentage as well as the rate of the internalisation. Banquy et al studied the uptake of nanoparticles of around 150 nm in size and 20-200 kPa in stiffness and suggested particles with different stiffness use different endocytosis pathways. While soft nanoparticles were internalised via micropinocytosis, stiffer ones were internalised by a clathrin-mediated pathway (Banquy et al., 2009). Those in the middle (30-140 kPa), however, could use both pathway and thus had a higher rate of internalisation.

Surface charge of the particles is another key factor in the internalisation of the particles. Studies showed an increased uptake of positively charged particles compared to that of negatively charged or neutral particles (Albanese et al., 2012). The explanation to this is that the cell membrane has a negatively charged surface and it is the electrostatic force that binds the

particles onto the membrane surface before the internalisation. This explanation was also confirmed by the interaction between microcapsules and cells. By measuring the force between the capsules and cell using AFM, Javier et al revealed that the adhesion between positively charged capsule and cells is indeed stronger than that of the negatively charged capsules (Javier et al., 2006).

It is also worth mention here that the colloidal particles might display totally different properties in the serum containing cell media compared to deionized water. As serum containing cell media contains hundreds of different proteins and other chemicals, many of which are highly reactive. This phenomena of nanoparticles coated with proteins inside the cell media is called protein corona (Nazarenus et al., 2014). The composition of protein corona is complicated, due to the diversity of the ingredient inside the cell media. Its effect on the zeta potential of the polyelectrolyte microcapsules were reported by Ai et al. The change in zeta potential after incubated with cell media is illustrated in Figure 2.6 (Ai et al., 2005). It suggested that after one hour of incubation, all the microcapsules with positively charged outer layer experienced a dramatic decrease in the zeta potential.

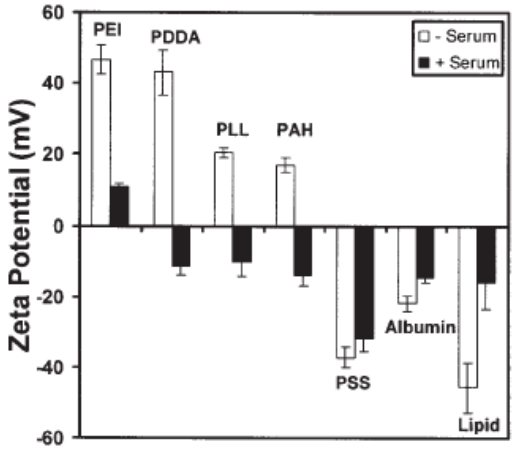

Figure 2.6 Zeta potential of polyelectrolyte microcapsules with different outermost layer before (white columns) and after (black columns) incubated in serum containing cell culture medium. (Ai et al., 2005)

2.3.2 Internalisation of polyelectrolyte microcapsules

Successful internalisation of polyelectrolyte microcapsules loaded with various macromolecules have been observed in several types of living cells (De Geest et al., 2006, Javier et al., 2006, Javier et al., 2008, Glinel et al., 2003, Sukhorukov et al., 2005). The internalisation of microcapsule shares commons with the internalisation of nanoparticles and microparticles as described before. The interaction between a wide variety of different microcapsules and cells have been studied. Factors that affect the internalisation of nanoparticles and microparticles, such as size (Foster et al., 2001), stiffness (Yu et al., 2016) and surface charge (Ai et al., 2005) also affect the internalisation of microcapsules. Apart from these, the interactions between functionalized microcapsules, such as PEG grafted capsules (Foster et al., 2001) and degradable capsules (De Koker et al., 2007, De Geest et al., 2006) and cells were also studied.

According to our knowledge, the first study on the internalisation of microcapsule was published in 2005 by Sukhorukov et al. Internalisation of microcapsules of 5 μm in diameter by breast cancer cells MDA-MB-435s was observed using optical and fluorescent microscopy (Sukhorukov et al., 2005). With the help of 100× oil immersion objective, internalised capsules could be distinguished from those attached to the cell membrane (Figure 2.7). The internalised capsule located around the nuclei but not inside the nuclei and had a squeezed appearance. It was suggested that the capsules were squeezed by the pressure present in the endocytic vesicles.

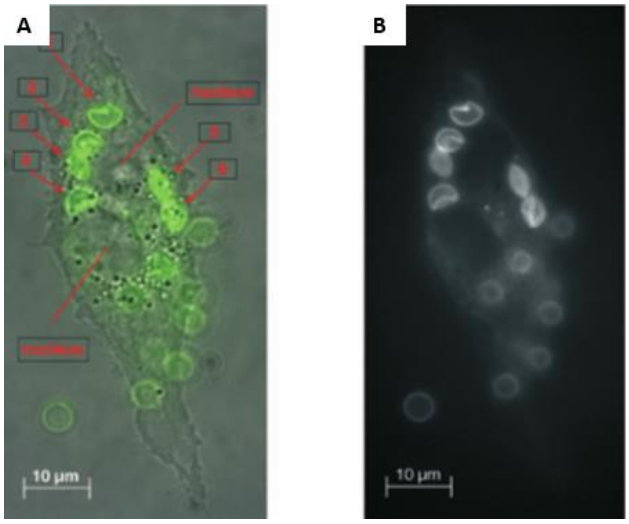

Figure 2.7 Optical (A) and fluorescence (B) images of capsule internalised by MDA-MB-435s breast cancer cells. Those internalised capsules had squeezed appearance while the un-internalised ones remained their spherical shapes. (Sukhorukov et al., 2005)

In that same year, Ai et al reported the internalisation of polyelectrolyte microcapsule of 1 µm in diameter by MCF-7 breast cancer cells. Cell uptake was examined by flow cytometry and confocal laser scanning microscopy (Figure 2.8). For flow cytometry analysis, the cells were washed with 5 mM EDTA at pH 5.0 for 15 minutes. This protocol was first introduced by Behrens et al to cleave sulphide-bonds of mucin (Behrens et al., 2002) as it was suggested that it is the mucus secreted by the MTX-E12 cells that bounds the particles to the cell membranes.

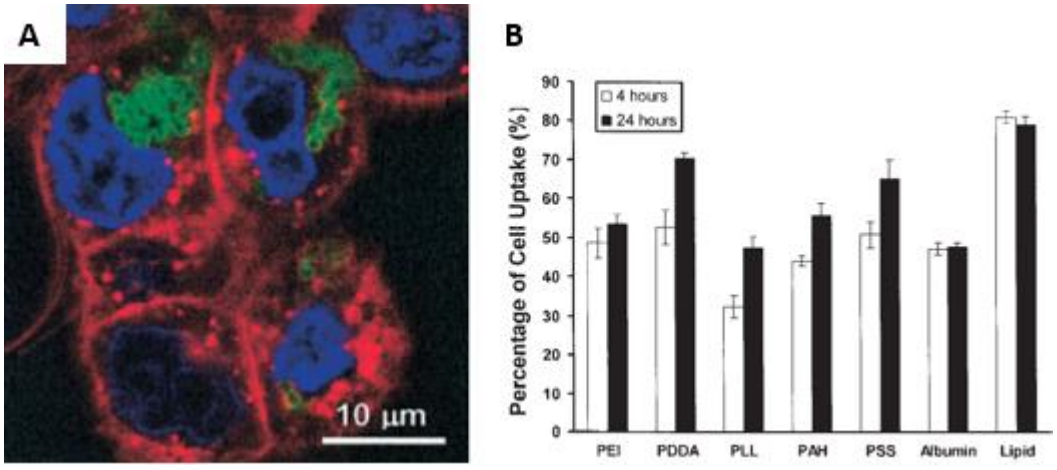

Figure 2.8 Internalisation of polyelectrolyte microcapsule of 1µm in diameter by MCF-7 breast cancer cells examined by confocal laser scanning microscopy (A) and flow cytometry (B).(Ai et al., 2005)

In 2006, Javier et al compared the statistic of internalisation using fluorescence microscopy and 3D confocal microscopy (Javier et al., 2006). The results showed the number of internalised capsules counted by conventional optical microscopy was significantly higher than that determined by 3D confocal microscopy. Javier et al suggested that this overestimation of internalisation rate was due to the counting of those microcapsules that adsorbed to the outside of the cell membrane as internalised.

In 2007, Kreft et al introduced the pH-sensitive fluorescent dye SNARF1 to the study of microcapsules internalisation (Kreft et al., 2007). SNARF1 alters its fluorescence emission under different pH conditions. It emits red fluorescence in alkaline condition and green fluorescence in acidic condition. It was used to investigate the destination of the microcapsules after the internalisation. As in Figure 2.9, the green fluorescence given by the capsules indicated they were in an acidic environment suggesting that the capsules were inside endosome after they had been internalised. With this fluorescence label, capsules that internalised by the cells could easily be distinguished from those only attached to the cell membrane surface. Based on this study, a flow cytometry based assay was developed by Semmling et al in 2008 to quantitatively analyse the internalisation of microcapsules (Semmling et al., 2008). By recording the fluorescence intensities from the red and green channels, the flow cytometry analysis allowed a more detailed quantitative analysis that could distinguish between the capsules attached to the cell membrane and those got internalised.

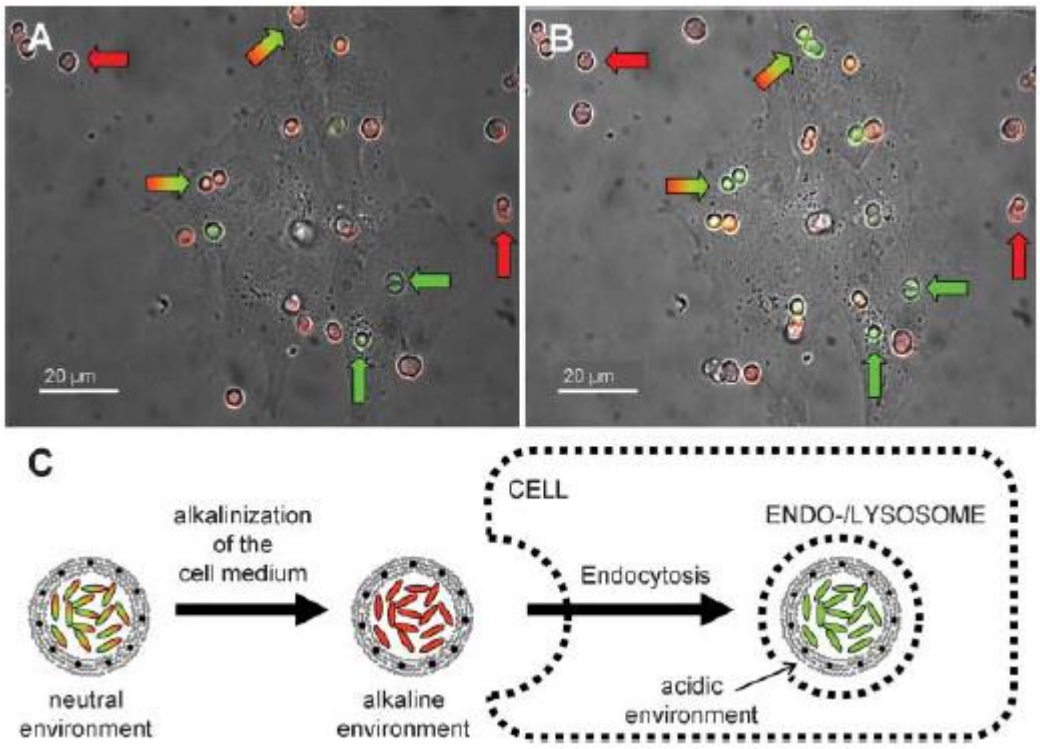

Figure 2.9 SNARF-loaded capsules change from red to green fluorescence upon internalisation (Kreft et al., 2007)

In 2013, Kastl et al employed electron microscopes to the characterisation of internalisation process (Kastl et al., 2013). The results suggested that multiple internalisation pathways are involved in the uptake of the microcapsules. The process of internalisation as suggested by Kastl et al was as follows. First, the capsule attaches to cell membrane as a result of electrostatic interaction. Then, phagocytic cup forms to stabilize the capsules by the reorganization of actin and the formation of filopodia (Figure 2.10). Lipid raft mediated macropinocytosis might also play an important role in this process. After the capsule has entered the cell, the capsule is then transported into its final location inside phagocytic vesicles.

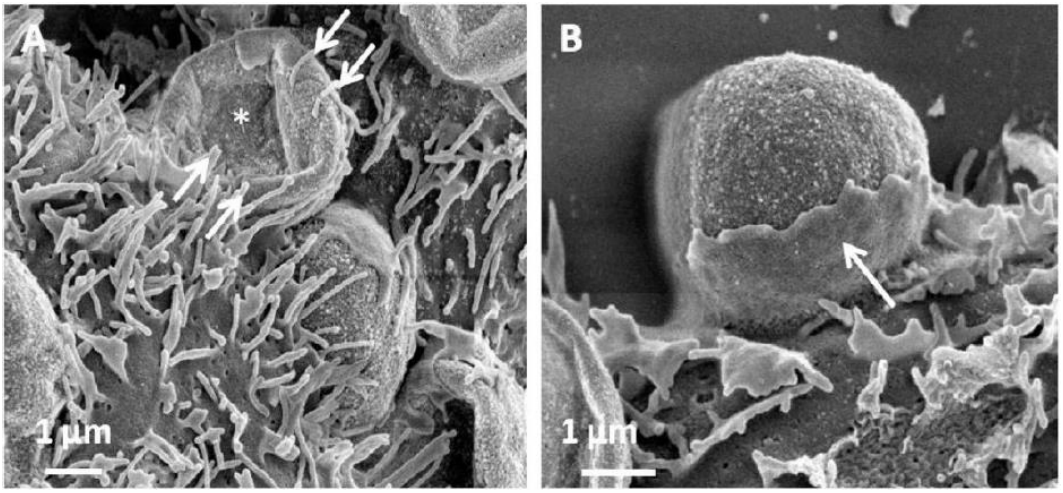

Figure 2.10 SEM images of the morphology of cultured MDA-MB-231 breast cancer cells during the capsule (*) internalisation. The formation of filopodia (arrows in A) and phagocytic cup (arrow in B) can be seen respectively in these images (Kastl et al., 2013).

To conclude, the internalisation of microcapsules was mainly studied using these four characterization methods: conventional optical/fluorescence microscopy (Sukhorukov et al., 2005), 3D confocal microscopy (Liu et al., 2014, Javier et al., 2006), flow cytometry (Semmling et al., 2008, Reibetanz et al., 2007), or electron microscopy (Pavlov et al., 2011, Kastl et al., 2013). Most fluorescence-based microscopy techniques struggled with distinguishing between internalised and simply adhered capsules. Different methods were developed to improve the precision and reliability in examining the capsule internalisation, such as pH sensitive dye SNARF (Kreft et al., 2007). However, due to the limitation in the resolution of these conventional microscopy techniques as well as the lack of specific fluorescent labels, the process of internalisation remains unclear.

2.4. Scanning Ion Conductance Microscopy

2.4.1 Principle of scanning ion conductance microscopy

Scanning ion conductance microscopy (SICM) is a type of scanning probe microscopy technique. It consists of an inverted microscope, a pipette, a micromanipulator, an amplifier and a computer. The principle of SICM is

illustrated in Figure 2.11. A nano pipette with electrolyte inside is used to scan the surface of the sample. The ion current between the bath and the electrolyte inside the pipette is monitored by two Ag/AgCl electrodes and sensitive current amplifier. When the pipette tip approaches the surface (before touching it) using a z-axis piezo actuator, the ion current drops as the pathway of the ion current is partially blocked by the sample. The relative height of the sample at that imaging point can be estimated as the z-axis coordinate of the nanopipette at which the current drops to a certain predefined value (setpoint). Usually, the pipette scans the surface in a raster scan manner and the topography of the sample is integrated by collecting the relative height at each imaging point. (Hansma et al., 1989)

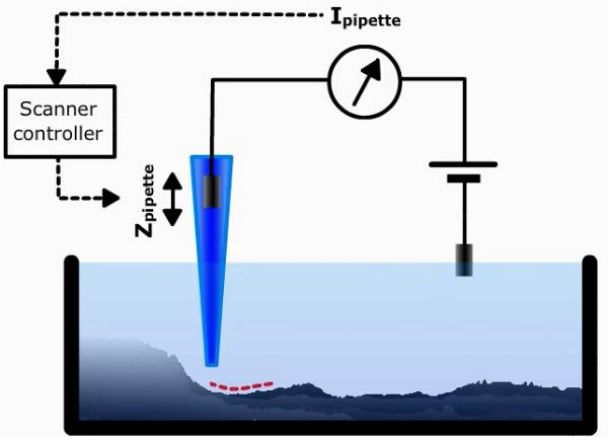

Figure 2.11 The principle of SICM.

Due to its unique feedback system, the SICM has the advantage of maintaining a gap between the pipette's tip and the surface without making any direct physical contact. This makes SICM a perfect tool for cell imaging (Korchev et al., 1997b). Fine surface structure that were once only observed by scanning electron microscopy could be visualised without fixation and staining. This opened the opportunity for live cell imaging at nanoscale. With SICM, the movement of the cell and the transformation of the cell membrane upon stimulation could be recorded with live time lapse topography images.

As mentioned before for conventional SICM, a continuous scanning mode of

feedback control is employed, where the gap between the pipette and the surface is kept constant (usually equals to the inner radius of the tip) by moving the pipette up and down using a z-axis piezo actuator. As a result of this, the conventional SICM is restricted to imaging relatively flat surface, as the probe might collide into the sample when it approaches a vertical structure. To eliminate this limitation of SICM, Novak et al developed a novel imaging mode, called Hopping Probe Ion Conductance Microscope (HPICM) (Novak et al., 2009). In HPICM, continuous feedback and raster scan is no longer employed. Instead of maintaining a constant gap, the pipette approaches the sample from a starting point far away from the sample. The pipette keeps approaching until the current drops by a predefined amount, which is typically in the range of 0.25- 1% (Novak et al., 2009). After acquiring the height information of this point, the pipette is drawn back to its original position and the sample is moved to the next imaging point, then the pipette is lowered to re-approach the sample. Figure 2.12 shows the scanning mechanism for both modes and also demonstrates the imaging artefacts of the conventional SICM.

Apart from its ability to image convoluted samples, HPICM also use smart algorithm to minimize the scanning time. It is achieved by scanning the surface square by square, the roughness of each is estimated by measuring the height difference of the four corners. This square could then be scanned with different resolution and scan rate according to its roughness. The amplitude of the withdrawal could also be adjusted according to the roughness of the sample to accelerate the rate of scanning. With these improvements in the algorithm, the time required for each scan is shortened significantly, for instance, it only took 15 min to acquire Figure 2.12D, while Figure 2.12C took 45 min. The capability of fast scan could not only save the time for imaging, but also provide better quality image of live cell and able to capture the movement of the live cell more precisely by time elapse images. After HPICM was introduced in 2009, it immediately replaced the

conventional continuous scan mode and draw more and more interest in the past few years.

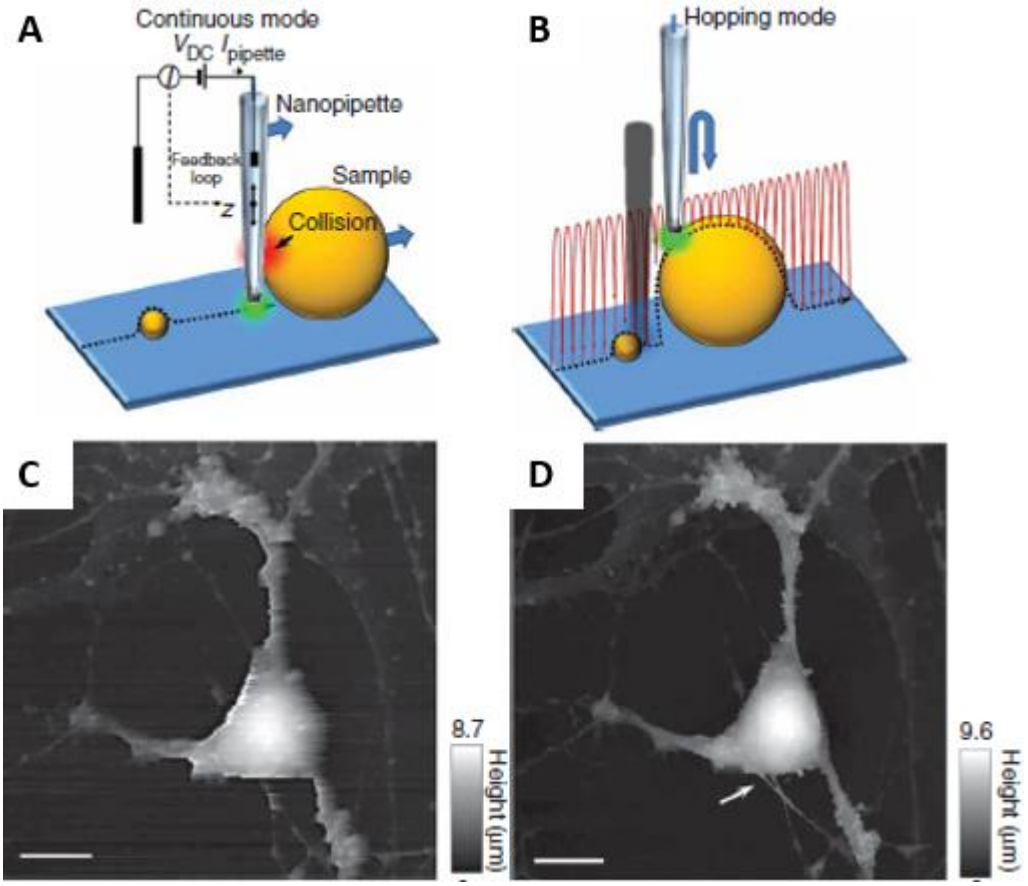

Figure 2.12 Principle of HPICM. (A) Illustration of a pipette operating in continuous scan mode colliding into a spherical object possessing a steep vertical slope, (B) Illustration of the hopping mode showing the pipette hops over the spherical object, (C, D) Topographies of same fixed hippocampal neuron obtained with continuous scan mode (C) and hopping mode (D). Arrow in (D) points out the fine structure that unable to be acquired by the continuous mode. (Novak et al., 2009)

2.4.2 Resolution and fidelity of SICM

The resolution and fidelity are two of the most important things of a characterization technique. The discussion on the true resolution of SICM is still ongoing. This discussion is further complicated by the fact that there are several different ways to define lateral and vertical resolution (Rheinlaender and Schaffer, 2009). In most of the articles, the resolution of the SICM is suggested as the equivalent of one inner radius of the pipette tip opening.

However, one of the recent reports concludes the lateral resolution equals to three times the inner radius of the pipette tip opening (Rheinlaender and Schaffer, 2009). This claim is made by assuming the resolution is the smallest distance at which two individual particles on a planar surface can clearly be resolved from each other in an image (Figure 2.13).

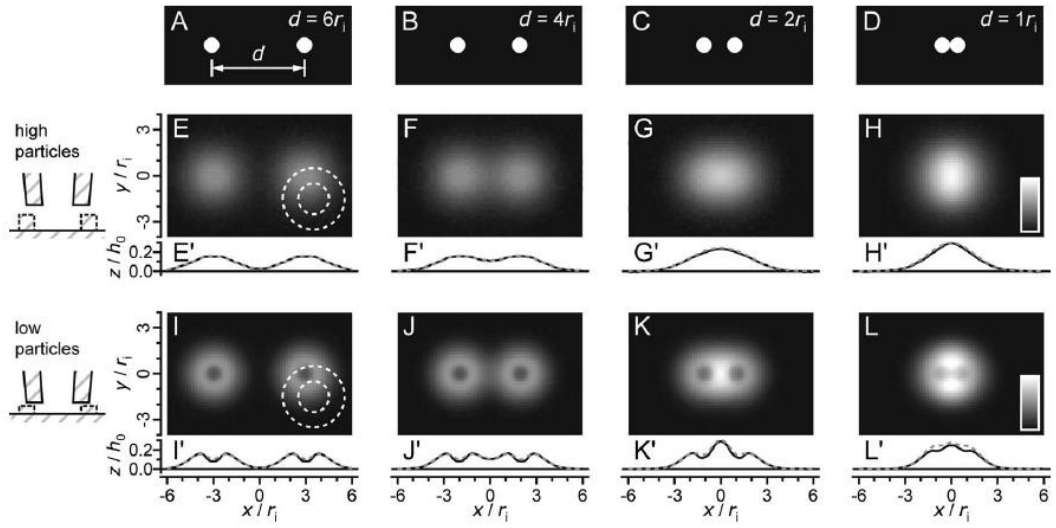

Figure 2.13 Calculated topography images of two cylindrical particles of radius r=r_i/2 on a planar surface. (Rheinlaender and Schaffer, 2009)

Before SICM was introduced for cell study, AFM was the most widely used characterization technique in surface morphology. Although the deformation of surface upon the contact of the AFM tip is always a problem for imaging soft samples, there are still few trails on applying AFM to cell imaging (Nowakowski and Luckham, 2002, Ushiki et al., 2000). As for the fidelity of the SICM, a comparison of SICM with AFM was made by Rheinlaender on fixed cell (Rheinlaender et al., 2011). Force mapping AFM and hopping mode SICM were used to scan the fixed sample of bulky shaped fibroblast cells and myoblast cells. The results showed that in the AFM image, the edges of the cell could not be imaged accurately (Figure 2.14). A characteristic stripe pattern appeared on one edge of the cell and a tail-like feature appeared on the other side (arrows and the dash-lined area in Figure 2.14e). The profiles of the cell topology show the SICM could accurately detect steep slopes while the AFM tends to miss all these information. Rheinlaender et al

suggested it was the geometry of the AFM tip that caused these artefacts. Because of its pyramid shape, the tip could not reach those crevices. However, for SICM, the pipette had typically a half-cone opening angle of 3° (Caldwell et al., 2012). It was also worth noting that this comparison was done on the fixed cell, which was much stiffer than the live cell.

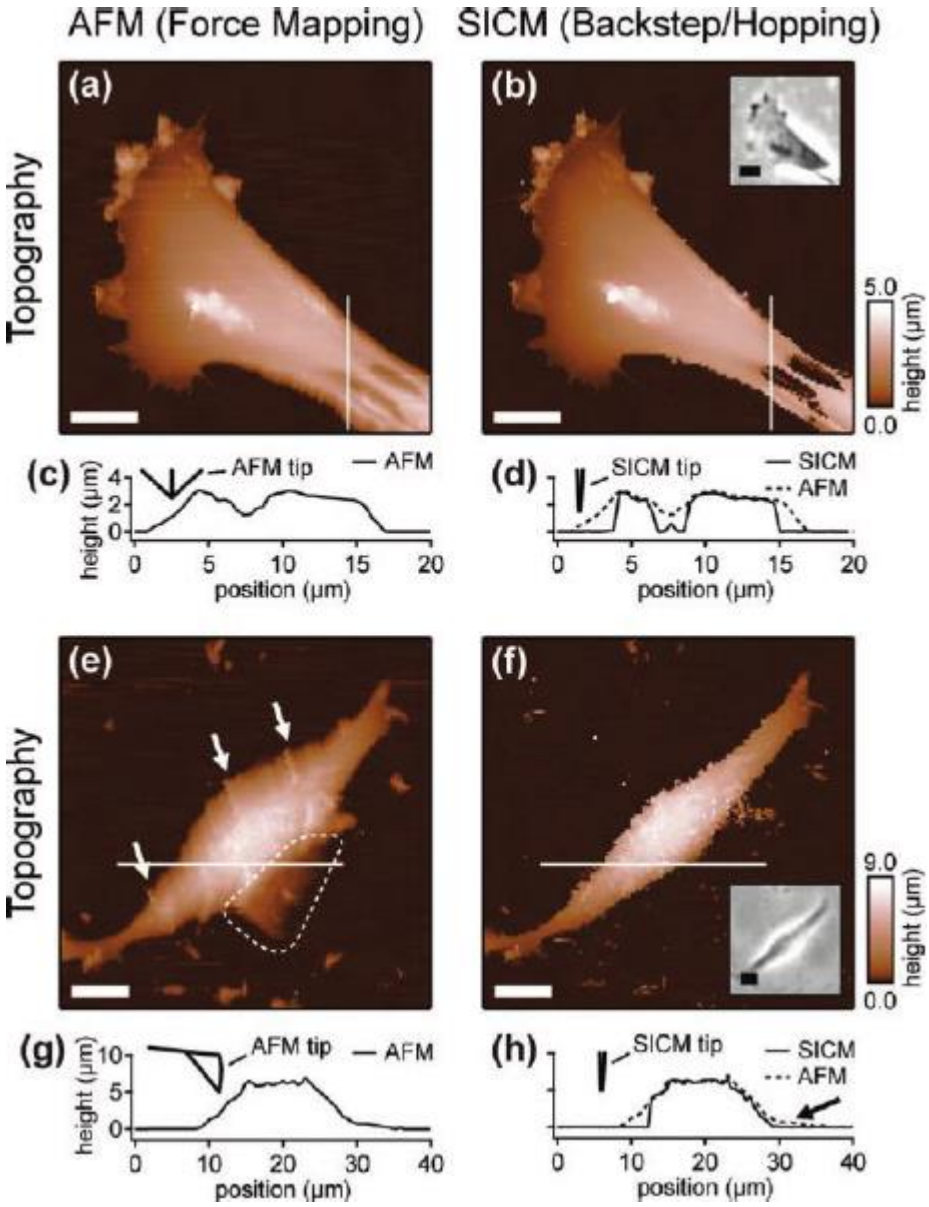

Figure 2.14 Comparison of SICM with AFM in imaging steep structure. (a) Force mapping mode AFM image and (b) hopping mode SICM image of fixed fibroblast cell. (e) Force mapping mode AFM image and (f) hopping mode SICM image of fixed myoblast cell. (c, d, g, h) Profiles of the cell surface along the white lines in their corresponded images. (Rheinlaender et al., 2011)

2.4.3 SICM in studying particle internalisation

The ability of SICM to scan live cells in real time with high resolution and fidelity opens the possibility of following biological processes of the cell membrane. When talking about the living recording, apart from spatial resolution, temporal resolution would be another major concern for achieve nice recordings. Shevchuk et al showed that SICM could be employed to study the movement of the microvilli-like structures and the opening and closing of the endocytic pits (Shevchuk et al., 2012). The fastest temporal resolution reported so far is 6s for a 1.2 μm×1.2 μm area at a resolution of 20×20 pixels (60 nm pixel width) (Novak et al., 2014).

The application of SICM to the study of particles cell entry in live cells was first introduced by Gorelik (Gorelik et al., 2002). Simultaneous recording of cell surface fluorescence and high resolution topography was realized by incorporated a laser scanning confocal microscopy into the SICM setup (Scanning surface confocal microscopy, SSCM). SSCM acquired both the topographical information and the fluorescence distribution in just one scan so that the position of the fluorescent labelled particles could be related directly onto the cell surface (Figure 2.15A). To study the cell entry, fluorescently labelled virus like particles and live COS7 cells were used. The surface of the cells was repetitively scanned by SSCM every 20 min for 4 hours. The disappearing of green fluorescence from the membrane surface confirmed the internalisation (Figure 2.15B).

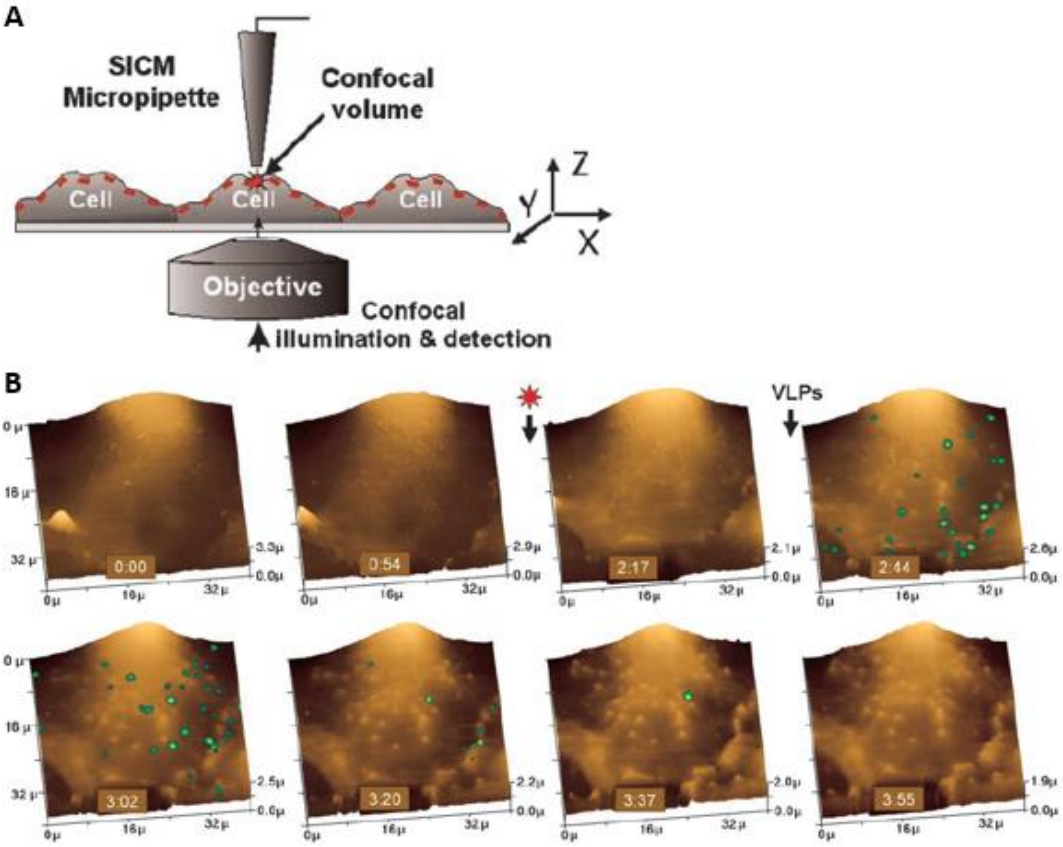

Figure 2.15 Investigating the particles cell entry using SSCM. (A) Schematic of the SSCM. (B) The particles internalisation process revealed by overlays of topography images and fluorescent information. The green dots visible on the topography represented fluorescently labelled particles. (Gorelik et al., 2002)

The experimental details Gorelik et al used in his study served as a guideline for the future study of particle internalisation (Gorelik et al., 2002). (1) Due to the limitation of scan rate, the size of the scanning area and the time span of the cell entry process should be considered carefully. (2) Although the fluorescence image could be captured during each scan, the photobleaching and photodamage limit the observation time of fluorescence. (3) Once the particle has passed through the membrane, it could no longer be traced using the topographical information. However, it could still be detected by moving the laser focus below cell surface. (4) The fluorescently labelled particles could be locally delivered to the cell surface by the same pipette used for scanning using voltage. (5) The imaging should start once the particles had a chance to strongly attach to the surface but not yet entered the cell.

2.4.4 Measurement of elastic modulus of cells using SICM

Mechanical properties of biological samples have been attracting growing level of interest over the last two decades. Mechanical stress has been reported to affect the morphology and behaviour of the cell (Janmey, 1998, Pollard and Borisy, 2003). Traditionally, AFM used to be the technique of choice when it comes to simultaneous topography imaging and elastic modulus measurement of living cells. Force mapping mode, force modulation mode and multi-harmonic tapping mode were developed for this purpose (Dufrene et al., 2017). Recently, the possibility of conducting elastic modulus measurement on biological sample with SICM was also explored (Rheinlaender et al., 2015, Schaffer, 2013, Rheinlaender and Schaffer, 2013, Clarke et al., 2016, Sanchez et al., 2008). So far, two methods for elastic modulus mapping have been established. The method developed by Rheinlaender and Schaffer uses a pressure-induced microfluidic flow out of the nanopipette tip to produce the force (Rheinlaender and Schaffer, 2013) while the method developed by Clarke et al uses an intrinsic pressure between the tip and the sample (Clarke et al., 2016).

The basic idea of the Rheinlaender and Schaffer's method is that pressure could be applied through the scanning pipette to measure the elastic modulus of the cell (Schaffer, 2013). When a pressure is applied to the wide back end of the nanopipette, a highly localised pressure builds up at the sharp tip of the pipette and this pressure could be utilized to indent the sample surface (Figure 2.16A, B). The feedback control of SICM is used to maintain a constant distance between pipette tip and sample surface. When the sample surface is indented by the pressure from the pipette tip, it displaces its surface away from the tip. The feedback control then lowers the pipette to maintain that constant gap. The distance that pipette lowered is recorded as the displacement of the sample (Rheinlaender and Schaffer, 2013). The larger the applied pressure and the softer the sample, the larger the displacement of the sample. To demonstrate the ability of SICM elastic modulus measurement,

Rheinlaender and Schaffer used their method to image changes in actin cytoskeleton in living fibroblast cell (Figure 2.16C). The resultant time lapse image sequence compared the fluorescence images, the topography images and the elastic modulus mapping of the fibroblast cell. The results showed the contrast in elastic modulus revealed the presence of actin cytoskeleton, which corresponded to the fluorescence images (Figure 2.16C).

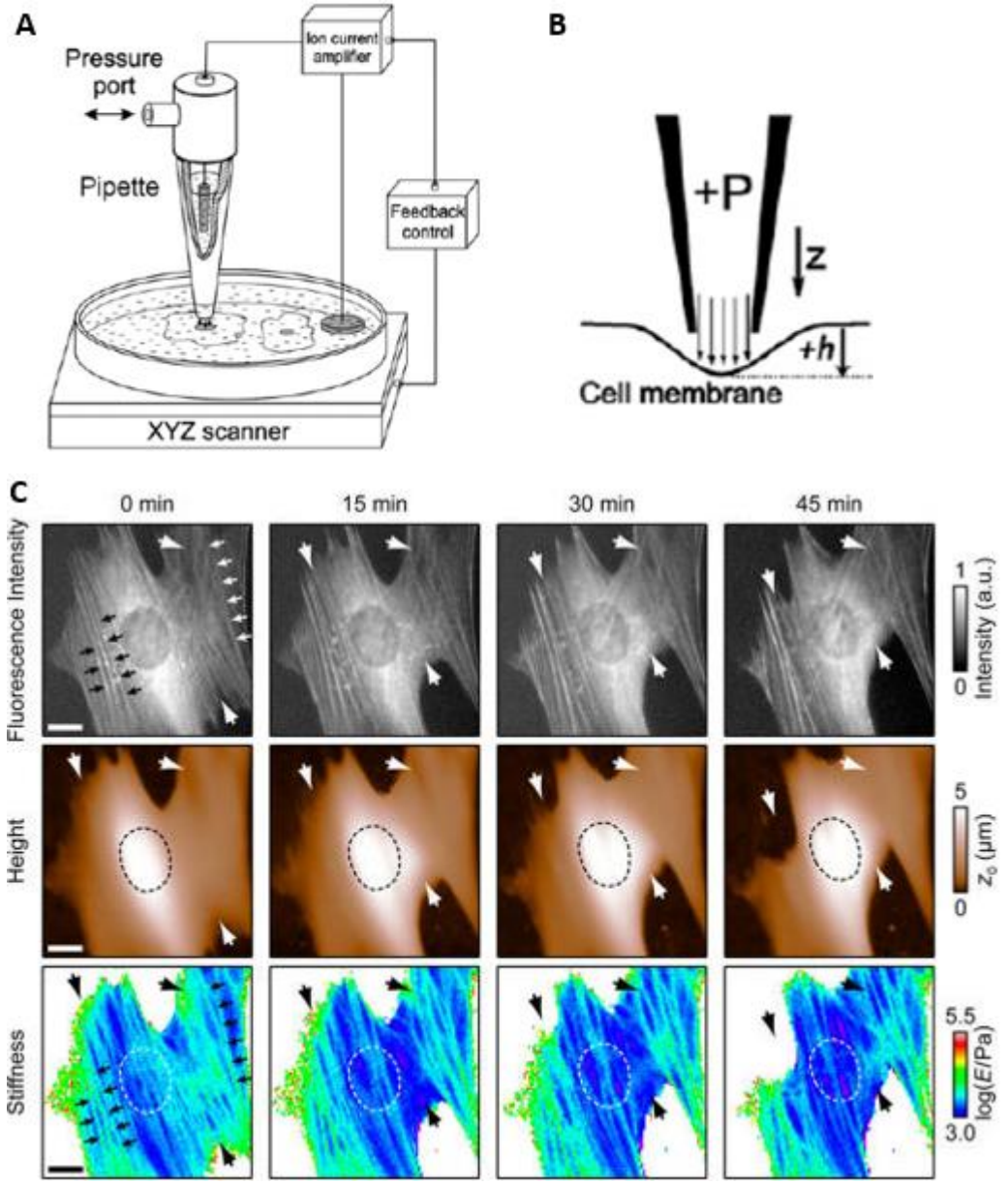

Figure 2.16 Elastic modulus mapping of live cells using Rheinlaender and Schaffer's method. (A) Schematic of the pressurised pipette. (B) Schematic of the indentation of cell membrane by the pressurised flow. (C) fluorescence images, the topography images and the elastic modulus mapping of the fibroblast cell showing the changes in actin cytoskeleton caused by cytochalasin D. (Rheinlaender and Schaffer, 2013)

The principle of the method developed by Clarke et al is similar to that of Rheinlaender and Schaffer method as described before with the main difference being that the stress applied to the cells is the intrinsic colloidal pressure between the cell surface and the glass pipette tip opening (Clarke et al., 2013) instead of the hydrostatic pressure in the Rheinlaender and Schaffer method. Since the method by Clarke et al does not rely on the use of pressure which may block pipette tip from inside, it can be used with shaper nanopipettes and therefore achieve higher spatial resolution (Figure 2.17) (Clarke et al., 2016). So far, there is no time lapse live cell imaging reported using this method.

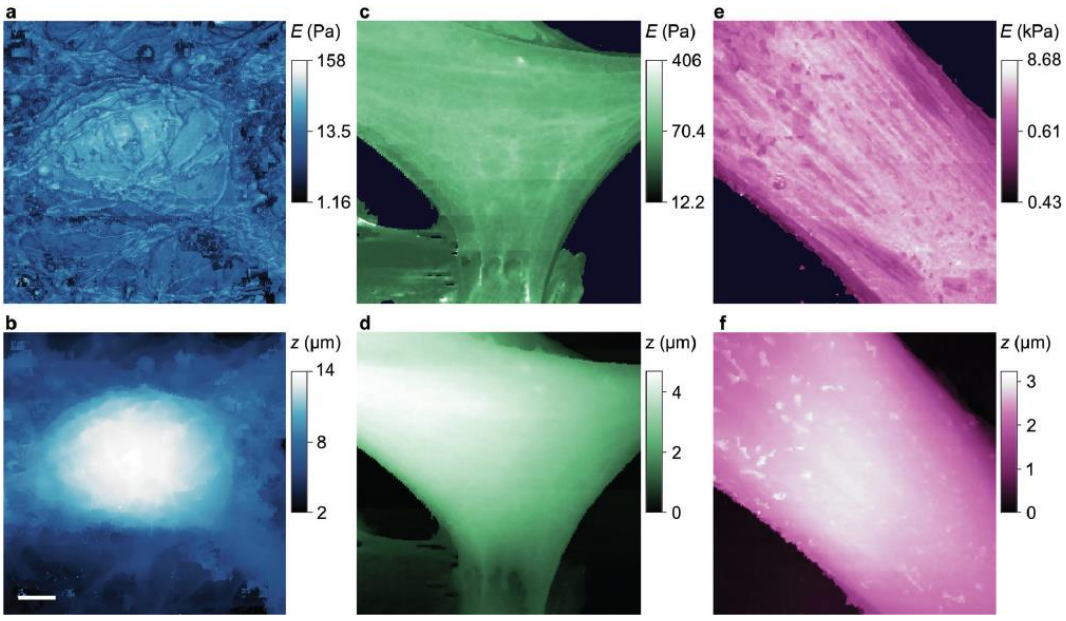

Figure 2.17 Stiffness and topography of three cell types, Human Neuron (a, b), HpL mouse hippocampal neurons (c, d) and Human Mammary Fibroblast (e, f) imaged at high resolution using Clarke method. (Clarke et al., 2016)

3. Aims and objectives

Polyelectrolyte microcapsule is considered as a promising strategy for targeted drug delivery (Johnston et al., 2006). The interaction between the microcapsule and cell need to be understood in order to improve the drug delivery efficiency of the microcapsule. However, current imaging techniques could only be used to confirm the internalisation of microcapsules (Sukhorukov et al., 2005, Ai et al., 2005). Due to the lack of resolution and specific fluorescent markers, these imaging techniques are struggling with providing further details to the internalisation process.

This study aims to exploit the live cell imaging ability of SICM to study the live internalisation process of polyelectrolyte microcapsules. Improvements in SICM has demonstrated its capability of imaging sophisticated cell structure with nanoscale resolution (Novak et al., 2009). The ability of imaging live samples allows the study of live process, such as the internalisation of nanoparticles (Novak et al., 2014). Recent implement of elastic modulus mapping opened up the possibility of measuring the mechanical properties of live cells (Clarke et al., 2016). However, none of these abilities have been tested before for imaging a process as complex as the internalisation of a microcapsule.

For imaging live internalisation process, we expected difficulty posed by the tall profile of microcapsules and the dynamic activities of cell membrane. In previous research, those sophisticated cell structures imaged were considerably still (Novak et al., 2009) and those live cell process recorded such as the internalisation of nanoparticles did not involve scanning convoluted structures (Novak et al., 2014). As for the elastic modulus mapping, it has not been tested on any dynamic processes before (Clarke et al., 2016).

This project will address the issues stated above through the following set of objectives:

- Determine the suitability of SICM for imaging topography and local elastic modulus of microcapsule internalization
- Characterise the behaviour of membrane processes during microcapsule internalisation and identify key aspects
- Characterise mechanical properties of the internalisation process
- Examine the effect of commonly used inhibitors on the internalisation from the viewpoint of label-free topographical imaging

Successful visualisation of the internalisation process would shed more light on the mechanism of particle internalisation. A better understanding of the interaction between particles and cells could help to develop drug carriers with desirable size, shape and surface properties to optimize their targeting efficiency.

4. Methods and materials

4.1 Materials

4.1.1 Materials for capsule synthesis

Polyelectrolytes used for capsule fabrication were poly(sodium 4-styrenesulfonate) (70,000)(PSS), poly(allylamine hydrochloride) (15,000) (PAH).

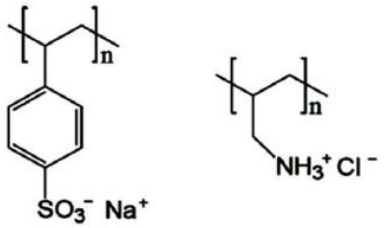

Chemicals used for core crystallization and dissolution were calcium chloride ($CaCl_2$), sodium carbonate (Na_2CO_3) and ethylenediaminetetraacetic acid (EDTA). Fluorescein isothiocyanate isomer I (FITC) was used to label the outermost layer of the capsule. All chemicals were bought from Sigma Aldrich and used without further purification.

4.1.2 Materials for cell culture and live cell imaging

Phosphate buffered Saline (PBS), DMEM, high glucose, GlutaMAX™ Supplement, pyruvate (DMEM), Fetal calf serum (FCS), penicillin and Trypsin-EDTA (0.05%) used for cell culture were purchased from Thermo Fisher Scientific.CellMask™ Orange Plasma Membrane Stain (CellMask™) and Leibovitz's L-15 Medium (L-15) were also purchased from Thermo Fisher Scientific.

4.2 Layer-by-layer capsules

4.2.1 The template for the synthesis of layer-by-layer capsules

In principle, the layer-by-layer capsules could be fabricated on any particles

followed by the dissolving of the original core. However, in application, considering the stability of the polyelectrolytes multilayer in the dissolving agent and the operability of the process, weakly cross-linked melamine formaldehyde particles (MF) (Donath et al., 1998), $CaCO_3$ particles prepared by colloidal crystallization (Volodkin et al., 2004b, Volodkin et al., 2004a), charged polystyrene latex particles (Sukhorukov et al., 1998b) and the mesoporous silica (MS) (Yu et al., 2005) are the most widely used cores for the synthesis of multilayers capsules. In this project, $CaCO_3$ particles were used as the template for the layer-by-layer capsules. $CaCO_3$ particles were chosen as they are the most feasible particles that could simply be synthesised in any lab and their size could be tuned easily by controlling the duration of precipitation.

Uniform and spherical $CaCO_3$ particles could be synthesized by colloidal crystallization from supersaturated solution. Spherical amorphous calcium carbonate (ACC) would form by simply mixing equal volume of $CaCl_2$ and Na_2CO_3. However, ACC is not a stable form of $CaCO_3$, so it will spontaneously transform into rhombohedral calcite crystal which is thermodynamically more favored. However, it is the spherical ACC that is needed as the substrate of layer-by-layer, so this transition must be avoided as much as possible. Volodkin suggested the transition occurs as long as the ACC particles are accessible to the water (Volodkin et al., 2004a). The most effective way to avoid the transition is to dry the particles or coat the particles with the polyelectrolytes multilayers as soon as the desired size of the particles has been reached.

To prepare the ACC particles, equal volume of $CaCl_2$ (0.33 M) and Na_2CO_3 (0.33 M) were rapidly mixed together by pouring one solution into another (Volodkin et al., 2004a). Then the mixture was intensively agitated on a magnetic stirrer. The duration of the agitation decides the size of the particle.

To achieve a size around 5 μm, a stirring time of 20 sec was applied. A shorter stirring time would be necessary if a smaller size is needed. 2 μm particles were synthesized with 5 seconds of stirring. Immediately after the stirring, the particles were separated from the supersaturated solution by centrifugation (Eppendorf centrifuge 5417C) and three rounds of washing. To avoid the phase transition, the ACC particles were immediately coated with the first layer of the polyelectrolyte or be dried for the further use. As the centrifugation would be frequently required throughout the process, the particles were transferred into a 2 ml Eppendorf tube right after the stirring and from now on all the operations were conducted with the Eppendorf tube.

4.2.2 The procedure of layer-by-layer process

In our experiment, microcapsules were labelled with fluorescent dextran to give emission under the confocal and fluorescence microscope. FITC-dextran is the most widely used fluorescent label for microcapsules. According to the purpose of the experiment, the dextran could either be incorporated inside the capsule cavity or inside the capsule wall (De Geest 2006). In this experiment, PAH-FITC was used as the outermost layer of the capsules to fluorescently label the capsule. FITC is a derivative of fluorescein widely used in the study of microcapsules (Kohler et al., 2007). FITC labelled microcapsules have a green colour under excitation, which allow the capsules to be more easily identified under the microscope.

The procedure for layer-by-layer deposition followed the protocol suggested by Volodkin (Volodkin et al., 2004a). The particles were first immersed into 2mg/ml oppositely charged polyelectrolyte. It could be either polycation or polyanion for $CaCO_3$ particles as $CaCO_3$ particles are positively charged as well as negatively charged due to the existence of both Ca^+ and CO_3^-. In our experiment, PSS solution was used to deposit the first layer. After the adding of particles, the suspension was shaken on a Vortex (Vortex-genie 2) for at

least 15 min to allow the surface of the particles be fully covered with the polyelectrolytes. After the adsorption, the particles were centrifuged by Eppendorf Rotor and washed with Milli-Q water for three times to get rid of the excess polyelectrolytes. The speed and the duration of the centrifugation depended on the size and the weight of the particles. Usually, a speed of 3000 rpm and a duration of 30 sec was enough for particles to be separated from the solution. After carefully removed the previous solution with a pipette, the particles were ready to be coated with another layer of polyelectrolyte with the opposite charge by using exactly the same process. The particles were coated repeatedly for 6 layers (PSS/PAH/PSS/PAH/PSS/PAH-FITC). During the layer-by-layer process, the particles aggregation might occur from time to time. To prevent the further effect of the aggregations, ultrasonic bath (Elmasonic S 15H) was used before each shaking step. A few seconds of sonication would be enough for the separation of the aggregation, while a longer time of sonication might damage the multilayer structure.

After the deposition of the layer-by-layer structure, the original core for the particles need to be dissolved to finally get the multilayers capsules. The $CaCO_3$ core could be dissolved by adding EDTA. For dissolving $CaCO_3$ core, 1 ml of 0.2 M EDTA was added into the $CaCO_3$ suspension and the mixture was shaken manually. Soon air bubbles start to form. To prevent the accumulation of pressure inside the tube, the Eppendorf tube was left open to release the carbon dioxide. After most of the cores were dissolved and there was no large air bubble forming in the suspension, the particles were put onto the vortex for further shaking to get rid of the calcium carbonate residues inside the capsules. Usually three rounds of ETDA and washing were used to make sure the $CaCO_3$ is fully dissolved. The yielding polyelectrolytes microcapsules were dispersed in PBS and stored in fridge for further usage.

4.3 Cell culturing

The internalisation of microcapsules has been studied with a variety of cells lines, such as MDA-MB-435S, human breast carcinoma cell line (Javier et al., 2006), MCF-10A, human breast adenocarcinoma cell line (Javier et al., 2006), HEK 293T, human embryonic kidney cell line, VERO-1, African green monkey kidney cell line (De Geest et al., 2006) and A549, adenocarcinomic alveolar basal epithelial cells (Foster et al., 2001) .

In this project, A549 was chosen for study the internalisation of the microcapsules as it had already been used in several studies on cell entry (Huang et al., 2002, Chang et al., 2011), especially for those studies that employed SICM as characterization method (Yang et al., 2012). A549 cell line (passage 80) was purchased from European Collection of Cell Cultures, and cultured in Dulbecco's Modified Eagle Medium (DMEM,), supplemented with 10 % fetal bovine serum (FBS), 1 % penicillin in incubator at 37 °C in 95% air / 5 % CO_2. For the study of internalisation, A549 cells from passages 82 to 90 were used.

4.3.1 Trypsinisation

The A549 cells were cultured in T25 cell culture flasks. After they reached 80 % confluence, trypsin (0.25 % trypsin-EDTA) was used for cells passage. After empty the cell medium, the cells were washed using PBS buffer (2 ml). Then, 2 ml of trypsin was added in the flask, and the flask was gently shaken. Cells morphology was checked using an optical microscopy. After the cells became rounded and detached from the flask, 2 ml of culture medium was added to deactivate the trypsinisation. The cell suspension was centrifuged for 5 minutes at 1800 rpm. The liquid phase was discarded after the centrifugation and the cells were resuspended with 5 ml of cell medium. Then 1 ml of cell suspension was added to a new flask at a concentration around 5000 cells/ cm^2. The rest of the cell suspension was used for seeding cells in

petri dish. The cells were discarded after 10 passages.

4.3.2 Cryopreservation and reawakening

To ensure reproducible results and continuity in research, the stability of the cell line was preserved by cryopreservation. For cryopreservation, a population of cells could be stabilized by subjecting them to cryogenic temperatures that stops cell from aging. The cooling rate is the most crucial parameter in the cryopreservation. Mazur (Mazur et al., 1972) suggested a cooling rate of 1 °C per minute with cryoprotective additive that protect the cells during the freezing. The cryoprotective agents used in this study was dimethyl sulfoxide (DMSO). To provide the suggested cooling rate, the cryovials was transferred into a styrofoam-insulated Mr. Frosty container that had been frozen at 20 °C and placed in a low temperature freezer at -80 °C for 24 hours, then transfer into liquid nitrogen.

To reawaken the cells, a vial of frozen cells was taken from liquid nitrogen and placed into 37 ˚C water bath. It was then centrifuged for 5 minutes at 1800rpm to get rid of the DMSO and re-suspended with 5 ml of cell culture medium. Then the cell suspension was replaced into a T25 cell culture flask and incubated at 37 ˚C and 5 % CO_2.

4.4 Instruments

4.4.1 Laser-based micropipette puller

The pipettes used in this study were all fabricated from borosilicate capillary glass (Sutter Instrument Company) using a P-2000 micropipette Puller (Sutter Instrument Company) (Figure 4.1). The P-2000 is a microprocessor controlled, CO_2 laser-based micropipette puller. The design of P-2000 allows the fabrication of micropipette for intracellular recording, patch clamping, microinjection and microperfusion. The main advantage of using CO_2 laser

as a heating source is the ability to work with quartz glass. Glass capillary of different diameter could be processed with P-2000, ranging from 0.125 to 1.2 mm. The taper geometry of the micropipette is controlled by pre-entered program with command lines that set five parameters, including: HEAT (output power of the laser), FILAMENT (scan pattern of the laser beam), VELOCITY (velocity at which the puller bar must be moving before the hard pull), DELAY (the timing of the start of the hard pull relative to the deactivation of the laser) and PULL (the force of the hard pull).

Figure 4.1 P-2000 micropipette Puller (Sutter Instrument Company)

In this study, pipettes were pulled from borosilicate capillary glasses BF 100-50-75 (Sutter Instrument Company). These capillary glasses had an outside diameter of 1.00mm, an inside diameter of 0.50 mm and an overall length of 7.5 cm. Pipettes with tip diameter of 100 nm were pulled with pre-set program 40 (Line 1: HEAT=310, FILAMENT=3, VELOCITY=30, DELAY=160, PULL=0; Line 2: HEAT: 330, FILAMENT: 3, VELOCITY: 25, DELAY: 160, PULL=200). Pipettes with diameter of 200 nm were pulled with pre-set program 41 (Line 1: HEAT=310, FILAMENT=3, VELOCITY=30, DELAY=160, PULL=0; Line 2: HEAT: 310, FILAMENT: 3, VELOCITY: 25, DELAY: 160, PULL=150).

4.4.2 Scanning ion conductance microscopy

SICM is a noncontact scanning probe microscopy technique, based on electrolyte-filled glass nanopipette. SICM has been applied to study the dynamics of live membrane activities at nanoscale (Clarke et al., 2016, Takahashi et al., 2011, Novak et al., 2009) as well as their interaction with nanoparticles (Novak et al., 2014, Shevchuk et al., 2012, Ruenraroengsak et al., 2012). In this study, SICM was used to study the live internalisation process of polyelectrolyte microcapsules. The principle and application of SICM has been introduced before in Chapter 2.

Scanning ion conductance microscopy used in our study uses a custom-built scanning head controlled by a SICM scanner controller (Ionscope Ltd., UK). The scanning head consisted of a P-733.2DD XY Piezo-Nanopositioning Stage (Physik Instrumente, Germany) 30 μm travel (XY movement of the sample) and P-753.21 piezo actuator (Physik Instrumente, Germany) 25 μm travel (Z movement of pipette). All piezos were driven by 200 W peak power high voltage PZT amplifiers E-505 (Physik Instrumente, Germany). The XY piezo scanner incorporated into heavy stainless steel platform was placed onto an Eclipse TE300 Inverted Microscope (Nikon Corporation, Japan).

The pipette current was detected via an Axopatch 200B (Molecular Devices, USA) using a gain of 1 mV/pA and a low-pass filter setting of 2kHz. The internal holding voltage source of the Axopatch-200B was used to supply a DC voltage of +200 mV to the pipette. The locating of the microcapsules and the positioning of the pipette were facilitated by using optical microscopy with oil-immersion objective 100x 1.3 NA (Nikon Corp, Japan).

4.4.3 Confocal laser scanning microscopy

Confocal laser scanning microscopy (CLSM) is a non-destructive imaging technique used for visualisation and three-dimensional reconstruction of

biological samples. It is an integration system that consists of numbers of optical and electronic devices, including optical microscope, computer, laser systems with selective wavelengths. The samples for CLSM are usually fluorescently labelled to make selected subject distinguished from the rest of the sample. CLSM was first introduced by Marvin Minsky in 1957. Since that, the application of CLSM grew rapidly in the field of biological study.

The advantage of CLSM over traditional fluorescence microscopy is that CLSM can capture multiple two-dimensional confocal section at different depths (Nwaneshiudu et al., 2012). This is realized by placing a spatial pinhole in front of the detector to block the out-of-focus signals (Figure 4.2). As only one point in the sample is illuminated at a time, the laser beam scans in a raster pattern to give two-dimensional images. The scanning is controlled by using one or more oscillating mirrors. Signals at each scanning point are collected by a photodetector and translated into pixels. The final image is a point by point reconstruction of the pixels.

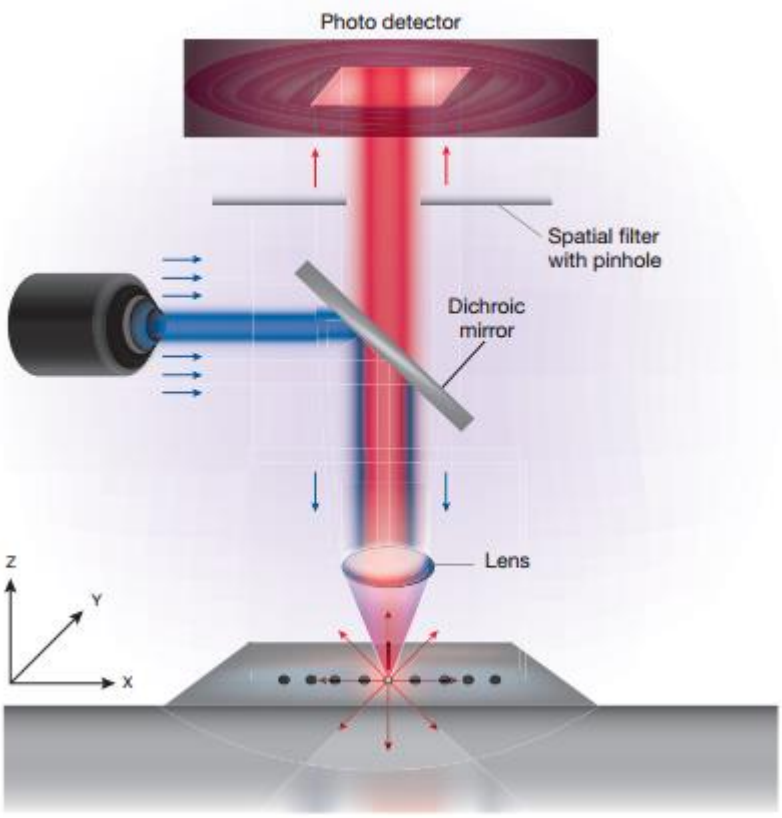

Figure 4.2 Schematic of a CLSM setup (Nwaneshiudu et al., 2012)

CLSM used in this study was a Leica TCS SP2 Spectral confocal & multiphoton system equipped with a 63x oil immersion objective lens. Ar-ion (488 nm) and He-Ne (543 nm) lasers were used as excitation sources. Microcapsules would emit green fluorescence as FITC was excited by 488 nm laser and the cell membrane would emit red fluorescence as the CellMask^{TM} plasma membrane stain was excited by 543 nm laser. To create a 3D reconstruction, the depth of confocal sections was selected at 0.5 μm. The start and the end depths were entered by adjusting the z-position. The software calculated the number of sections by dividing the total depth by the selected depth of each confocal section. Then the CLSM would automatically scan all the sections. 3D reconstruction could be created by stacking all the images from different sections using Leica Application Suite.

As for the live cell imaging, cells were cultured on a glass coverslip disc coated with collagen. Collagen was coated by spreading the surface of coverslip with diluted collagen solution (1:10 with 30 % ethanol) followed by air drying. Before imaging, the coverslip was carefully mounted on to the sample holder. The edge of coverslip was rubbed with a layer of Vaseline to seal the gap between the coverslip and the sample holder so that the culture medium would not leak through the gap. A thin layer of warmed L-15 culture medium was used to cover the surface of the coverslip to keep the cells alive. The sample holder maintained its temperature at 37 ˚C by connecting to a temperature control device. The operation software was set to capture an image every minute to record the live process.

5. Establishing the procedure for live imaging of the internalisation of microcapsules

Previously, SICM has been used to study the endocytic pathways of the cells (Shevchuk et al., 2012, Shevchuk et al., 2008b, Shevchuk et al., 2008a) and the internalisation process of 200 nm nanoparticles (Novak et al., 2014). In these studies, internalisation behaviours that resemble clathrin-mediated endocytosis were recorded with time lapse images. While there are certain similarities between imaging the internalisation of the nanoparticles and that of microcapsules, the increase in the size of the particles, from 200 nm to around 5 μm in diameter, not only changes the way cells internalise the particles, but also poses challenges for the scanning and imaging of the SICM. Here in this chapter, we explore the capability of SICM to record the internalisation of the microcapsules and introduce the procedure developed to cope with the problems encountered during recording of the whole internalisation process.

5.1 Selecting suitable cell culture for the SICM live cell imaging

5.1.1 Cell line

A variety of different cell lines were reported to have the ability of uptaking microcapsules (Reibetanz et al., 2010, Reibetanz et al., 2007, Palankar et al., 2013, Dierendonck et al., 2012, De Koker et al., 2007). Here we explored two of these cell lines, A549 and 3T3 for studying the internalisation behaviour. Initial proof-of-concept experiments on these two cell lines showed that both of them appeared to be suitable for SICM imaging. These initial experiments revealed that A549 cells appeared to be less motile and displayed less pseudopodia-like structures with sudden increase in height compared to 3T3 cells (Figure 5.1). In general, cells with simpler height profile require lower hopping amplitudes and therefore can be imaged at higher frame rate using the hopping mode of SICM. Lower cell motility

makes long-term tracking of cellular processes easier. All this would suggest A549 as more suitable for the purpose of our study than the 3T3 cell line.

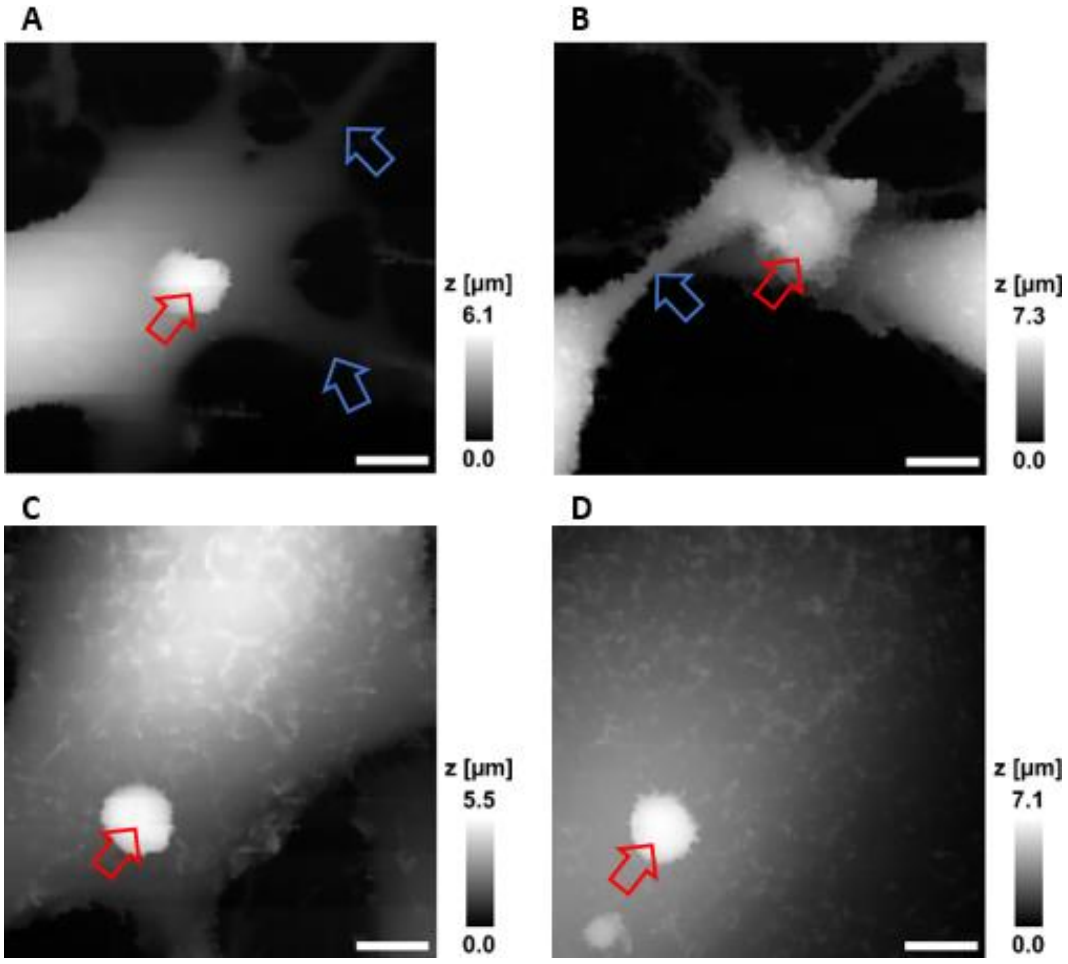

Figure 5.1 Comparison between the topography of the 3T3 cells and A549 cells. (A) Topography image of a 3T3 cell. (B) Topography image of the protrusions of two 3T3 cells. Note the existence of long pseudopodia-like structures (blue arrows) stretching out from the edges of the 3T3 cells. (C, D) Example topography images of two A549 cells. (Capsules are pointed with red arrows, scale bar: 5 µm)

To further investigate suitability of these cell lines for the project a fluorescence-based assay of capsule internalisation was performed. Laser scanning confocal microscopy (Leica SP2) was used to estimate the general time span of the internalisation events in A549 and 3T3 cells. With 3D reconstruction of confocal images, it was possible to distinguish internalised capsules (Figure 5.2 B) from those attached to the membrane surface (Figure 5.2 A). The rate of internalisation could be estimated by counting the

percentage of internalised capsules (Table 2), which was the number of internalised capsules divided by the total number of the capsules (capsule aggregations were excluded).

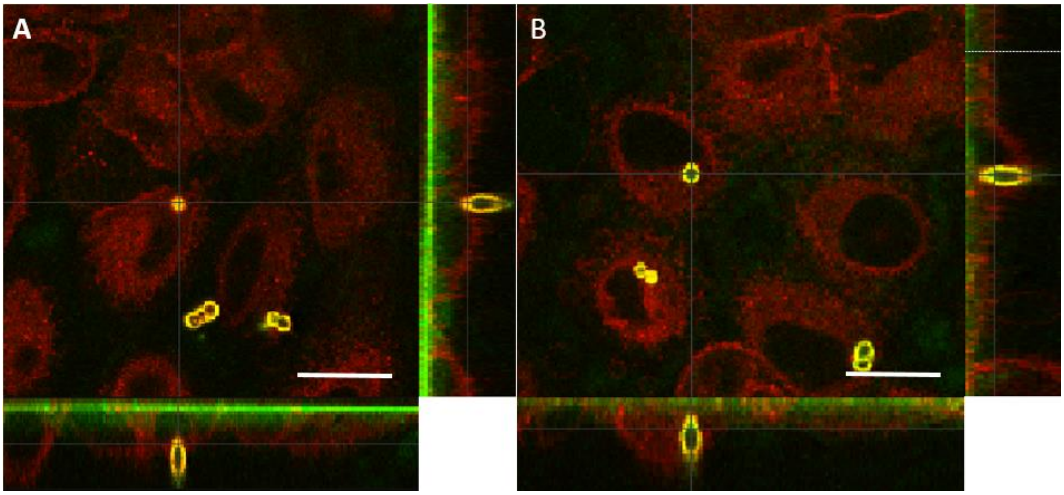

Figure 5.2 3D confocal images of uninternalised (A) and internalized (B) capsules. The side panels of (A) revealed that the capsule was on top of the cell membrane suggesting an uninternalised capsule. The side panels of (B) revealed that the capsule was inside the A549 cells suggesting an internalised capsule. (Scan bar: 25 μm)

Experimental data gathered from three different passages of the same cell line revealed that 55.7 % of capsules got internalised within one hour of incubation (Table 2). The data indicated that the internalisation process happened on minutes scale and complete internalisation was possible to be captured within the timespan of an hour. This meant imaging the process of capsule internalisation events using SICM was possible at least in terms of temporal resolution. The fastest frame rate previously achieved with SICM when imaging endocytosis of 200 nm particles was 4 frames per minute (or 15 seconds per frame of 1.2 μm×1.2 μm) (Novak et al., 2014). Internalisation of microcapsules is expected to require scanning of features approximately 25 times taller than the previously imaged 200 nm nanoparticles and so may result in the scanning rate slowed down to 10 minutes/frame in the worst case scenario, which, however, may still be enough to capture the progress of capsule internalisation lasting for up to an hour. At the same time the fact that the whole process could be captured within an hour means that the imaging

could be done without environmental chamber to keep cells viable during the imaging.

We tested the internalisation rate of A549 and 3T3 at two different incubation times (Table 2). The results suggest that A549 internalised higher proportion of capsules compare to 3T3. As expected, the longer the incubation time the more likely the capsules would get internalised. Based on these initial estimations A549 cell line was selected as the main target for the project.

	Cell Line	Incubation Time (h)	Percentage of internalised capsules (%)	Number of capsules analysed
1	A549	1	55.7	61
2	A549	2	80	10
3	3T3	1	44.4	36
4	3T3	2	60	25

Table 2 Rate of microcapsule internalisation in A549 and 3T3 cell lines determined from confocal images (Figure 5.2). The capsules were formed of 6 layers of polyelectrolytes and had diameters of 4.7 ± 0.8 μm (mean ± standard deviation of the mean)

5.1.2 Confluency

The place where the capsule first attaches to the cell membrane is likely to affect the outcome of internalisation massively, however this aspect has not received enough attention in previously published research into capsule internalisation. Certain regions of the cell are expected to be more likely to internalise capsules than others. From purely mechanistic point of view, internalisation of capsules which landed on parts where there is not enough volume to accommodate the capsule, such as above the nucleus or near the cell boundaries, would require more energy and are less likely to be fully internalised by the cell within one hour, if ever. Because our experimental setup is suitable only for studying over relatively limited period of time (not more than 1-2 hours), capsules that attached to certain regions of the cell

where the internalisation could take place quickly are more preferred objects for study than those capsules that require more time to get internalised.

Conventionally, the internalisation of the capsules or other particles were studied using cell culture that formed a confluent monolayer (Huang et al., 2002, Davoren et al., 2007). As for A549, which is a lung epithelial cell line, it is their natural state forming a uniform monolayer. However, we found the monolayer brought problems to the identification of the boundary of each individual cell as when cells reach their monolayer state, they fused together and formed a flat and uniform surface. This brought great difficulty to looking for those capsules that attached to the desired position of cells for the purpose of getting a higher chance of quick internalisation.

A situation that quite often occurred in the imaging of monolayer with 100% confluency was that the capsule often ended on the boundary of two cells where the internalisation was less likely to happen. As shown here in Figure 5.3, a capsule had attached to the boundary of two cells, one cell occupied the top right side of the image and the other bottom left (Figure 5.3B). However, the actual boundary was difficult to clearly identify. Both cells responded to the attaching of the capsule by forming long and solid protrusions (Figure 5.3A, cyan arrow and blue arrow) towards it, the one on the top right responded first followed by the one on bottom left. It appears that there was a short period of time in which two cells competing over this single capsule, as two protrusions were reaching the capsule from both sides (Figure 5.3A, 17 min, 21 min, 24 min). However, despite the highly active response in the first 30 minutes of the recording, there was no further sign of internalisation hereafter. At 35min, both protrusions receded without leaving any remarkable trace (Figure 5.3C).

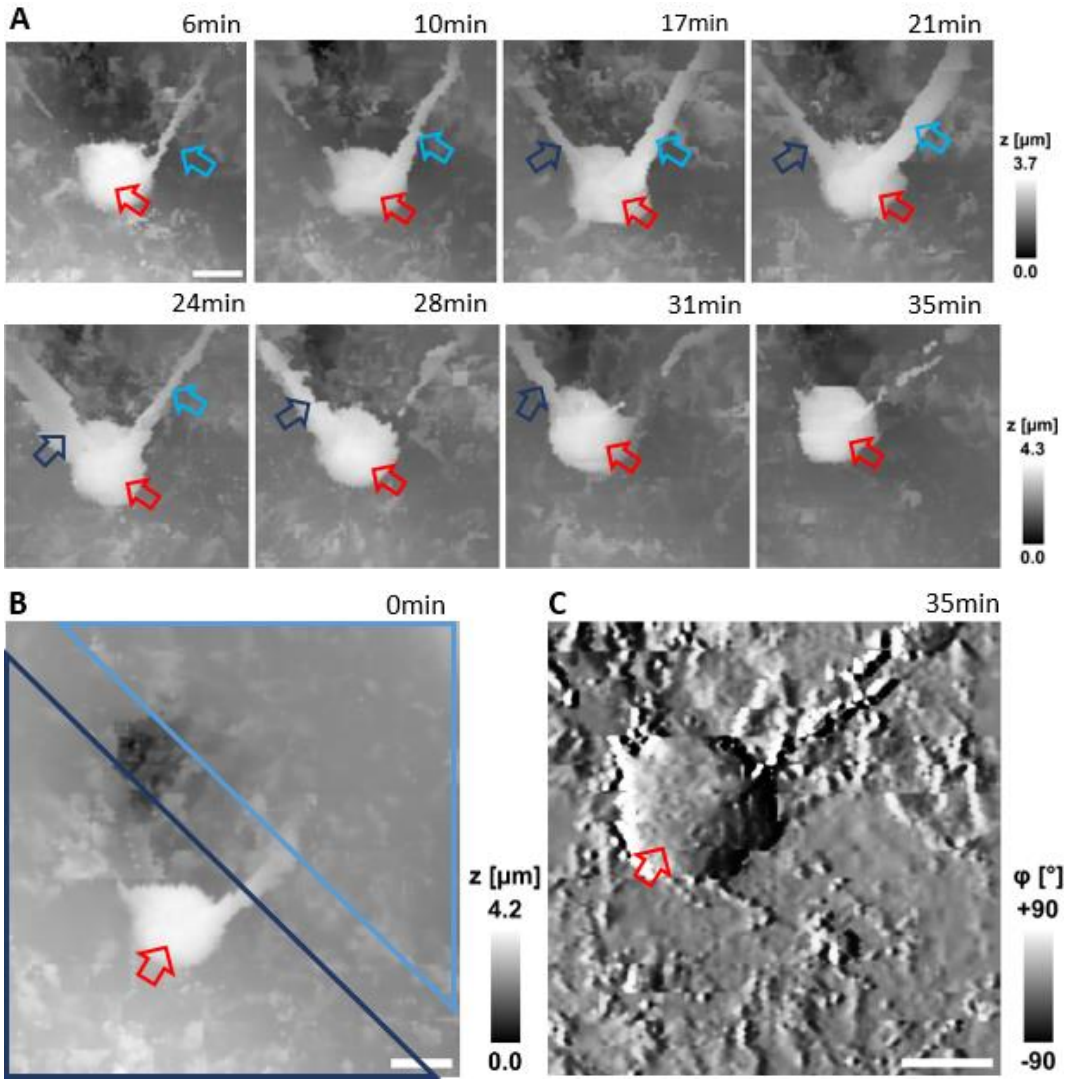

Figure 5.3 Capsule that landed near the boundary of two cells. (A) Time lapse topography images, note two distinct membrane protrusions that stuck out from the cell on the bottom left (blue arrow) and from the cell on the top right (cyan arrow). (Capsules are pointed with red arrows, scan size: 10 µm×10 µm, scale bar: 2 µm) (B) Two cells are highlighted, the bottom left one is highlighted with dark blue rectangular area and the top right one is highlighted with cyan rectangular area. (Scan size: 15 µm×15 µm, scale bar: 2 µm) (C) Slope image at the end of the recording, note the relatively rough surface of the capsule (red arrow), indicating the capsule was partially covered by membrane protrusions. (Scan size: 10 µm×10 µm, scale bar: 2 µm)

This situation of capsule attached to the boundary of the cells was a result of the higher density the capsules have in comparison to the cell culture medium. So, by the pulling of gravity, they sediment in the medium and there is this tendency that those capsules would gathered at those lower places, for instance the bottom of the petri-dish or the boundaries between two cells in

cell cultures with 100% confluency. In the first 10 sets of experiments in which the monolayers were used for the study and the capsules were randomly chosen for imaging, 5 out of 10 capsules we imaged were situated on the boundary of the cells and from these 5 capsules, none of them was internalised in the time span of imaging. The high possibility of capsules attaching to the boundaries and the seeming consequence of no internalisation were not ideal for the imaging of internalisation process. As it is almost impossible to identify the boundaries of the cells in monolayer, to avoid the above-mentioned issues linked to 100 % confluency monolayer, we reduced the confluency to 40-50 % for all of our experiments. Later experiments showed with 40-50 % confluency cell cultures, each individual cell could be clearly identified from the observation of optical microscope (Figure 5.4).

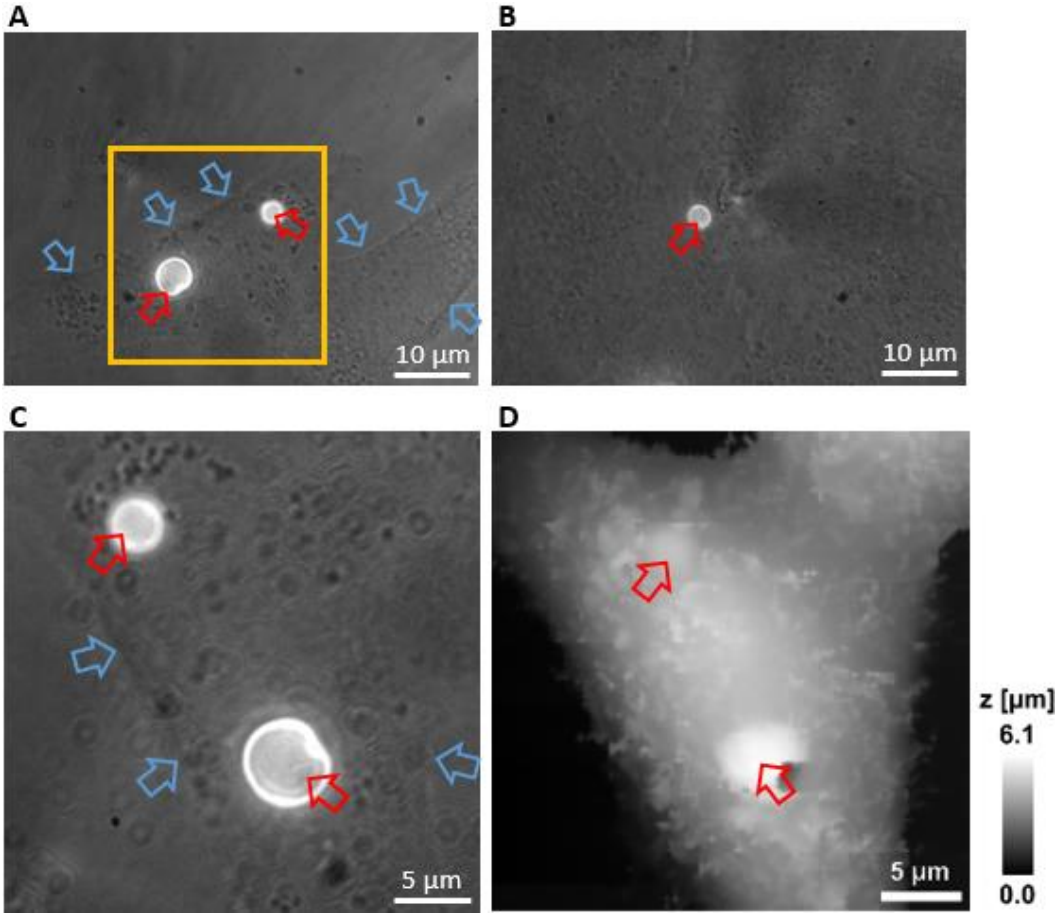

Figure 5.4 Individual cell could be identified from optical microscope when the cells were at low confluency. (A) Optical microscopy image of cells. The boundary of these two cells (blue arrows) could be clearly identified. There were two capsules (red arrows) that attached to one of these two cells, their position could be roughly estimate from the image. (B) Optical microscopy image of cells at their monolayer state. The monolayer was almost invisible under the optical microscope. (C) Detailed view of the area in (A) marked by yellow square. (D) SICM topographical image of the same area shown in (C). Note the capsule (red arrow) on the top left was almost internalised.

5.2 Optimising the SICM setup and imaging procedure for live visualisation of capsule internalisation

5.2.1 Temperature control

The initial experiments were performed on live samples at room temperature. The microcapsules would often successfully attach to the cell membrane, however no visible progress in internalisation would take place over one hour, as illustrated in example recording shown in Figure 5.5. It was further made clear by the slope images (Figure 5.5B), where the capsule surface remained

perfectly smooth suggesting no membrane protrusion had formed around the capsule, which is a behaviour we found later that involved in the process of internalisation. This was further confirmed by other 3 trails (4 in total) that imaged at room temperature and all 4 experiments gave this same result. This finding corresponded with previous knowledge (Kastl et al., 2013, Bischof and He, 2005, Beney and Gervais, 2001). Though the exact temperatures at which each endocytic pathway stops are unclear as far as we understand, it is reported that the fluidity of membrane lipid is temperature dependent (Beney and Gervais, 2001). Lowered temperature causes phase transition of membrane lipids, which in turn effects the functions of certain membrane proteins (Beney and Gervais, 2001, Bischof and He, 2005). As a result, all the endocytic pathways eventually stop at 4 ˚C (Kastl et al., 2013).

The only noticeable change that happened during the observation was the change in the position of the capsule (Figure 5.5C). This suggested that while the internalisation function of the cell was frozen at room temperature, the cell still possesses its motility. Apart from that, the cell morphology appeared normal and the membrane protrusions could be seen spreading all over the cell membrane throughout the entire length of observation.

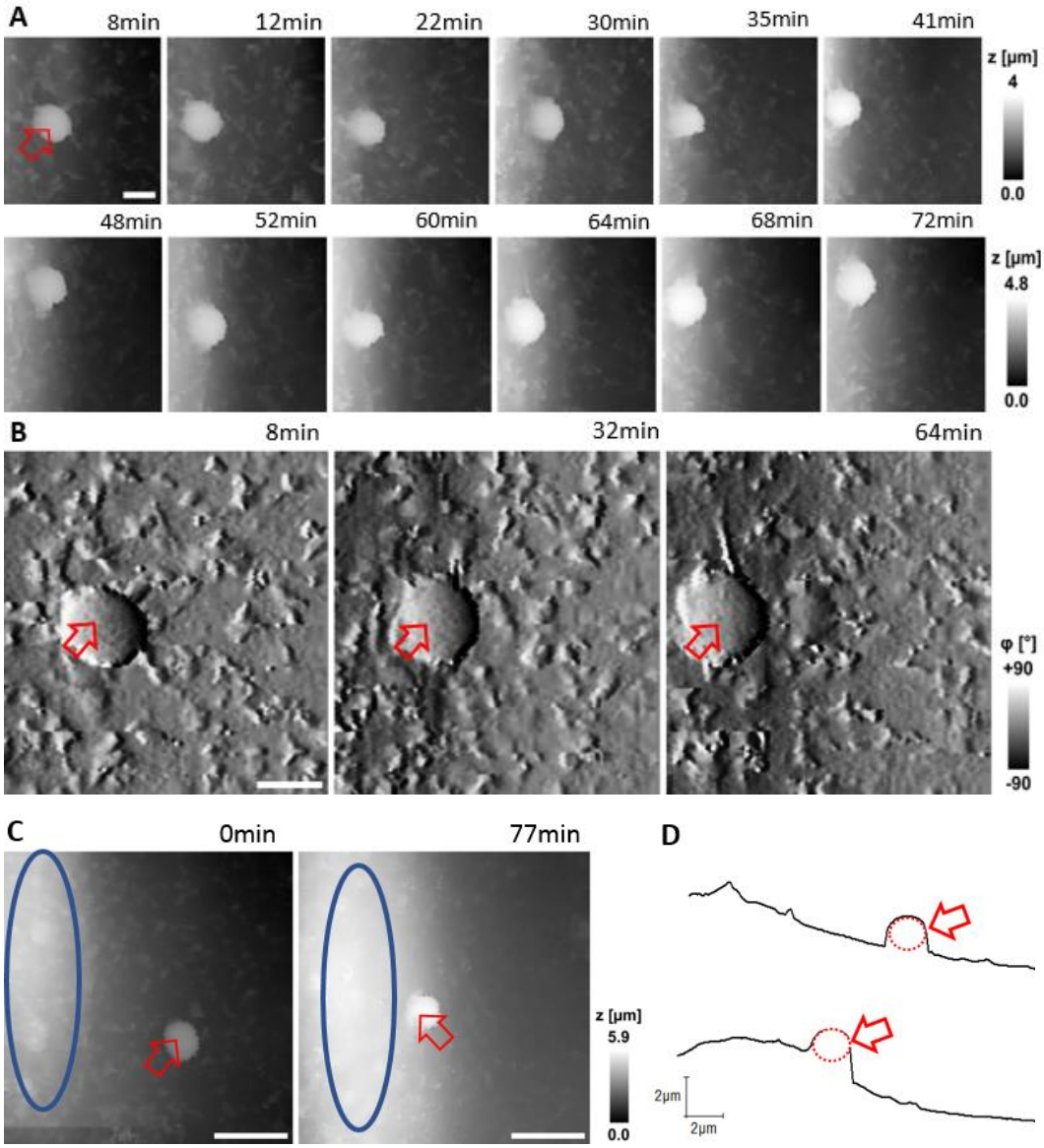

Figure 5.5 Capsule and cell interaction at room temperature. (A) Time lapse topography images of the capsule (red arrows) and cell interaction, no remarkable membrane behaviour could be seen from the images (Scan size: 10 µm×10 µm, scale bar: 2 µm). (B) Slope images at beginning (8 min), middle (32 min) and end (64 min) of the recording, note that the surface of the capsule (red arrows) stayed smooth throughout the entire length of the recording. (scan size: 10 µm×10 µm, scale bar: 2 µm) (C) The relative position of the capsule (red arrows) in comparison to the cell nuclei (blue circle), note the change in position of the capsule. (Scan size: 30 µm×30 µm, scale bar: 5 µm) (D) The profile of the cross section showed the change in the position of the capsule (red dotted circle pointed with red arrows).

After confirming the inhibition effect of low temperature on internalisation, a heating device was installed onto the setup. We chose temperature controller (CL-100) and objective lens heating mantle (ALA Scientific Instruments) for our purpose. This heating method was previously proved

effective to controlling temperature for SICM (Shevchuk et al., 2012, Novak et al., 2014). Objective lens heating mantle have few advantages over circulation bath by preventing the flow caused by circulation. Debris flowing in the cell medium might attach to the pipette tip and cause pipette blockage. The flow might also carry away the capsules before they attached to the cell membrane. Objective lens heating mantle prevents these problems by only heating a small area directly beneath sample. By doing this, it also reduces the evaporation of the cell culture medium and maintains the concentration of the medium.

After the installation of the objective lens heating mantle, all experiments were carried out with the heating device at 37 ˚C. Apart from the results showed in Figure 5.5, all successful and unsuccessful internalisation events that were recorded and showed in this thesis were imaged at 37 ˚C with the help of the heating device.

5.2.2 Establishing the ability of hopping mode SICM to image microcapsules

Compared to the relatively flat surface profile of epithelial cells displaying just small membrane protrusions of few hundred nanometres tall, a spherical microcapsule with diameter of 5 micrometres attached to the cell membrane is considered as a relatively tall, overhanging structure. It has been widely known that structures with steep slopes or overhanging structures are challenging for scanning probe microscopy (Novak et al., 2009). In conventional scanning mode, the distance between the tip of the probe and the sample is kept constant by maintaining the set point (also known as constant-distance mode). However, because this feedback control system could not predict the height information in advance, the tip might collide into overhanging structures high above the surface and cause sample or probe damage. The hopping mode of SICM was proved effective in avoiding collisions in samples with convoluted topography while keeping nanoscale

resolution and authenticity of the soft and sophisticated sample (Novak et al., 2009). Here we explore the possibility of scanning this convoluted structure with hopping mode SICM.

5.2.3 Topographical imaging of capsules adhered on a petri dish

Capsules used in our experiment are hollow spheres of approximately 5 μm in diameter. Let us consider a single capsule with 5 μm in diameter (Figure 5.6A). From the viewpoint of the horizontally moving scanning nanopipette, the capsule represents an overhanging structure with the bottom half (2.5 μm in height) of the capsule effectively not accessible to the nanopipette. The hopping mode deals with the problem of overhanging structures by setting the hopping amplitude higher than the height of the structure (in this case higher than 2.5 μm) which worked well for most of biological structures imaged previously (Takahashi et al., 2012, Miragoli et al., 2011, Novak et al., 2014, Velez-Ortega et al., 2014). However, in case of large capsules attached additional aspect of SICM imaging needs to be considered. The nanopipette tip has typically the shape of a truncated cone with angle of 6˚ (or 3˚ for half angle) (Rheinlaender and Schaffer, 2009). This means when the side wall of the nanopipette may get in contact with the side of capsule while the nanopipette tip is still approximately 0.13 μm (estimated as $\tan(3°) \times 2.5$ μm) away from the edge of capsule (Figure 5.6A). In this case, the side wall of the pipette may start to exert force on the side of the capsule before the nanopipette tip had a chance to detect the presence of capsule wall and may push the capsule out of its original position if it is not firmly attached to the substrate. In the initial attempts to image freshly prepared microcapsules, significant number of capsules were displaced while the nanopipette was in process of imaging the edge of capsule.

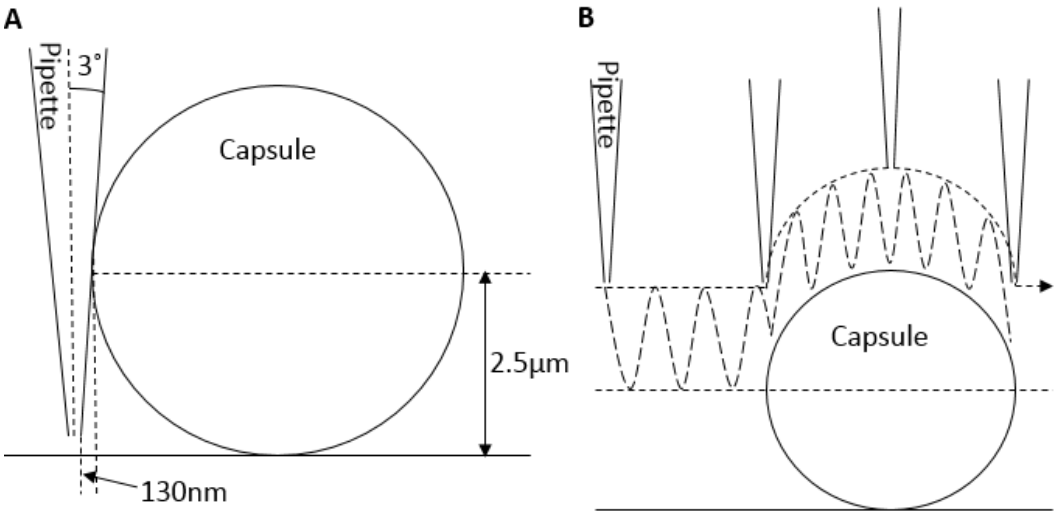

Figure 5.6 (A) the schematic of the situation when the pipette starts to make contacts with the capsule. (B) the schematic of the scanning method in which the pipette is prevented to fall below a certain pre-set height (approximately 2 µm) to scan only the upper surface of the capsule.

A possible way to address the problem with scanning of freshly prepared capsules that are loosely attached on the bottom of the glass petri dish is to prevent the pipette tip from reaching the substrate and let it hop at a distance 2-3 µm away from the substrate (Figure 5.6B). This can be done simply by limiting the vertical range of the z-axis piezo or by withdrawing the z-axis motor, on which the z-axis piezo is mounted on so that the surface cannot be reached even if the z-axis piezo is fully extended. This way only the upper surface of the capsule is scanned and contact between the side of the capsule and the side wall of the pipette is eliminated. However, the topographical information of anything that is out of the reach of the pipette tip would be missing from the image. Thus, this method is only applicable when the substrate is of no interest of the imaging. This could be used for locating the position of the capsule and for imaging the topography of the capsule. Figure 5.7A&C shows typical images of a capsule imaged by this method.

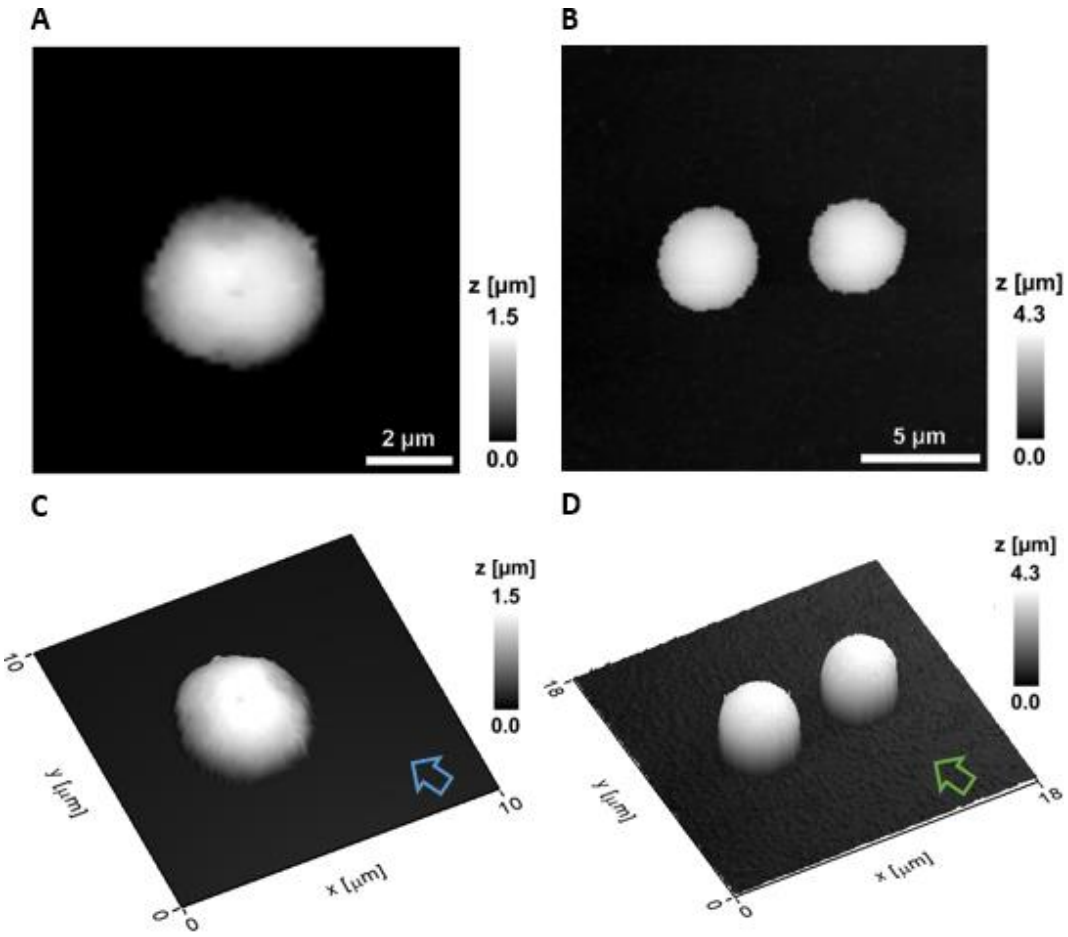

Figure 5.7 SICM images of capsules on the substrate of petri dishes. (A, C) Typical topography image (A) and its 3D reconstruction (C) of capsule imaged with pipette hopping 3µm away from the substrate. (B, D) Typical topography image (B) and it 3D reconstruction (D) of capsules on petri dish treated with PEI imaged with normal hopping. Note the difference in the heights of the images, which is 1.5 µm in A, C and 4.3 µm in B, D. Also note the backgrounds of the images, which is entirely smooth in A, C (cyan arrow) and relatively rough in B, D (green arrow).

Another possible way to address the above problem is to increase the bond between the capsule and the substrate. To increase this bond, the surface of the petri dish was treated with PEI to give it a positive charge. The capsules were coated with PSS as the outermost layers to ensure a negative charge. The capsules were dipped onto the bottom of the petri dish and left for days to allow the negatively charged capsules to settle on the positively charged substrate and form electrostatic interactions. These stronger interactions made possible the successful scanning of capsules together with the substrate. However, even with this type of sample preparation the lowest possible set point has be used to minimise the chances of pushing the capsule away.

Figure 5.7B&D shows typical images of a capsule imaged by this method.

5.2.4 Imaging capsules on the surface of cell membranes

Without the attractive force between the capsules and cell membranes, the capsules that land onto the cell would most likely roll from top of the cell onto the bottom of the petri dish. Fortunately, as the cell membranes are mostly negatively charged and the capsules (with PAH as outermost layers) are positively charged, they appear to form a relatively strong binding that is capable of stopping the capsules from rolling downhill. This binding also appeared to be strong enough to hold the capsule in its place during SICM imaging in most of experiments with only few exceptions in which the capsule rolled. All these happened from the early stage of the imaging. In most of these cases the capsules were still around but only slightly dislocated. Only in 2 (of over 50) cases, we observed the entire rolling away of capsule (Figure 5.8). Figure 5.8 illustrates imaging artefacts caused by loosely attached capsule rolling down the membrane from 1 of those 2 cases. As the nanopipette moves from the bottom left corner of the image to top right corner during the scan in a bidirectional pattern, the loosely attached capsules are pushed from both left and right alternately. In the case illustrated in Figure 5.8, the capsule rolled from its original position on top of the cell (bright red circle) towards the location near the edge of the cell (dark red circle) where it detached entirely from the cell membrane. Rolling of capsules was typically observed during the early stage when the capsule had just attached to the cell membrane. Therefore, to minimise the risk of rolling issue, we introduced a 5 minutes wait before the start of imaging.

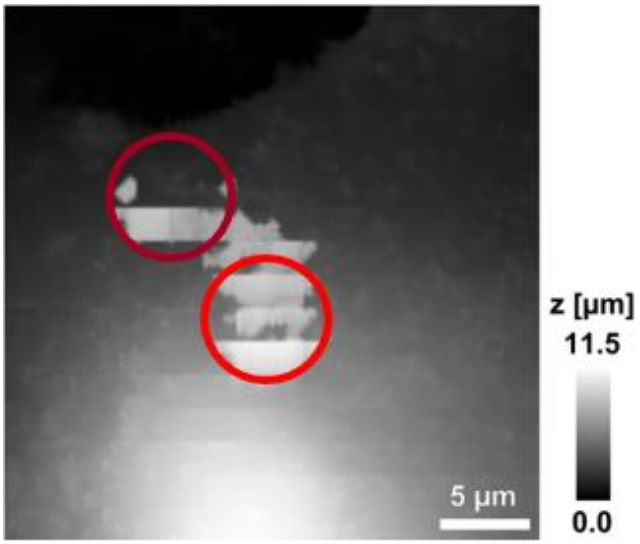

Figure 5.8 Capsule rolling during the imaging due to the failure in its attachment to the cell. The capsule rolled from top of the cell (bright red circle) to the bottom of the cell (dark red circle) where it was last seen, before disappearing entirely. (Scan size: 30 µm×30 µm)

5.3 Imaging artefacts due to nanopipette tip blockage

Generally speaking, the A549 cells used in our experiments had relatively flat height profile with membrane populated with small membrane protrusions. When imaging the cell membrane alone, it is unlikely that the pipette would collide into the cell membrane if the SICM setup is operated properly and a low setpoint is used. However, in the case of internalisation, cell membrane become more active and tall membrane protrusions forms in respond of the attachment of the capsule. In this case, it is more likely for the pipette to crush into this mobile and sophisticated tall membrane protrusions. When the pipette accidentally crushes into these membrane protrusions. The remnant of the disrupted cell membrane attaches to the tip of the pipette and causes the increase in the electric resistance and the instability in current. This is the situation we call the blockage of the pipette tip. This is a fault that happened frequently during the imaging. Fortunately, this is generally less crucial and the scanning and recording could continue most of the times.

When the current was unstable, the sudden increase of the current resulted in the error in the recorded height of that image point. As it happened, it creates

noises which appeared as white dots (Figure 5.9A, C, cyan arrow) in the images. When the instability was relatively low, the scanning was still under control (Figure 5.9A) and the resulting white dots could be removed by post imaging processing. There is a built-in noise reduction function in our image software, SICMImageViewer, that could eliminate those single image points with sudden increase in height and replace them with the height information of the mean height of the surrounding area. After applying the noise reduction function, all sudden increases in heights were filtered and the result was a decent topography image with no sign of unstable current (Figure 5.9B). However, when the instability was too severe, large continuous areas of noises appeared in the images (Figure 5.9C). As there is too much information missing from the image, those continuous white areas were impossible to remove (Figure 5.9D, yellow arrow). Force removal of continuous noise left an area that is without detail (Figure 5.9D, green arrow). This severe blockage of pipette happened when cell's response to the capsule is too dramatic and form membrane protrusions too tall for the pipette to avoid. The pipette crushed into those irregular structures of membrane and severely blocked. In the case of severe block, the pipette would no longer work properly and may even disrupt the whole imaging by damaging the cell.

The blockage of the pipette after crushing into the membrane could be carefully avoided by choosing a slower pipette falling rate, a higher pipette hopping height and by using a smaller setpoint so the pipette is more sensitive to the drop in the current. However, a slower falling rate and a higher hopping height also mean a slower scanning speed. So, in practice this way of preventing pipette blockage was rarely used in time lapse imaging. As for the setpoint, a lower setpoint of 0.3 % is generally used. In those cases when the severe blockages did happen, the imaging need to be paused immediately. Emergency operation to clear the blockage is to retract the pipette to a safe distance from the cell surface (25 μm) and then apply a high voltage to drive away the charged debris that block the pipette tip. If this emergency operation

is not effective to clear the blockage, the pipette need to be withdrawn and quickly replaced before continuing the imaging.

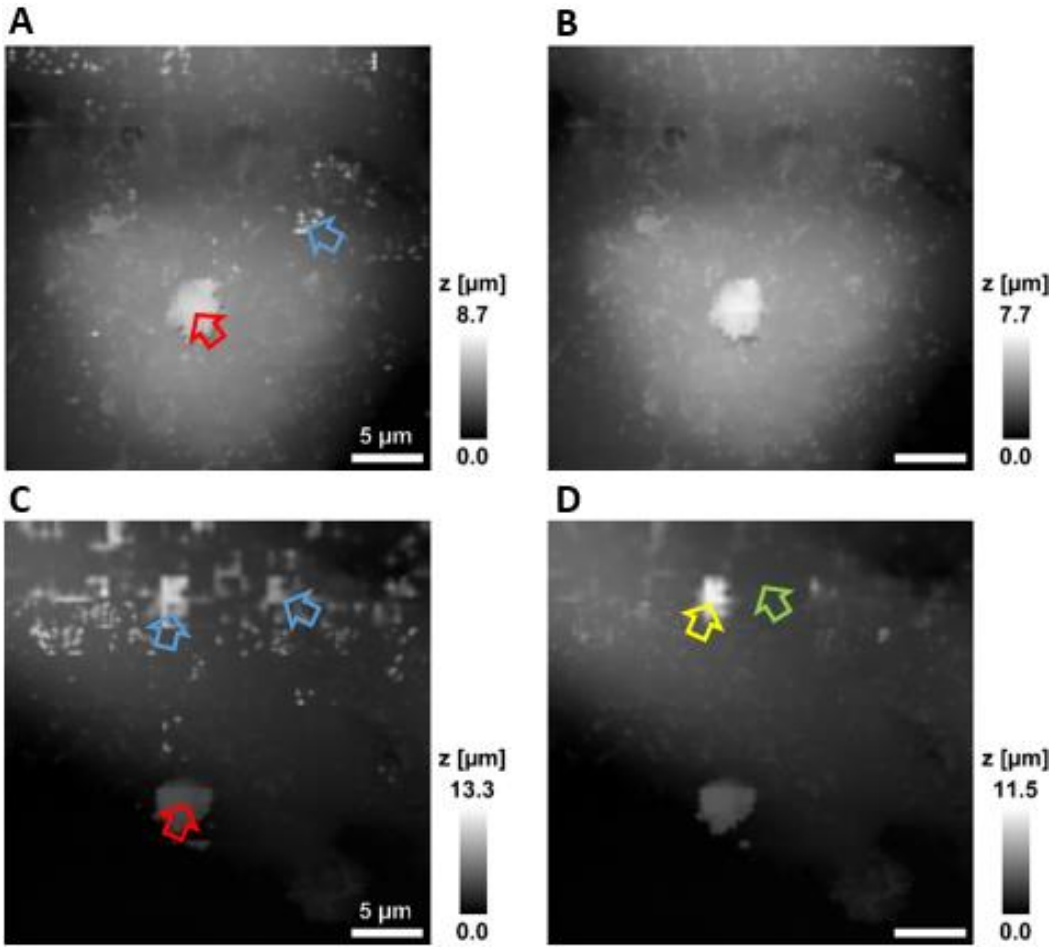

Figure 5.9 The SICM images with noise before (A, C) and after (B, D) applying Noise Reduction in SICMImageViewer. Note the existence of white dots (A, C, blue arrows), a batch of white (D, yellow arrow) and an area of missing detail (D, green arrow). (Capsules are pointed with red arrows, scan size: 30µm×30µm)

5.4 Elastic modulus mapping

With the SICM, it is possible to conduct elastic modulus measurement of the sample (Rheinlaender et al., 2015, Schaffer, 2013, Rheinlaender and Schaffer, 2013, Clarke et al., 2016). Knowing the change in the elastic modulus could provide valuable insights into the understanding of the internalisation process. However, previously the elastic modulus measurements had only been conducted on relatively stationary objects (Rheinlaender and Schaffer, 2013,

Clarke et al., 2016) and the effect of external force on a live process like internalisation was still unknown. Apart from the problem of external force, high structure of the capsules again poses a great problem to the scanning of the pipette. In this section, we will demonstrate the ability of SICM to measure the elastic modulus change in the membrane during internalisation.

Previously, two elastic modulus mapping methods were developed and reported, the Rheinlaender and Schaffer method that uses the pressure-induced microfluidic flow to produce the force (Rheinlaender and Schaffer, 2013) and the Clarke et al method that uses the intrinsic pressure between the tip and the sample (Clarke et al., 2016). We tested both methods on the study of internalisation and found the Clarke method more suitable for our study. We found the Clarke method to be much easier to operate and could record images with higher resolution. Later we decided to use Clarke method as our way to measure the elastic modulus and all the elastic modulus data presented in this thesis were collected using the Clarke method.

With Clarke method elastic modulus measurement, the morphology of the cell membrane could be captured with high fidelity (Figure 5.10A). However, when imaging the internalisation, the increase in setpoint might bring unwanted side effect and even disruption to the internalisation of the capsule. As a result, significant artefacts (Figure 5.10B, C) appeared in the images as the pipette hopped closer to the sample. These artefacts revealed clear signs that the capsules, or more likely the membrane underneath them, were deformed by the pushing of the pipette during the elastic modulus measurement. In the first 8 attempts we tried with elastic modulus measurement, 4 out of 8 attempts showed considerable imaging artefacts as illustrated in Figure 5.10B&C. The artefacts looked similar to that of the rolled capsule showed in the previous section (Chapter 5.2) caused by the general scanning of the SICM. The difference was, in the case of topography imaging, capsule rolled away only occasionally when attachment between

the capsule and the cell was poor. However, in the case of elastic modulus mapping, the capsule moved even when the attachment was firm. Even with the rest 4 case where the capsules were appeared to be relatively intact from the images, certain degree of imaging artefacts could still be seen (Figure 5.10C). These artefacts differed from the previous one in their appearances. The grey strip (Figure 5.10C, yellow arrow) indicated a lower profile compared to its surrounding which was likely to be the deformation of the cell membrane underneath the capsule caused by the pushing of the pipette. In these 4 cases, only one case had the capsule finally internalised.

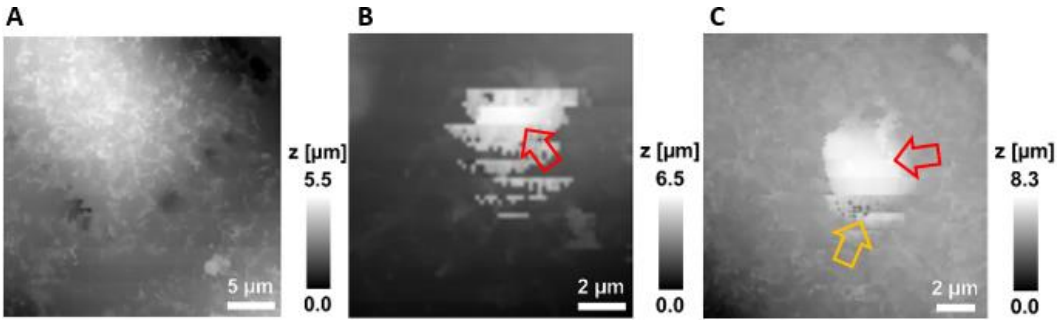

Figure 5.10 Topography images captured with the elastic modulus measurement on. (A) The topography of the cell membrane showed no significant artefacts. (B) The capsule (red arrow) was severely moved by the pipette. (C) The cell membrane beneath the capsule was slightly deformed (yellow arrow) by the pushing of the pipette, the overall appearance of the capsule (red arrow) was relatively intact.

In order not to interrupt the internalisation too much with the elastic modulus measurement, the frame rate of the elastic modulus measurement was considerately reduced. While the elastic modulus could be measured at the same time as the regular topography imaging at a frame rate around 4 min/frame, a lower frame rate of around 10 min/frame was used to minimize the interference of the mechanical force in internalisation. This compensatory practice was regularly followed in the later experiments, in hope of the cell would have time to recover from the interruption and continue its internalisation process. Another practice we frequently used to reduce the effects of the elastic modulus measurement was to not capture the first frame of the image sequence with elastic modulus measurement. As we observed that the capsules were more likely to be severely pushed away by the pipette

when it had just landed on the cell and the bond between them was weak. We also kept the setpoint low at 0.3 % for topography and 1.3 % for the second setpoint.

The results shown that though the pipette constantly exerted force to deform the sample during the elastic modulus measurement, and occasionally collided with the capsule causing imaging artefacts, the interruption was still considered tolerable as the internalisation process could still progress without apparent disruption. In the extreme case showed in Figure 5.11, the capsule was entirely blurred throughout the whole span of imaging. However, after 54 min the cell still managed to internalise the capsule regardless of the constant agitation of the pipette (Figure 5.11A, 54 min). Note that these severe artefacts appeared in the images were not permanent and irreversible. Once the scanning was switched back to topography mode, all the details that failed to be captured with the elastic modulus mode (Figure 5.11B, 3 min, 26 min) could still be resolved faithfully with the topography mode (Figure 5.11B, 6 min, 28 min). In this case, the capsule was also internalised, it was half inside in the cell at 28 minutes (Figure 5.11A) and was totally inside the cell after 48 minutes. However, due to the lack of fidelity, these images sequence with significant artefacts were not considered as good showcase of representative internalisation process. They were showed here only to demonstrate the effect of elastic modulus measurement on the internalisation of the capsule.

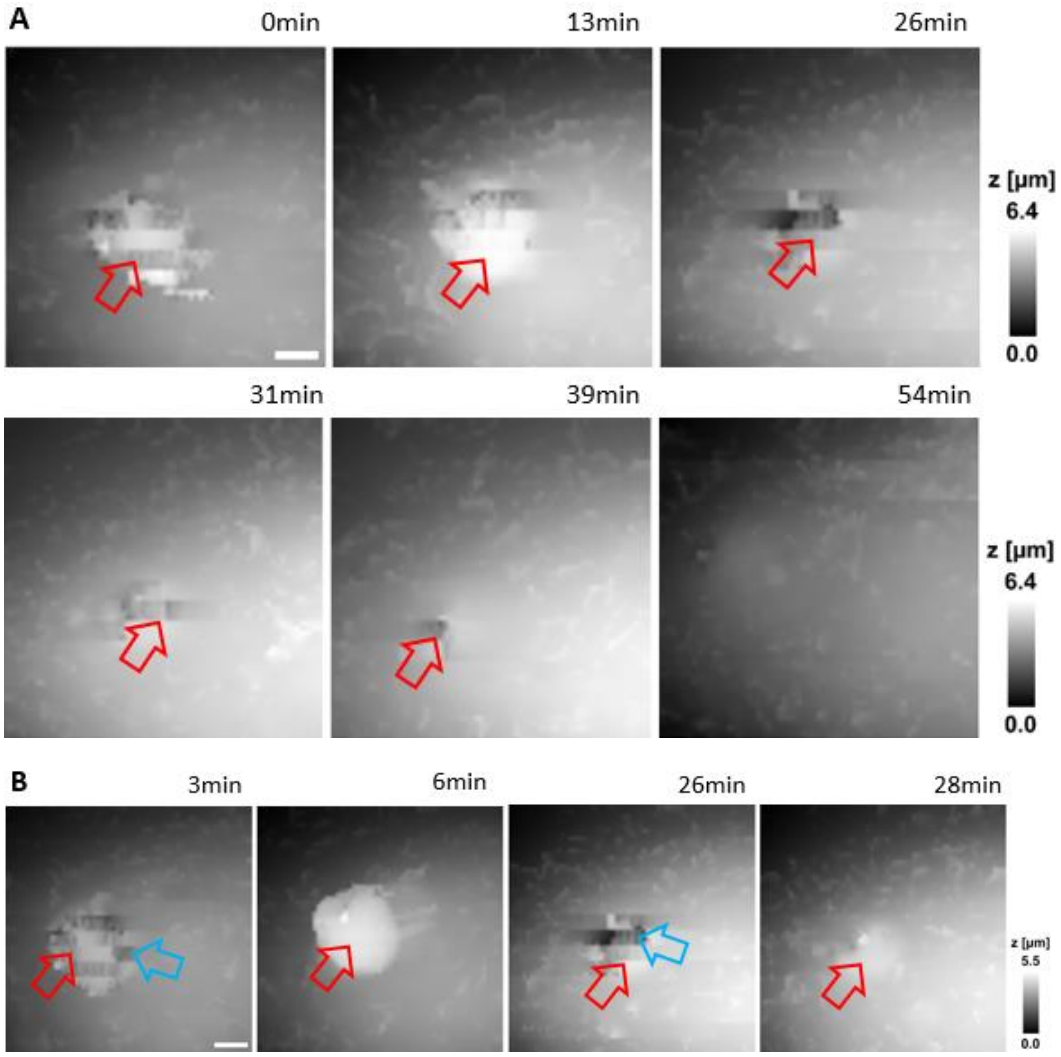

Figure 5.11 Time lapse topography images captured with the elastic modulus measurement on. (A) a whole internalisation process in which the pipette interfered with the capsule (red arrows) severely and the capsule was still internalised. (Scan size: 15 µm×15 µm, scale bar: 2 µm) (B) The same capsule (red arrows) imaged with (3 min, 26 min) and without (6 min, 28 min) elastic modulus mode. Note the presence of artefacts (cyan arrow) in the images captured with elastic modulus mode and the normal images captured with topography mode with no sign of artefact.

5.5 The detailed procedure for visualising the internalisation event with SICM

Here we are going to introduce the detailed procedure we designed for imaging the internalisation of microcapsules using SICM as a summary of those technical problems and solutions mentioned previously in this chapter.

Polyelectrolyte multilayer capsules (PSS/PAH/PSS/PAH/PSS/PAH-FITC)

with diameter range from 4 μm to 6 μm were prepared in advance and stored in PBS. Immortalised human lung cancerous epithelial cell line A549 cells were seeded on glass bottom petri dishes FluroDish^{TM} with 10mm well at a density of 1×10^5 cell per petri dish after trypsinised from T25 cell culture flasks. The cells were left in incubator at 37 ºC, 5 % CO_2 for around one or two days until they reached a confluency of 50 %. Nano-pipettes of 100 nm in diameter were pulled using P-2000 laser puller several days before the imaging.

On the day of imaging, the SICM system was turned on about 15 minutes before the imaging to allow the objective lens heating mantle to warm up. When the system was ready, the cells were taken out of the incubator. The original DMEM cell culture medium was replaced by warm serum-free Leibovitz's L-15 medium after three rounds of washing with warm L-15. After that, the petri dish with cells and warm L-15 inside was immediately mounted onto the sample stage. After mounting the sample, a pipette was filled with PBS and mounted onto the pipette holder. Then the two electrodes were placed, one inside the pipette and the other one in petri dish immersed by L-15. This setup is illustrated in Figure 5.12.

Pipette was immersed and lowered down towards the sample surface using SICM software. The setpoint we used for approaching as well as imaging was 0.3-0.4 %, which meant the pipette stopped approaching after detecting a 0.3-0.4 % drop in current and started to hop at a hopping amplitude of 2 μm. Generally speaking, a lower setpoint of 0.3 % was preferred as it allowed the pipette to hop further away from the membrane surface and reduced the risk of collision. At this point, the setup was ready for imaging. The next step was adding capsules.

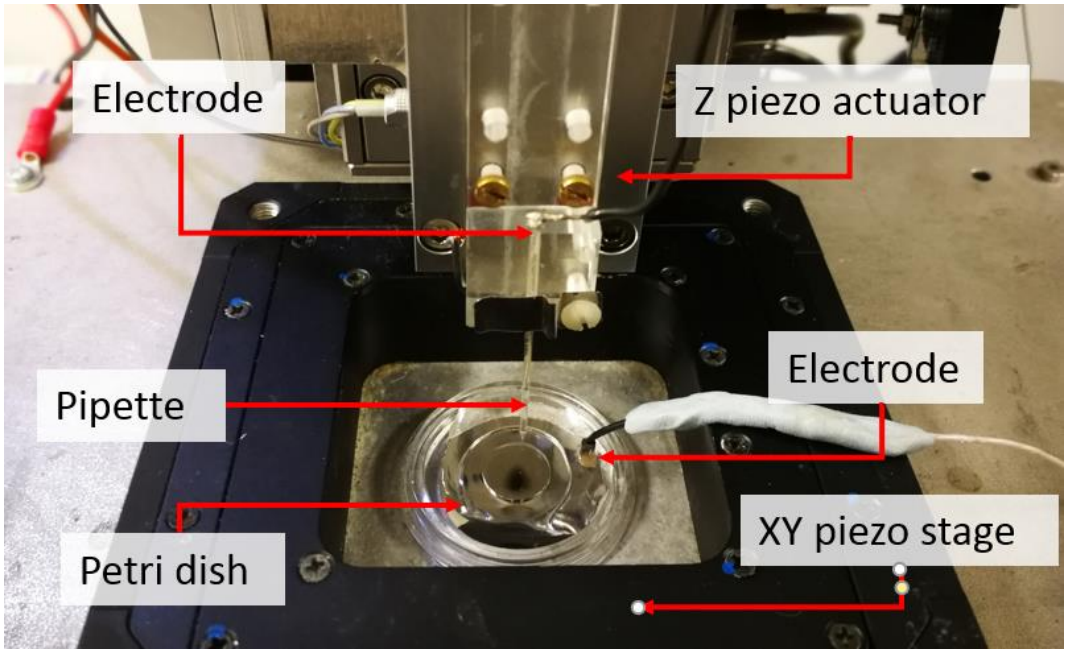

Figure 5.12 The setup for SICM imaging.

For adding capsules, pipette was slight moved up for 25μm to avoid the slight vibrations caused by handling from breaking the pipette tip. Capsules were added by dipping 100 μl of capsules/PBS suspension (~10^5 of microcapsules) into the L-15 using an Eppendorf Pipette without extensive stirring or mixing the solution to reduce the risk of breaking or blocking of the pipette tip as it had already been in close vicinity of the cell membrane surface. Instead, the operation we used was to bring the tip of the Eppendorf Pipette with the capsule suspension close to the glass nanopipette without touching it and allow the drop of capsule suspension to run down the glass pipette side-wall to ensure a good capsule concentration around the pipette tip. After the capsules were added, we waited for at least 5 minutes to allow the capsules to settle and firmly attached to the cell membrane surface before we started scanning.

In the meantime, we started to look into the optical microscope in searching for capsules that appeared to be attached to the cell membrane. The searching and choosing of capsule that had the best chance of getting internalised was probably the most crucial and most challenging step in this entire procedure.

A 100× oil immersion objective lens was used for this task. There are a variety of facts that might affect the possibility of witnessing the internalisation of microcapsule within the time span of an hour, such as the size of the capsules (Foster et al., 2001), the size and shape of the cells, the position of the capsules that attached to the cells, etc. However, we have no unarguable statistics confirming the effect of these facts on the internalisation of microcapsules, apart from the case of those capsules that attached to the boundary between cells, which we had described in previous section and which we knew for sure would not lead to a successful internalisation. Nevertheless, according to our own experience, in most of the internalisation events (22 out of 23) we recorded, we had the capsule attached to a relatively flat cell (with height ranging from 4 μm to 8 μm) and the position of attachment was usually somewhere away from the periphery of the cell (Figure 5.13).

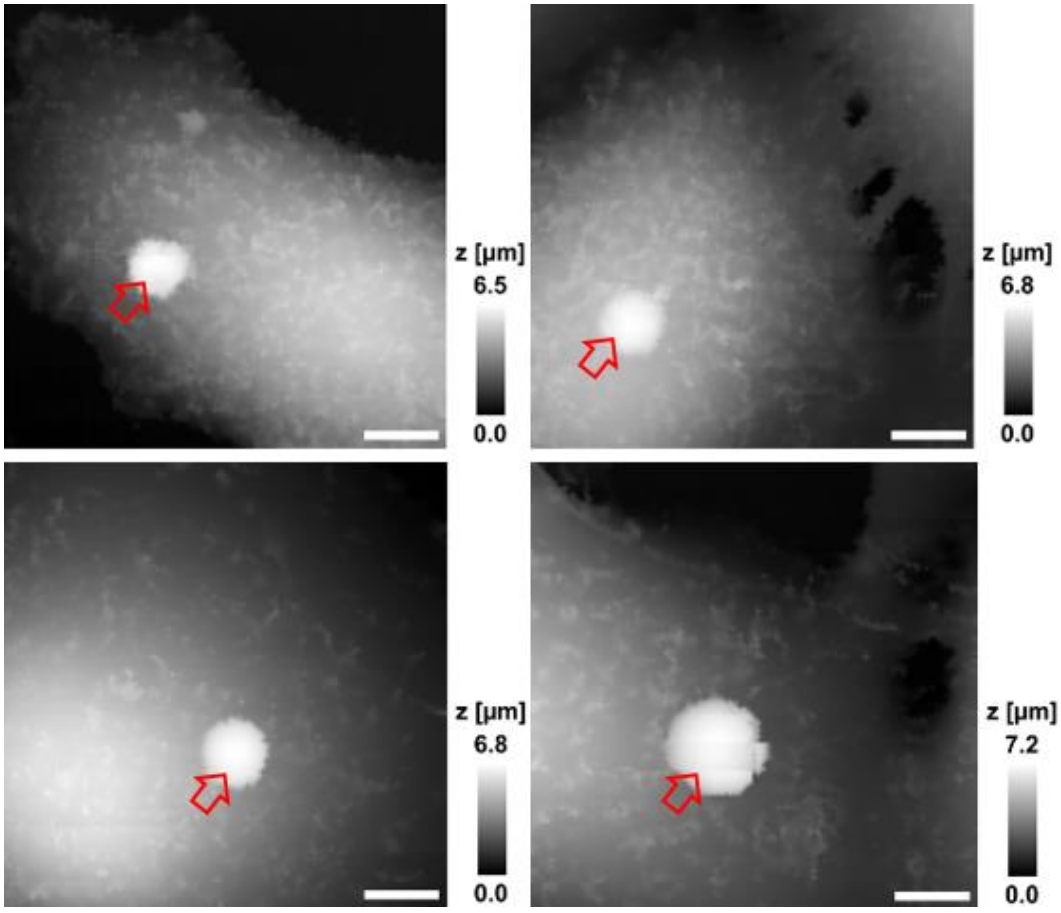

Figure 5.13 Typical situations of capsule (red arrows) and cell that would lead to a successful internalisation. (Scale bar: 5 µm)

This searching might sometimes take more than 5 minutes. In those cases in which the searching took over 10 minutes, it was likely that the initial interaction of the internalisation would be missing from the recording. If the searching took less than 5 minutes, we waited for the capsule to settle before starting the scanning. Usually, a 30 µm×30 µm image with resolution of 320 nm was first scanned to give an overview of the capsule and the cell and confirm that the situation was the same as that was observed form the optical microscope. After that, a smaller area was scanned to improve the resolution of the images without increasing the scanning time. The size of the small area scanning ranged from 10 µm×10 µm to 20 µm×20 µm depending on the extend of membrane activities. Most frequently, a 15 µm×15 µm area was scanned, which gave images with a resolution of 156 nm at frame rate of 5 min/frame. If dislocation or deformation of the capsules was seen from the images, which suggested the scanning of the pipette was disturbing the

internalisation process, a 5 minutes waiting time was introduced in between each frame. This setting gave a frame every 10 minutes, but each frame still took just 5 minutes to finish.

As for the elastic modulus measurement, a second setpoint was set. After reaching the first setpoint, the pipette travelled further down until the current detected was reduced by another 1 % (1.3-1.4 %). No further operation was needed for recording the elastic modulus. After each scan, the original data could be instantly processed using the built-in function of SICMImageViewer to get the elastic modulus reading.

That smaller area was scanned repeatedly until the capsule got internalised. After the internalisation, we continued to scan this same area if the capsule could still be detected by elastic modulus measurement until all signs of capsule disappeared. For those uninternalised cases, the scanning was usually aborted after 90 minutes of imaging, as the longest internalisation event recorded by us was 71 minutes. After the imaging finished, the used pipette and the cell culture were discarded accordingly.

5.6 Conclusion

We have successfully established a procedure for capturing topographical images of microcapsules internalisation and observed 23 events of internalisation.

In 14 out of these 23 events, we captured the entire internalisation process from right after the first contact to the final internalisation of capsule. In the remaining 9 events, the internalisation had already begun and the capsules were already half way inside when we started the imaging. However, we still managed to capture few frames before its final internalised. The fail in capturing the whole process was usually because we spent too long (more

than 10 minutes) in searching for a good capsule/cell combination and missed the first contact of capsule and cell. Other reason was sometimes something went wrong with the setup during the scanning, such as pipette blockage. In that case, we had to stop the scanning and replace the pipette, thus missed few frames. Nevertheless, the percentage of capturing the whole internalisation process (60.9 %, 14 out of 23) was overall good. This percentage was also dependent on the operational skills of the operator, which showed signs of improvement with time as the operator gained more experience.

In 9 out of these 23 events, severe artefacts appeared in the images, which were caused by the pipette blockage or by the pushing of pipette under elastic modulus measurement mode. Though the internalisation could still be confirmed with those image sequences, those images had limited assertion in demonstrating the internalisation process. For those 14 complete internalisation events we recorded, 10 events had image sequence of good resolution and fidelity without significant artefacts.

In conclusion, the SICM live cell imaging technique as well as the procedure we established were proved capable of capturing the internalisation of microcapsules. The success rate of capturing true and complete recording of the internalisation (43.8 %, 10 out of 23) was considerately good for imaging a highly sophisticated process like this.

6. Characterising microcapsule internalisation using SICM

Previously, the internalisation of microcapsules was mainly studied by four characterization methods: optical/fluorescence microscopy, 3D confocal microscopy, flow cytometry and electron microscopy. Each method has its own advantages and its own applications in the study of capsule internalisation as discussed before in chapter 2.3. However, the limitations of these methods are also undeniable. In this chapter, we are going to present the internalisation process as revealed by SICM.

6.1 The high-resolution details revealed by live SICM imaging

For time lapse SICM imaging, we used a frame rate of 5min/frame. With this frame rate, an area of 30 μm×30 μm could be imaged at lateral resolution of 320 nm. Higher resolution could be achieved by scanning a smaller area. With the same frame rate of 5 min/frame, a smaller area of 15 μm×15 μm could be imaged at lateral resolution of 156 nm. This resolution was proved high enough to resolve details regarding the forming of fine membrane protrusions during the internalisation process of the microcapsule. Figure 6.1 shows an image of 20 μm×20 μm in size, imaged using a lateral resolution (pixel size) of 156 nm. In the image, fine membrane protrusions formed in the vicinity of the capsule (cyan arrows) resembling the forming of phagocytic cup reported before (Kastl et al., 2013). However, these details had only been visualised before in fixed samples using electron microscopy. With SICM, these details were captured with live cells for the first time. Note the relatively thin protrusion (yellow arrow) that appeared to cling to the capsule, which was beautifully captured by SICM time lapse imaging.

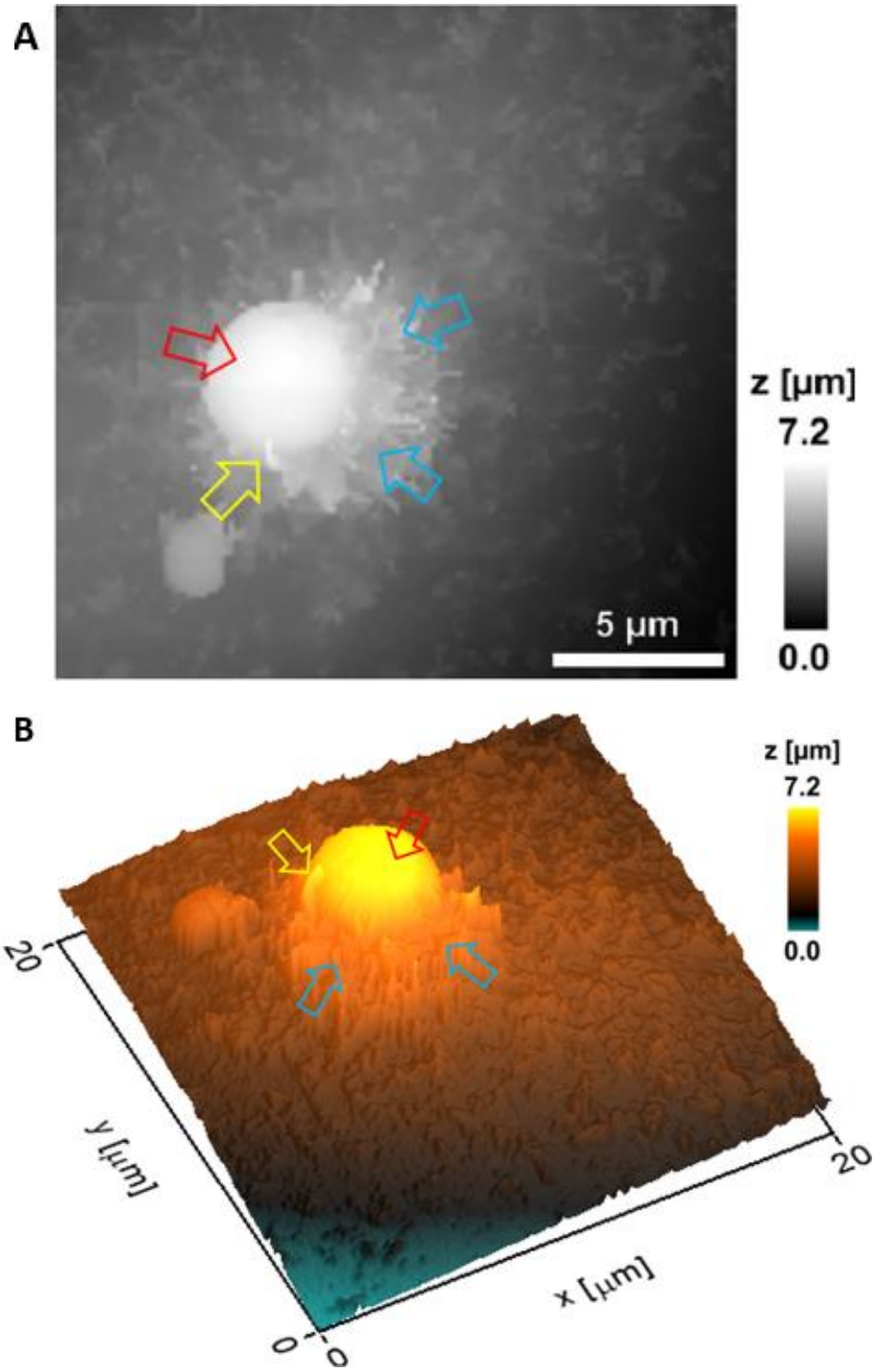

Figure 6.1 Forming of fine membrane protrusions around the capsule captured by SICM at a resolution of 156 nm. (A) SICM topography image. (B) 3D reconstruction of the topography image. Note the fine details of the membrane protrusions (cyan arrows), especially with the one pointed with the yellow arrows. This image was captured 9 minutes after recording the first frame in which the capsule had just attached to the cell membrane. (Capsules are pointed with red arrow)

6.2 Confirming the internalisation of the microcapsules with SICM

In our experiments, we studied the process of internalisation by observing its topographical change. We considered a capsule internalised if the capsule was entirely inside the cell as viewed from SICM topography images. After full internalisation, the cell membrane would typically display topography similar to the one observed before the exposure to the capsule, with no features identifiable as capsule left on the surface of the membrane (Figure 6.2A, B). The membrane protrusions were typically still present on the cell membrane (Figure 6.2B) as before the landing of the capsule (Figure 6.2A). While the capsules could no longer be identified in the topographical images of the cell membrane (Figure 6.2B, D, G), the presence of the capsule underneath the cell membrane could still be proved with optical microscopy (Figure 6.2E, H). The SICM topography of the cell membrane together with the optical image of the capsule confirmed that the capsule was without doubt inside the cell. We observed 27 cases of interactions between individual capsules and cells and successfully recorded 14 cases of full capsule internalisation.

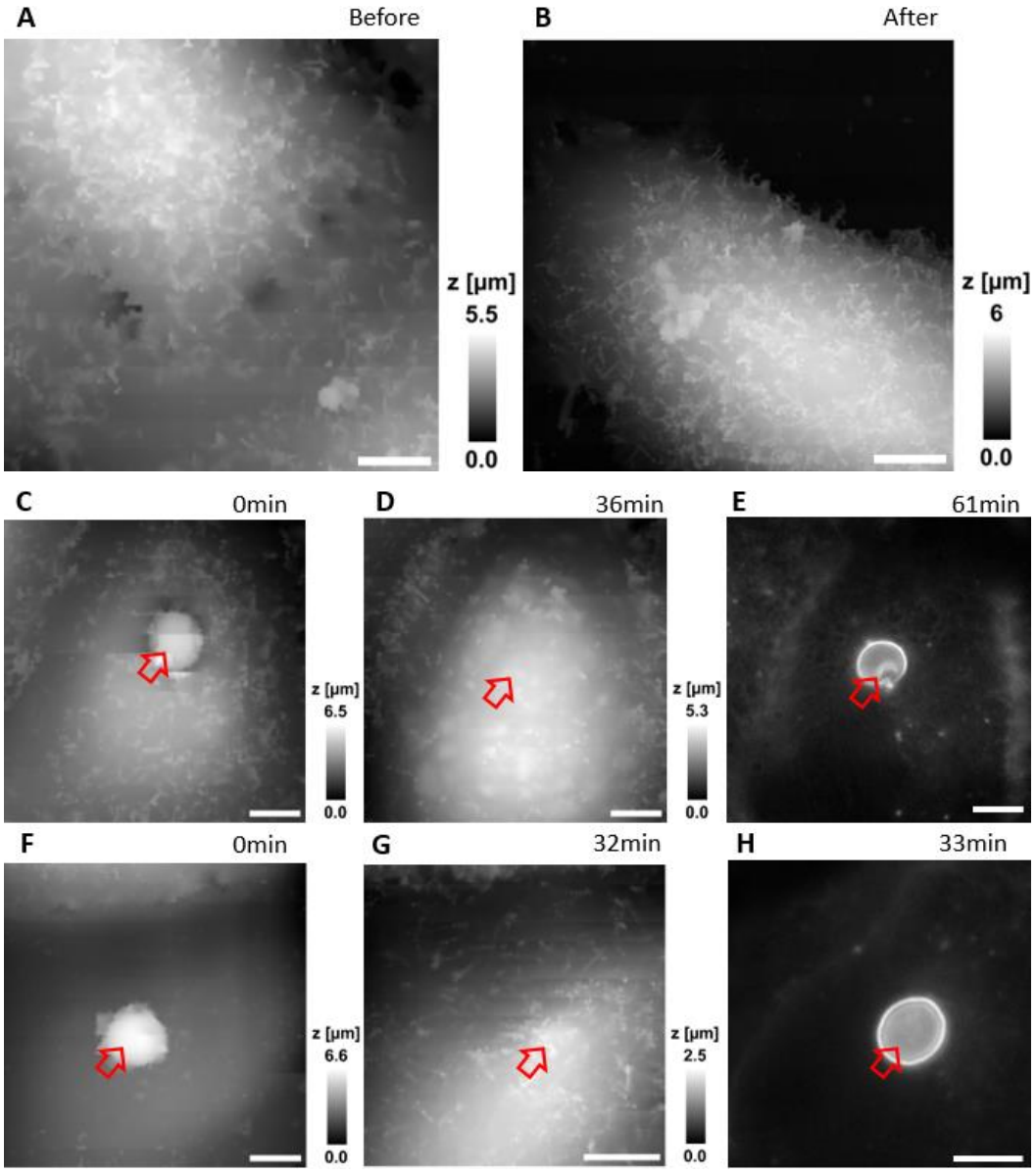

Figure 6.2 The confirmation of internalisation. (A, B) SICM topography images showing the morphology of cells before the attachment of the capsule (A) and after the internalisation of the capsule (B). Note that the cells presented in A and B were two different cells. (Scan area: 30 µm × 30 µm, scale bar: 5 µm) (C-E, F-H) Two demonstrations of capsule internalisation proven by the SICM topography images and optical microscopy images. Capsules were sitting on the cell membranes at the beginning of the recording (C, F) and disappeared from the topography images by the end of the recording (D, G). The optical images showed the presence of capsules underneath the cell membrane (E, H). (Scale bar: 5 µm)

In 6 out of the 14 cases, no sign of capsule could be observed after the capsules were internalised (Figure 6.3A). In 5 out of the 14 cases, the patch of the membrane where the capsule was internalised remained slightly elevated above the surrounding membrane (Figure 6.3B). The height of the membrane patch above the substrate before the internalisation in these cases

was often smaller or comparable to the diameter of internalised capsule. This suggested that the bulging membrane patch was most likely caused simply by the internalised capsule pushing the soft membrane upwards due to the limited existing cytoplasmic space underneath the membrane. These capsules were considered fully internalised, because the top part of the capsule was entirely covered with membrane and the characteristic smooth spherical profile of the capsule wall was no longer identifiable in the topography. On the contrary, if the whole spherical profile capsule or some part of it was still identifiable above the surrounding membrane surface (Figure 6.3D), we would consider it as not-internalised even if it was partially covered by membrane protrusions. In 3 out of 14 cases, the membrane activities reduced after the internalisation of the capsule (Figure 6.3C). In these cases, considerable large bumps could be observed at the location of internalisation suggesting limited cytosolic space. Due to low incidence of this behaviour, we could not conclude a direct relation between the reduced activities of membrane protrusions and presence of the bump left by the capsule on the membrane surface.

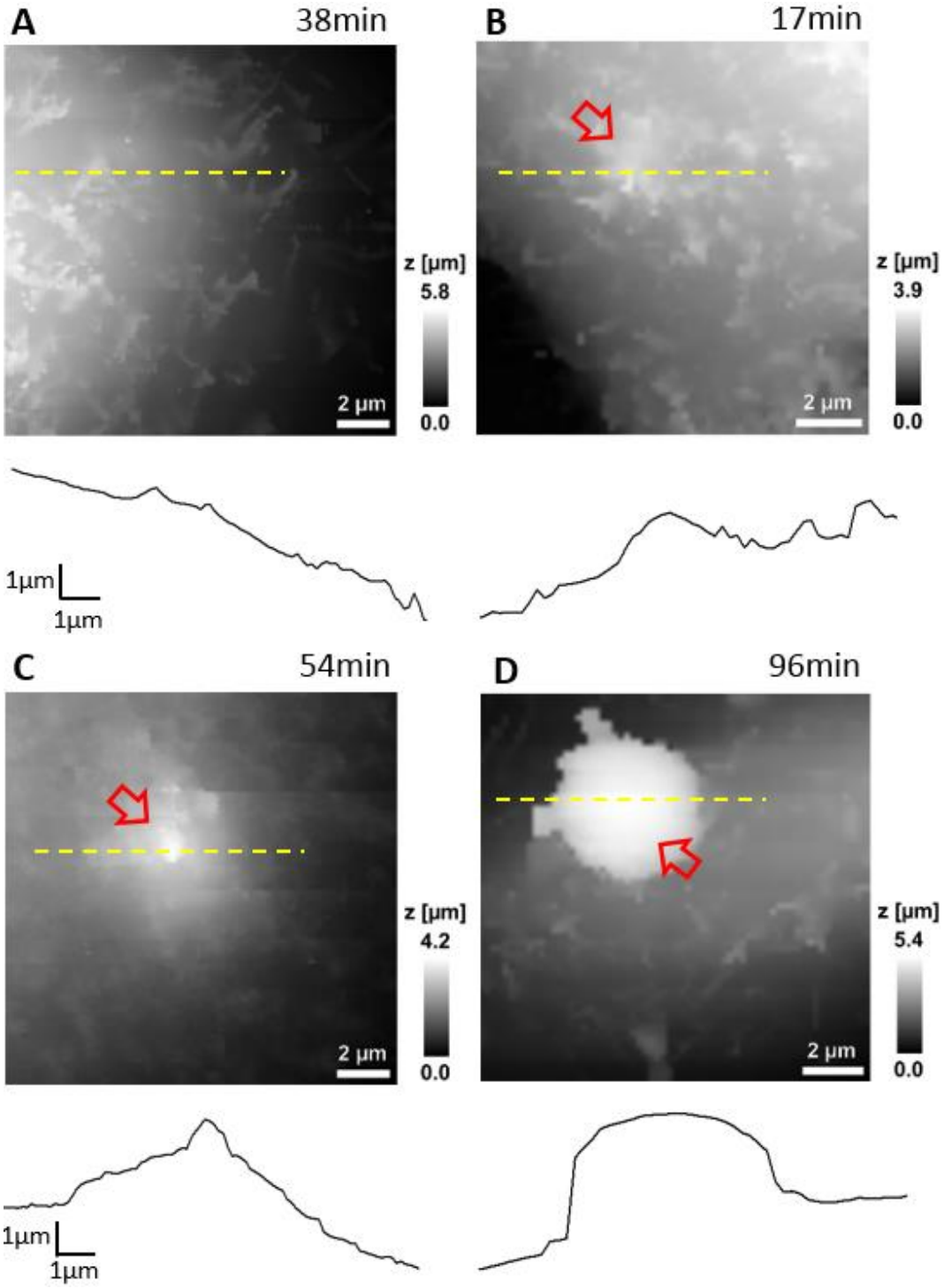

Figure 6.3 Topography images of the interaction between the capsules and the cells by the end of the recording in 4 different cases (A) No sign of capsule could be observed after the capsules were internalised. (B) Slightly elevated membrane (red arrow) left by the internalised capsule. (C) Bump (red arrow) left on the surface of the membrane and reduced membrane activities after the internalisation. (D) Uninternalised capsule (red arrow) that stick out of the cell membrane by the end of 96 minutes of recording.

6.3 Internalisation events recorded with live SICM time lapse imaging

6.3.1 The time span for complete internalisation

In the 14 cases in which we observed complete capsule internalisation (Chapter 5.6), full internalisation happened within 17 to 71 minutes from the beginning of the recording, with average duration of 43.2 ± 19.3 minutes (mean ± standard deviation of the mean, Figure 6.4A). The duration of internalisation showed weak, statistically insignificant dependence on the diameter of microcapsules ($R = 0.315$, $p > 0.05$, Figure 6.4B). This was in agreement with results obtained using confocal fluorescence imaging where 55.7 % (34 out of 61) of capsules appeared to be internalised after one-hour incubation (Chapter 4.1.1), suggesting the SICM imaging had not negatively affected the rate of capsule internalisation.

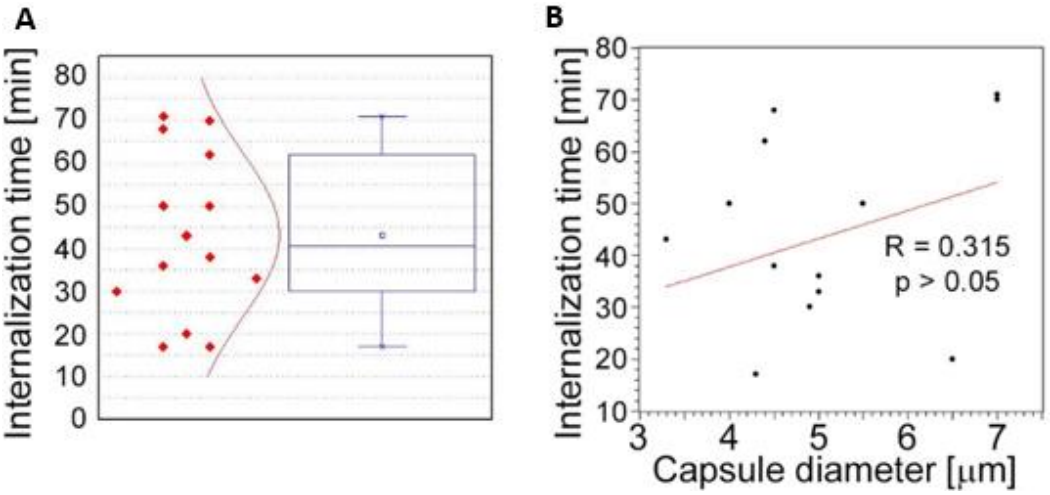

Figure 6.4 (A) The distribution of the internalisation time. (B) The correlation between internalisation time and capsule diameter.

The fastest internalisation event we recorded was 17 minutes (Figure 6.5). Recording started 5 minutes after adding the suspension of capsules into the bath solution. Due to random character of the motion of capsules, the actual time of attachment to the membrane could not be identified and can only be specified as within 5 minutes before the recording started. The perfectly spherical, smooth profile of the capsule (Figure 6.5, 0 min, red arrow)

indicated that the cell membrane had not started to cover the capsule, also suggesting that the capsule had only recently landed on the cell membrane before the starting of first imaging. However, just 17 minutes after the recording started, the capsule was completely internalised by the cell. So, after adding the 0 to 5 minutes of waiting time before the start of the recording, the entire internalisation happened within 22 minutes. It was truly remarkable that an unmodified particle 4 μm in diameter could be fully internalised by a cell not specialised in phagocytosis at such a speed.

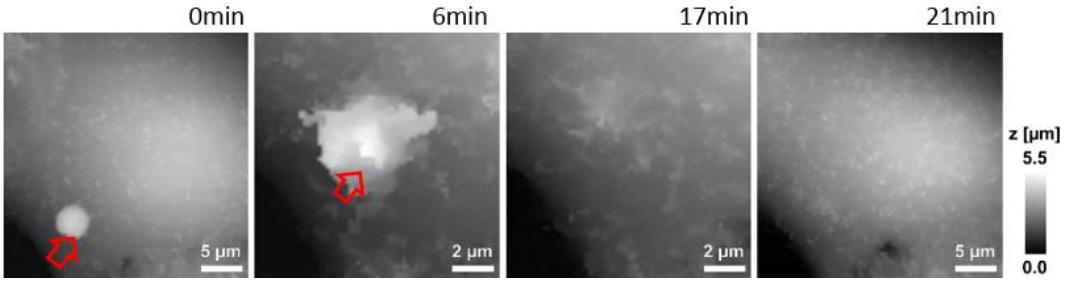

Figure 6.5 The fastest internalisation event recorded. Note the disappearance of capsule (red arrow) from the membrane surface at 17 min.

6.3.2 The topographical and morphological changes during the internalisation

From the viewpoint of topographical and morphological changes we observed two markedly different ways in which the capsules were internalised. In the first type of internalisation (Figure 6.6), the fine, finger-like membrane protrusions normally present on the cell first started to concentrate mainly around the bottom of the capsule (green arrowheads, Figure 6.6). Some of these protrusions gradually restructured into membrane ruffles (yellow arrowhead, Figure 6.6) and were followed by a number of apparently separate sheets of membrane gradually extending over the top of the capsule in a process similar to the zipper model of phagocytosis (Swanson, 2008). The gradual engulfment of the capsule happened mainly by extension of membrane sheets over capsule without noticeable "sinking" of the capsule into the cell until the very last stage. While the internalisation events we observed here displayed certain characteristics resembling receptor mediated phagocytosis, we would like to note here that these capsules were not

modified in any way to specifically trigger the Fc or C3bi receptors previously identified as responsible for phagocytosis, and it remains unclear which, if any, receptor is involved in the processes described here.

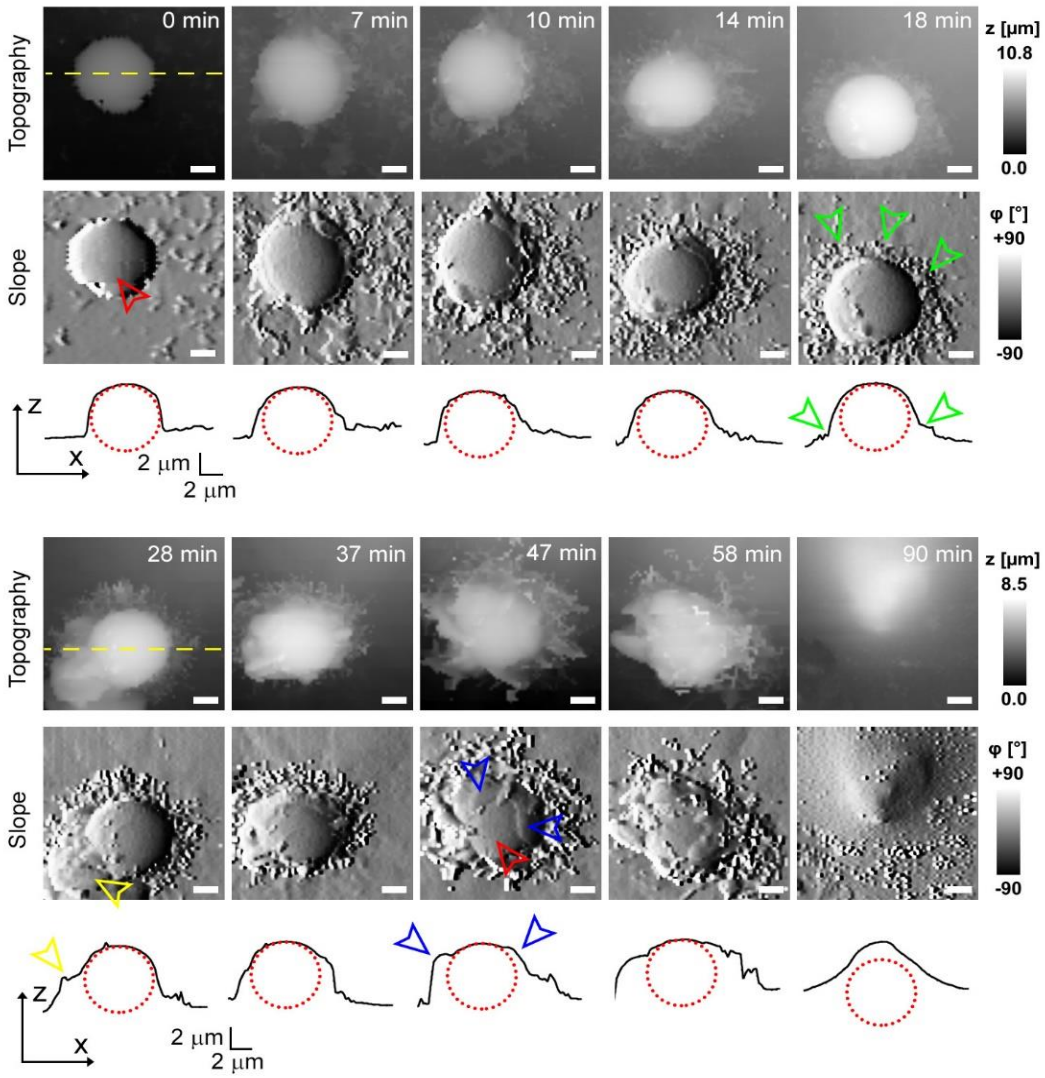

Figure 6.6 Representative internalisation of polyelectrolyte capsule involving formation of extracellular phagocytotic-like cup. Time lapse imaging of topography is shown together with corresponding slope images (first derivative of topography) and line profiles (black curves) across the centre of the capsule as indicated by the yellow dashed lines. The time 0 min marks the beginning of the recording, the exact time when capsule landed on the cells is uncertain. The red dotted circle represents the capsule. Note how the bare capsule (red arrowhead) is gradually surrounded by fine finger-like protrusions (green arrowheads) at the bottom of the capsule, later morphing into larger membrane protrusions (yellow arrowhead), and finally how the top of the capsule gets gradually covered by thin layers of membrane (blue arrowheads). (All scale bars: 2 µm)

In the second type of internalisation (Figure 6.7), the capsule appeared to sink into the cell almost simultaneously with the growth of membrane protrusions around and above the capsule (Figure 6.7B, C), resembling previously described process mediated by CR3 (Swanson, 2008). No apparent concentration of membrane protrusions around the capsule was observed in this type of internalisation. Few relatively large membrane protrusions remained at the site of internalisation in some cases for considerable amount of time (almost 30 minutes in the case shown in Figure 6.7B)

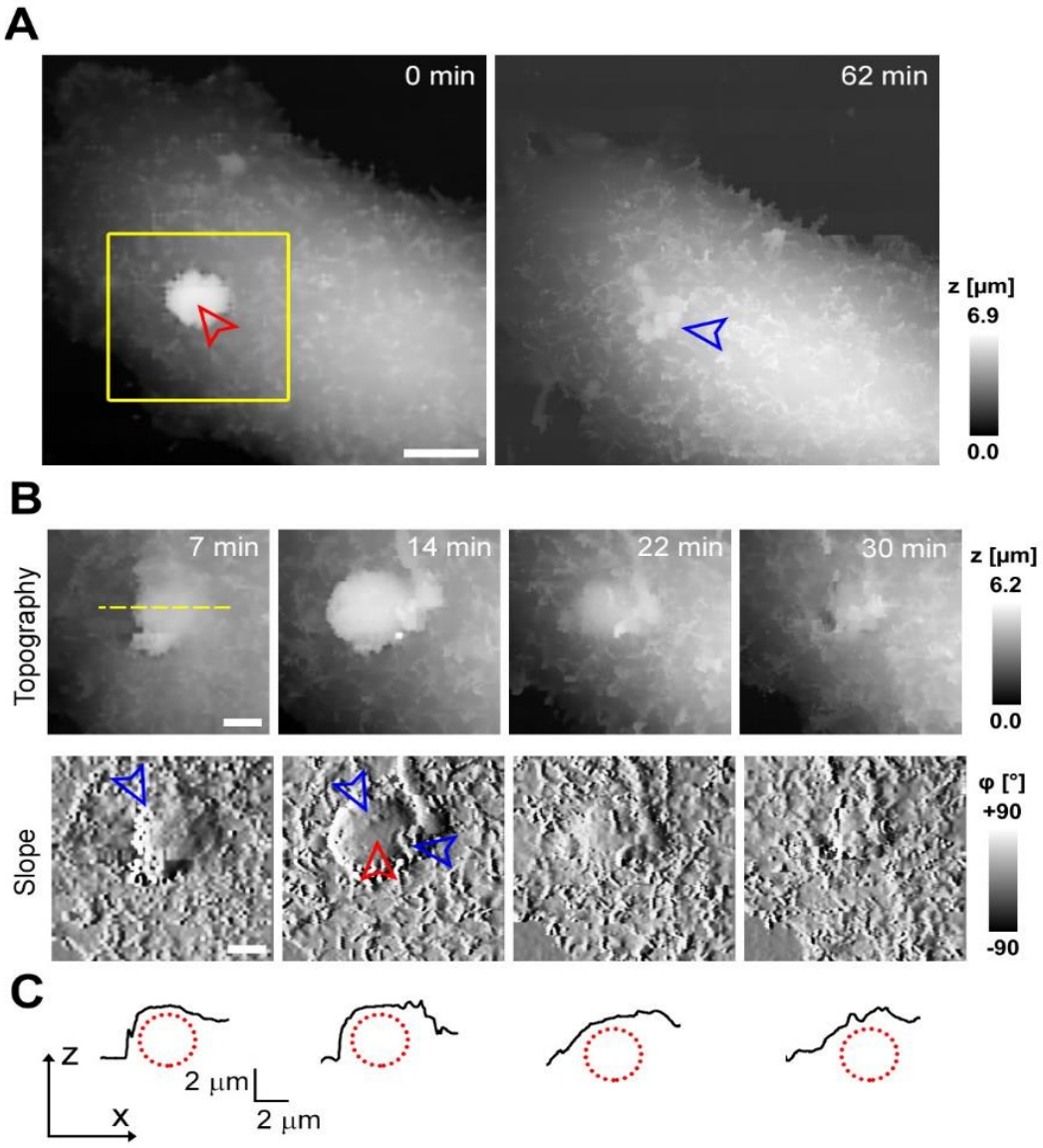

Figure 6.7 Representative internalisation of polyelectrolyte capsule with no apparent formation of extracellular cup. (A) Topographical image taken shortly after a capsule (red arrow) landed on the cell surface and 62 minutes later, after full internalisation of the capsule. Note the protrusions remaining at the location of internalisation (blue arrow). (Scale bar: 5 µm) (B) Time lapse topographical imaging within area marked by the yellow square in (A). Note protrusions (blue arrowheads) appearing halfway through the internalisation process. (Scale bar: 2 µm) (C) Line profiles across the centre of the capsule as marked in (B). Note gradual flattening of the line profile suggesting the capsule (illustrated by red dotted circle) sank into the cell.

6.4 Stalled internalisation events

The initial formation of membrane protrusions interacting with a capsule attached to the cell membrane appeared to be triggered regardless of the

position of the capsule on the cell or the eventual fate of the capsule. In 13 out of 27 experiments (in which we got images sequence without significant artefact), we observed this initial interaction between cell membrane and the capsule appeared to "stall" in the early stages (Figure 6.8) and did not progress into development of membrane ruffles or sheets within the time span of recording. On average, we followed these stalled events for 83 ± 46 min (n = 13), with the longest recording reaching 202 minutes (Figure 6.8C, D) with no signs of progression into the phase where "sinking" of the capsule could be detected, or any other sign on internalisation. This suggests the formation of membrane protrusions around the capsule is a typical feature of initial interaction between A549 cells and capsules but not sufficient step in the process of internalisation. It appears that the important step leading to successful internalisation is restructuring of the finger-like membrane protrusions into membrane ruffles which then extend smooth sheets of membrane over the top of the capsule. This was not observed in the cases where internalisation appeared to "stall" (Figure 6.8). The existence of capsules "trapped" on the cell membrane as described here suggests that simple washing used in previous reported research (Ai et al., 2005) may not be sufficient to remove capsules that have not been internalised. Methods such as counting supernatant or epi-fluorescence microscopy are incapable of distinguishing the adhered capsules from the internalised ones, negatively affecting the conclusions made on the basis of results obtained with these techniques.

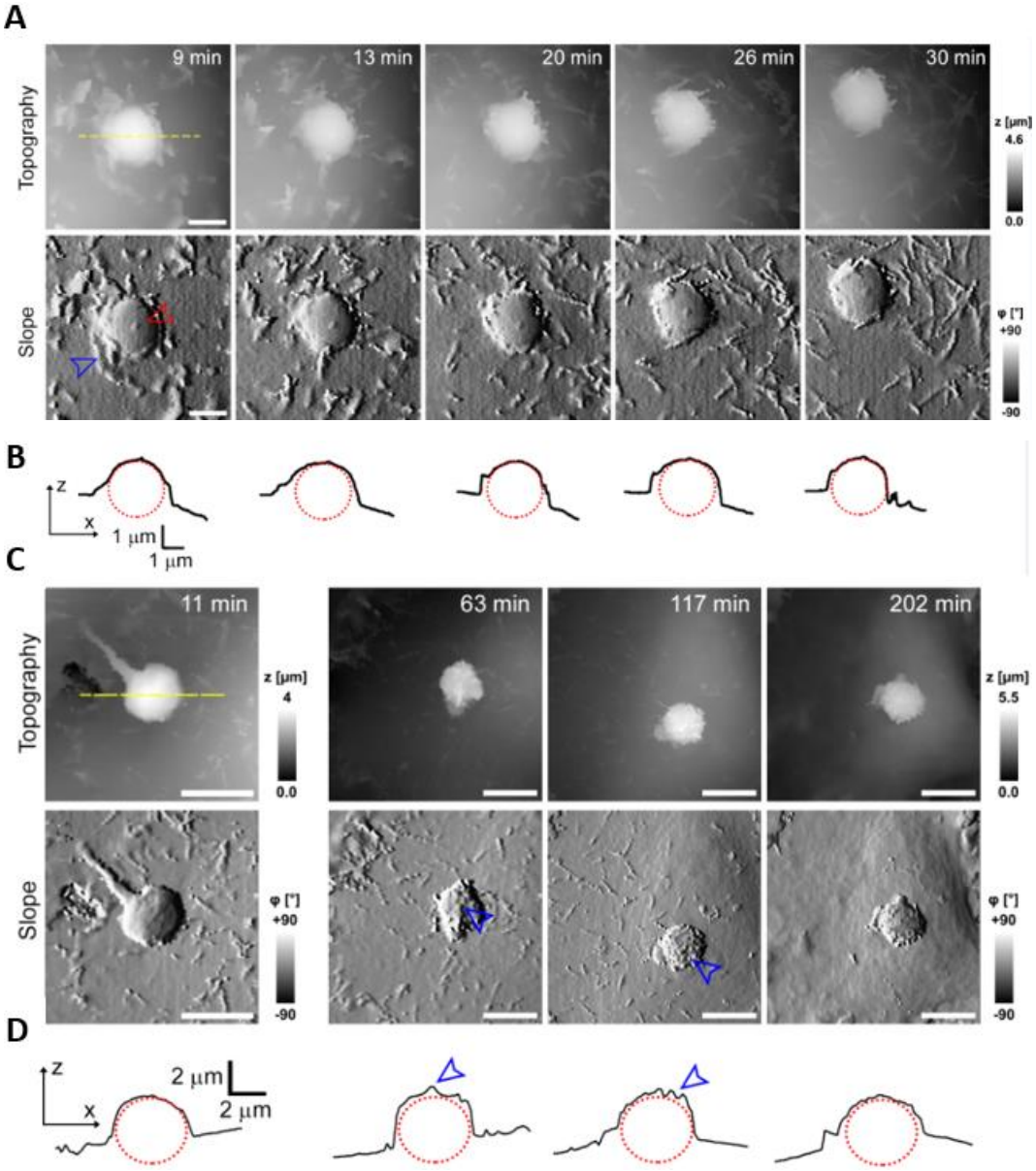

Figure 6.8 Representative time lapse SICM imaging of a "stalled" internalisation. (A) Topography and corresponding slope (first derivative of topography) images. Note that a number of protrusions (blue arrowhead) seem to be interacting with the capsule (red arrowhead), however the central area of the capsule remains almost intact. (Scale bars: 2 µm) (B) Line profiles across the centre of the capsule as marked by dashed yellow line in (A). The red dotted circle represents the capsule. No apparent sinking of the capsule was observed within the total recording time of 55 min. (C) Excerpts from a long-term time-lapse topography imaging of a stalled internalisation event. Note presence of fine protrusions (blue arrowhead) on the top of the capsule still present 1-2 hours after the beginning of recording instead of flat, smooth sheets of membrane observed in successful internalisation events. After 202 minutes, the cell membrane around the capsule became almost completely smooth. (Scale bars: 5 µm) (D) Line profiles across the centre of the capsule as indicated by dashed yellow line in (C). The red dotted ellipse represents the capsule at given z-x scaling. Note the presence of rough protrusions on top of the capsule (blue arrowheads). No apparent sinking of the capsule into the cell visible here within 202 minutes from the beginning of recording.

6.5 Mapping mechanical properties of capsule internalisation

To investigate the mechanical properties of capsule internalisation we used the recently implemented method for measurement of elastic modulus (Clarke et al., 2016). Thanks to the low stress and minimally invasive character of the imaging using nanopipettes we were able to map changes of mechanical properties without apparent disruption of the internalisation process. The area of the cell membrane above the cell nuclei and around the nuclei displayed mean elastic modulus of 4205 Pa ± 1284 (n = 9) and 1310 Pa ± 559 (n = 27), respectively. These values are comparable to previous observations using AFM (Byfield et al., 2011). The mapping of elastic modulus using SICM was sensitive enough to distinguish between the bare surface of a capsule and the surface already covered by cellular membrane (magenta & red arrowheads, Figure 6.9). The modulus of the membrane covering the capsule was similar to the modulus of the cell membrane away from the site of internalisation (black arrowhead, Figure 6.9), while the modulus of the large protrusions growing in the vicinity of the capsule (yellow arrowhead, Fig. 4a) was apparently higher suggesting higher density of actin in these protrusions.

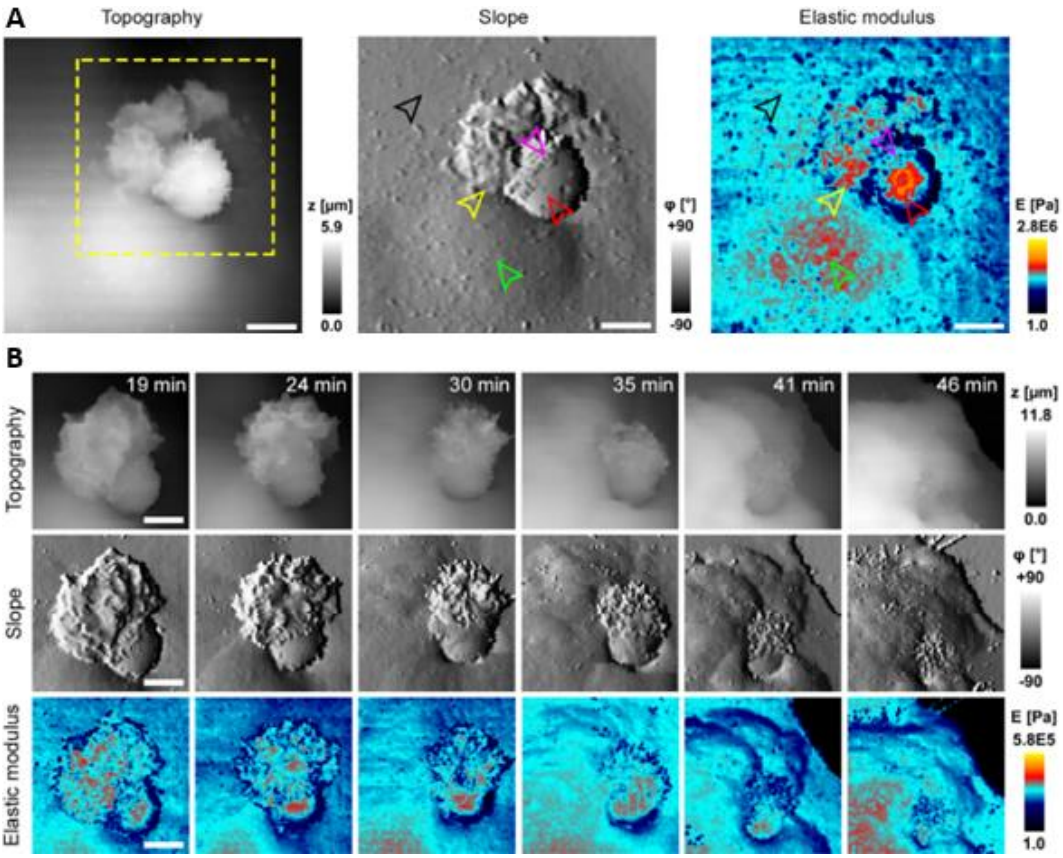

Figure 6.9 Representative time lapse imaging of mechanical properties during the internalisation. (A) Topography image of 30 µm × 30 µm area showing the early stage of the internalisation together with corresponding slope and elastic modulus images. Note the part of capsule covered with membrane (magenta arrowhead) displays lower elastic modulus than the exposed part (red arrowhead). Membrane protrusions (yellow arrowhead) formed in the vicinity of capsule and also membrane above the nucleus (green arrowhead) showed higher modulus than membrane (black arrowhead) away from the capsule. (Scale bars: 5 µm) (B) Simultaneous time lapse imaging of the topography (top row) and elastic modulus (bottom row) of the internalisation marked by yellow dashed square in (A). Elastic modulus of the substrate (glass bottom) was set to 1 Pa (black colour coded) for clarity. (Scale bars: 5 µm)

To analyse the morphological changes in Figure 6.9, we calculated the thickness and roughness of the membrane covering the capsule during the internalisation. The topographical line profiles across the centre of capsules undergoing internalisation were extracted from topographical images (Figure 6.9B) using Gwyddion (http://gwyddion.net/) and imported into Origin 8.1 (OriginLab, USA). Ideal circle equation

$$y = \sqrt{r^2 - (x - x_C)^2} + y_C$$

(where r is capsule radius, and x_C and y_C are coordinates of the centre),

representing microcapsules was fitted to sections of height profiles showing exposed capsule surface. Roughness of the membrane-coated and exposed surface of the capsules was calculated as standard deviation of the extracted line profiles after subtracting the fitted circle equation.

The elastic modulus of exposed capsules attached to the cell membrane estimated using our method (14372 Pa ± 10373 Pa, n=13) is few orders of magnitude lower than previously reported for polyelectrolyte capsules on glass coverslips (hundreds of MPa to few GPa (Dubreuil et al., 2003)), however, it is significantly higher ($p<0.001$) than the elastic modulus of cell membrane just outside the internalisation site (2100 Pa ± 1202 Pa, n=13).

As the membrane extended over the capsule, its roughness reduced (from 214 nm to 36 nm, Figure 6.10B) pointing to restructuring of the underlying actin-myosin skeleton from finger-like protrusions into smooth membrane sheets. The change in roughness was very likely due to restructuring of the membrane as the roughness of exposed capsule surface showed only slight changes (from 9 nm to 12 nm, Figure 6.10B). At its lowest thickness, the membrane sheet extending over the capsule was just 160 ± 70 nm thick (at 30 minutes, Figure 6.10B), compared to 355 ± 213 nm at the beginning of the process.

With the membrane sheet gradually thinning, the underlying stiff wall of the capsule could be detected when compressing the membrane to obtain elastic modulus. This was observed as transient increase of elastic modulus of the membrane (magenta line, between 15 - 30 minutes, Figure 6.10C) right up to the value comparable to exposed capsule (red line, Figure 6.10C), followed by decrease back to the value comparable to cytoplasmic membrane around the internalisation site. The transient increase in the elastic modulus reflected specifically the membrane processes happening on the upper side of the

capsule as indicated by the fact that elastic modulus of other parts of the membrane showed distinctly different trends (Figure 6.10C). Elastic modulus of membrane protrusions forming around the capsule (yellow arrowhead, Figure 6.9A) simply gradually decreased as the internalisation progressed (yellow line, Figure 6.10C), while the modulus of the cytoplasmic membrane around the internalisation site transiently decreased before recovering back to original value once the internalisation finished. The latter possibly reflects depletion of actin below the capsule as observed before during phagocytosis using fluorescence techniques (Swanson, 2008). Most importantly, the elastic modulus of membrane area above the nucleus remained relatively unchanged during the whole internalisation (cyan line, Figure 6.10C), further supporting the claim that the observed changes in elastic modulus described above were related to capsule internalisation.

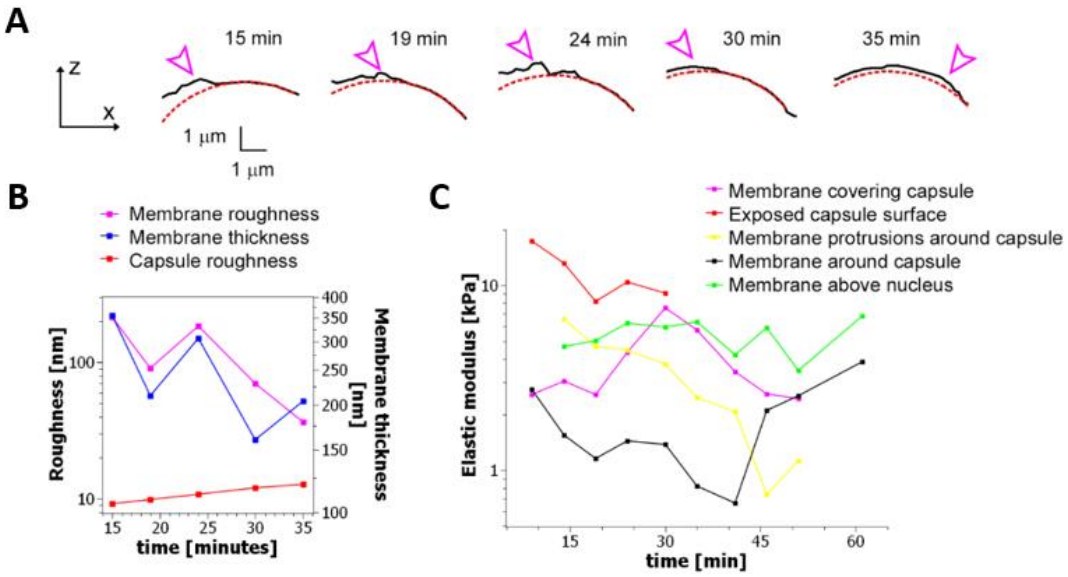

Figure 6.10 Roughness, thickness and elastic modulus analysis of the results presented in Figure 6.9B. (A) Height profiles extracted from sequence in Figure 6.9B showing extension of membrane (magenta arrowhead) over the capsule surface fitted to a circle with 3.8 µm radius (red dotted line). (B) Changes in the thickness (blue line) and roughness (magenta line) of the membrane as it keeps extending over the capsule surface shown in (A). Note that roughness of the exposed capsule surface (red line) remains low and steady throughout the whole process. (C) Changes in the mean elastic modulus of the different areas of membrane and capsule during the internalisation shown in Figure 6.9B.

6.6 Tracking the capsule after internalisation using elastic modulus mapping

After full internalisation, the capsule could no longer be identified in the SICM topography. However, we found out that using the elastic modulus measurement, it was possible to track the presence of the capsule even after the internalisation.

The exact timespan in which the elastic modulus mapping could detect the capsule after the internalisation varied in each case. We observed 6 out of 14 cases, in which the capsule disappeared from the elastic modulus map shortly after the internalisation. As illustrated in Figure 6.11, in this type of events, the elevated membrane patch in the topography due to capsule internalised in limited cytosolic space as described in chapter 5.2 was still clearly visible at 11 min (from the start of recording) and the elastic modulus of the capsule area was significantly higher than the surrounding area (Figure 6.11, 11 min). At 17 min, the bump on the membrane due to internalised capsule is barely recognisable in the topography, but it is clearly identifiable in the elastic modulus image (Figure 6.11, 17 min). However, within another 5 minutes, the presence of capsule was no longer clearly identifiable in neither the topography nor the elastic modulus images Figure 6.11, 22 min). In these cases, the relatively sudden decrease in elastic modulus points to either quick disintegration of the capsule wall or rather quick pulling away of the capsule from the surface of the cell membrane after the internalisation.

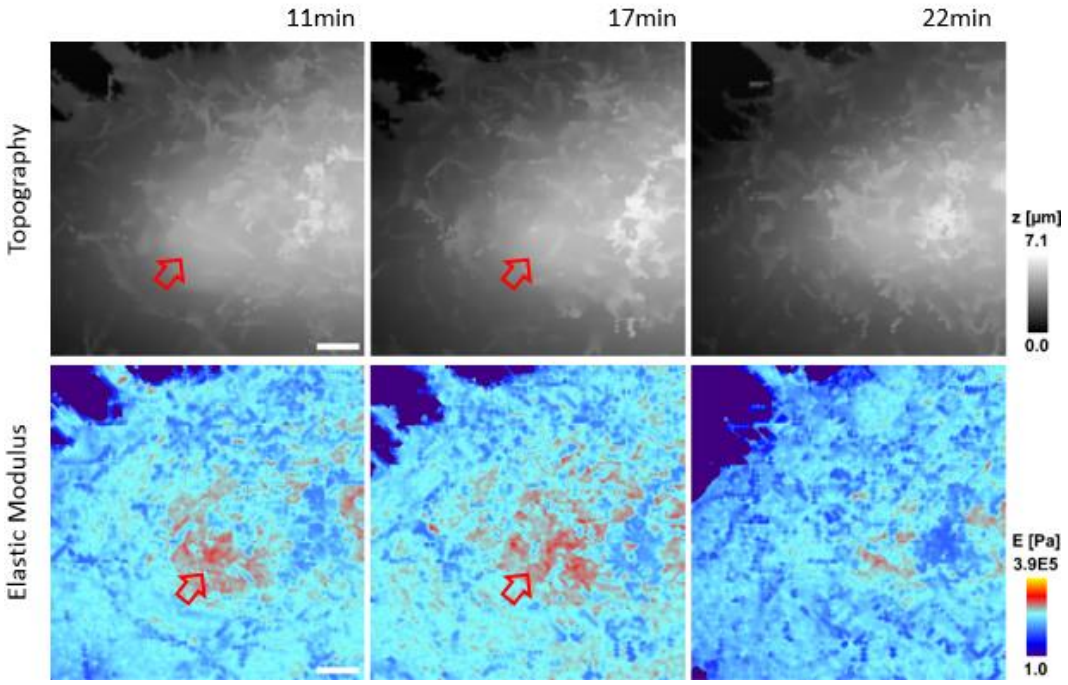

Figure 6.11 The case in which the capsule left the vicinity of membrane surface soon after being internalised. Note the red area with high elastic modulus at 17 min (red arrow) and the absence of this red area in the image at 22 min. (scan size: 12 µm×12 µm, scale bar: 2 µm)

In 8 out of 14 cases, the thickness of the membrane layer covering the microcapsule remained relatively low after the full internalisation. These included 5 cases in which the capsules left bumps on the membrane after internalisation and 3 cases in which there was no trace of capsule left from the topography of the membrane. In these cases, it was possible to visualize the microcapsule underneath the membrane using the mapping of elastic modulus for considerable period of time. As shown in Figure 6.12, at 24 min the surface of the capsule could no longer be distinguished from the cell membrane purely on the basis of the topography image. However, it could still be detected by the elastic modulus measurement as it presented a much higher elastic modulus compared to the surrounding cell membrane. The elastic modulus decreased gradually in the next 23 minutes, but still maintained an elastic modulus higher than the cell membrane. This pointed to persistence of the capsule close to the cell membrane for more than 20 minutes after the full internalisation.

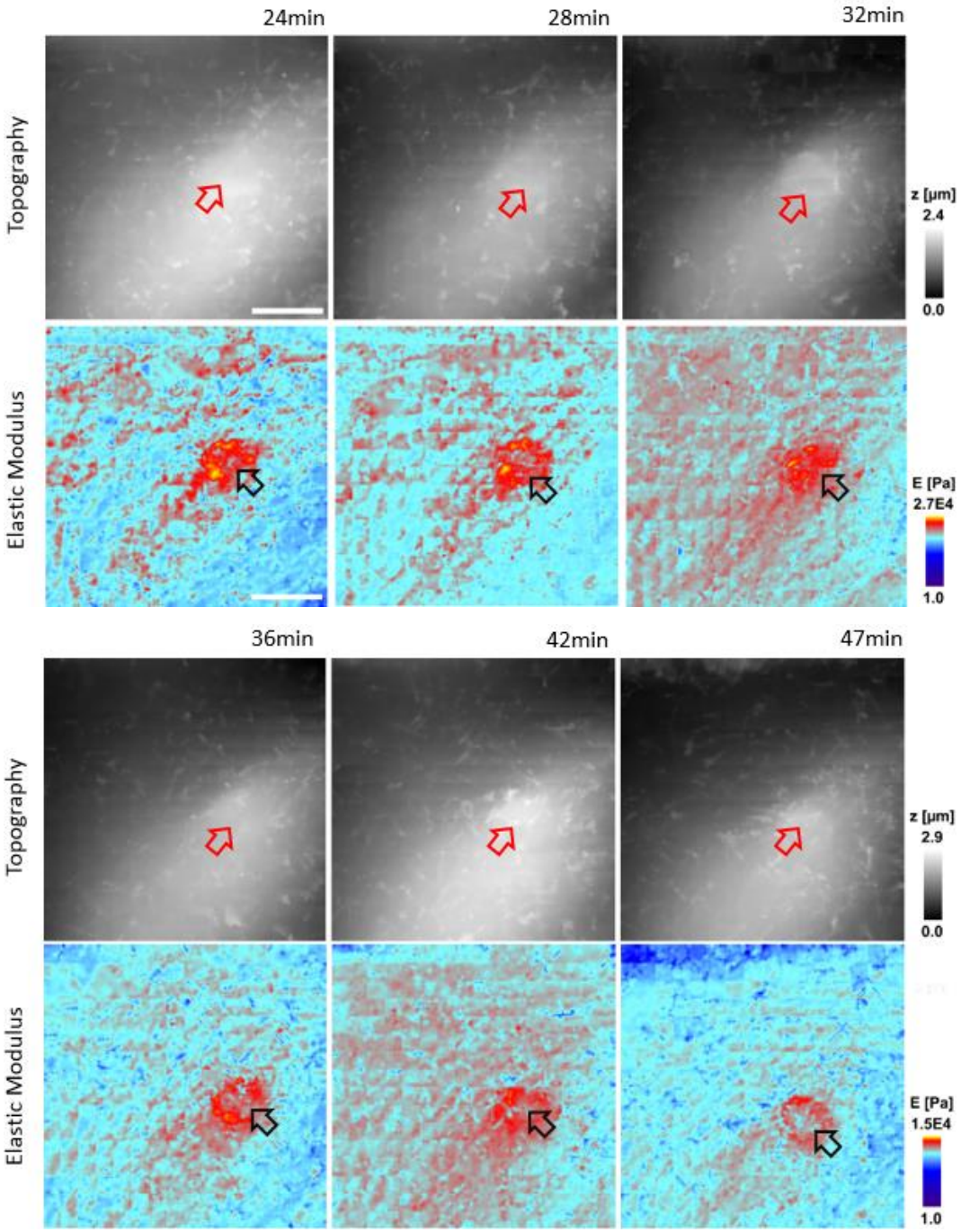

Figure 6.12 The case in which the capsule remained close to the membrane surface after being internalised and moved away from the membrane surface. The capsule pointed by red arrows is almost invisible from topography images. In elastic modulus images the capsule could be clearly identified as area of higher elastic modulus (black arrows). (Scan size: 20 µm×20 µm, scale bar: 5 µm)

What is also worth mentioning from Figure 6.12 is that by the end of the recording, at 47 min, capsule appeared as a red ring from the topography image, which reveal the morphology of the capsule after the internalisation. Therefore, in those cases in which the thickness of the membrane layer covering the microcapsule remained relatively low for substantial amount of time following full internalisation, it was possible to capture post-internalisation events such as buckling of the microcapsule wall (Figure 6.13). Before the internalisation the elastic modulus was higher in the centre of the capsule (red arrowhead, 7 minutes) while after full internalisation it was higher at the edges creating a ring pattern (red arrowheads, 58 minutes). Interestingly, our observations show that the membrane protrusions surrounding and covering the capsule prior the observed buckling appear substantially softer than the capsule and also softer than the surrounding cytoplasmic membrane (Figure 6.13A, at 27 minutes), and seem unlikely to be capable of applying force needed to deform the capsule.

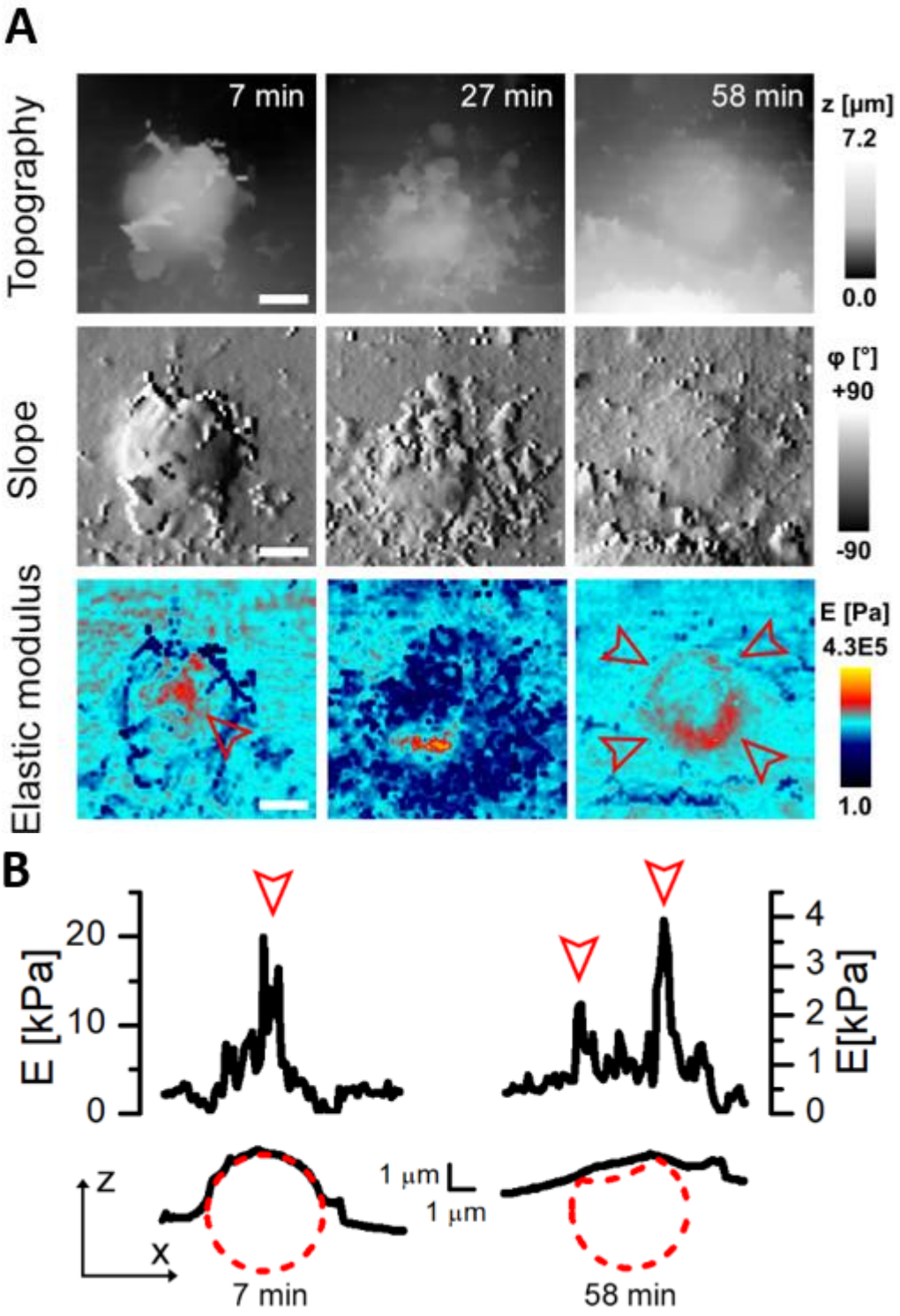

Figure 6.13 Mapping of elastic modulus can be used to study buckling of internalised microcapsules. (A) Topography, slope and elastic modulus images of 10 µm × 10 µm area showing example case of suspected capsule buckling. (Scale bars: 2 µm) (B) Elastic modulus (top) and topography (bottom) profiles across the centre of the capsule shown in (A) 7 min (left) and 58 minutes (right) after the start of recording. Circle with radius 2.4 µm (red dashed line) fitted to topography data represents the capsule before and after internalisation. Profile of elastic modulus observed at 58 minutes show two peaks suggesting collapsed centre of the capsule as illustrated by the red dotted line.

6.7 The effect of chemical inhibitors on the process of internalisation

In order to shed more light on the underlying processes responsible for internalisation of microcapsules we performed a set of experiments using chemical inhibitors. A wide range of substances known to affect endocytosis, micropinocytosis, or phagocytosis have been previously tested (Kastl et al., 2013). Particularly strong inhibition of capsule internalisation has been reported for cytochalasin D and methyl-beta-cyclodextrin (MβCD) (Kastl et al., 2013), however it needs to be noted that these are nonspecific inhibitors. Cytochalasin D inhibits polymerisation of actin, which is a fundamental component of cellular cytoskeleton and provides structural supports for wide range of membrane protrusions such as lamellipodia, filopodia etc. (Vieira et al., 2002). MβCD depletes cholesterol content of cell membrane and is reportedly affecting formation of membrane ruffles (Grimmer et al., 2002). Due to absence of other specific inhibitors relevant to the processes observed in our experiments we decided to investigate the effect of cytochalasin D and MβCD on microcapsule internalisation using SICM.

Due to nonspecific character of cytochalasin D and MβCD we first studied their effect on control group of cells not exposed to capsules. Cells were imaged continuously for half an hour before adding inhibitors at concentrations reported previously (Kastl et al., 2013).

6.7.1 The effect of cytochalasin D

Adding 20 μM of cytochalasin D led to the substantial collapse of the cellular morphology. As illustrated in Figure 6.14, the effect started to reveal at 20min after the adding of the inhibitor. After 38 min of exposing under cytochalasin D the cell loose its original spread out morphology. This result corresponded to the fact that cytochalasin D stopped the polymerisation of the actin. Similar morphological change was also previously observed using SICM by Rheinlaender et al (Rheinlaender and Schaffer, 2013). As the cellular

skeleton of actins decomposed, the cell no longer had its structural support and inevitably collapsed. The large scale morphological changes induced by the cytochalasin D made imaging capsules internalisation using SICM rather problematic. As a non-specific blocker, cytochalasin D also added too much uncertainty to the experiment. Therefore, after reconsideration, we aborted this study with cytochalasin D.

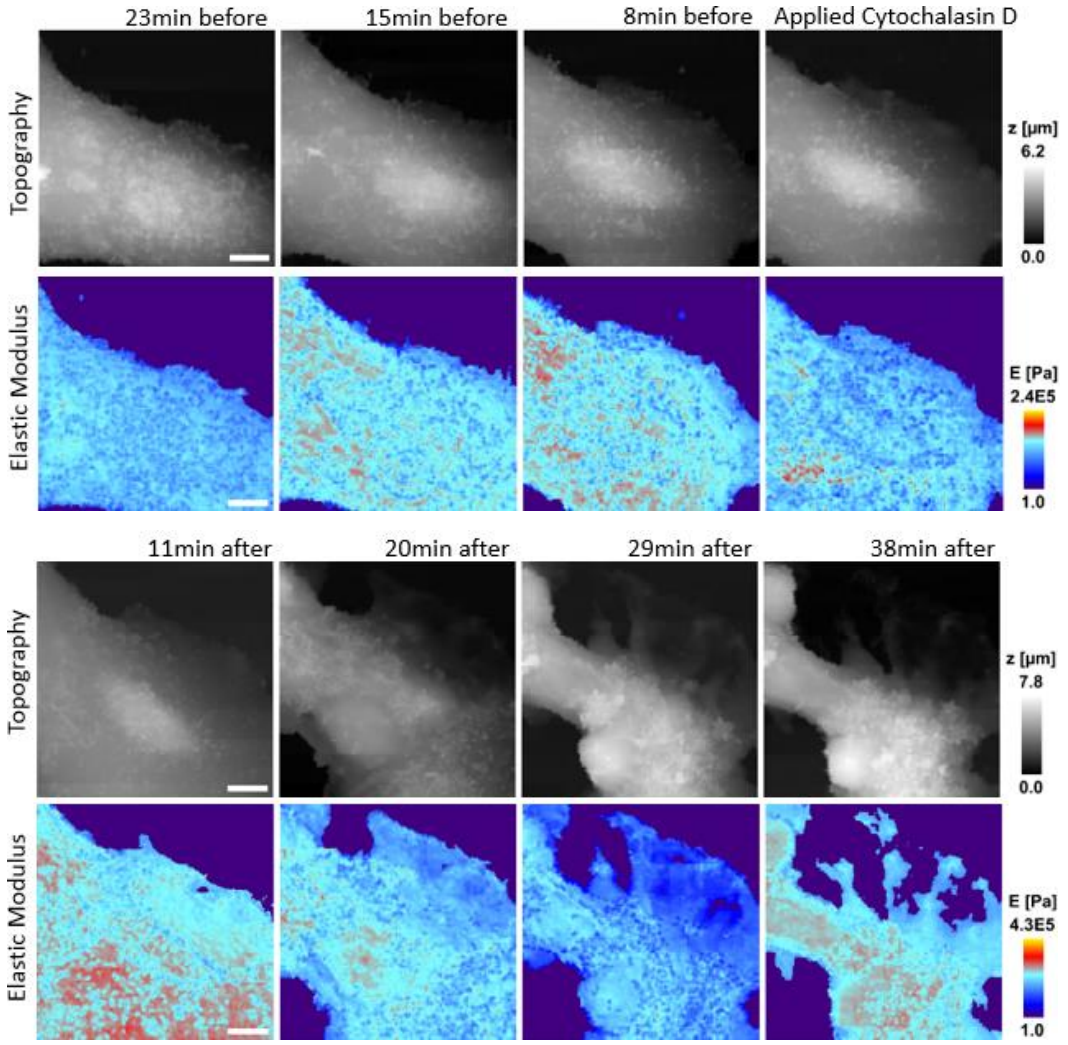

Figure 6.14 The effect of Cytochalasin D on the A549 Cell. (Scan area: 30 µm × 30 µm, scale bar: 5 µm)

6.7.2 The effect of MβCD

Compared to the large scale effect of cytochalasin D, the effect of the MβCD on cell morphology was a much subtler one. The appearance of the cells looked identically the same before and after exposure to the MβCD.

Membrane protrusions could still be seen from its topography after 26 mins of exposure (Figure 6.15). Longer exposure time over an hour leaded to the round-up of certain population of cells (Li et al., 2006). The percentage of cells that rounded up after one hour of exposure in MβCD of different concentrations were roughly estimated by counting under optical microscopy. After 1 hour of exposure, 43 % of cells (13 out of 30) rounded up in 5 mM of MβCD (a concentration suggested by Grimmer (Grimmer et al., 2002)). Meanwhile, only 10 % of cells (3 out of 30) rounded up in 2 mM of MβCD (a concentration suggested by Kastl (Kastl et al., 2013)). This was a promising result suggesting that while 2 mM of MβCD was reported to cause the total inhibition of the internalisation process (Kastl et al., 2013), it could maintain a good cell viability and its original morphology.

Further experiment was designed to investigate the effect of 2 mM of MβCD on the process of internalisation. In these experiments, after the mounting the petri dish with cell culture inside on the SICM stage, capsules and the inhibitors were added into the cell culture medium at the same time. The results showed clear evidence that 2 mM of MβCD effected the attachment of the capsules to the cell membranes. At the beginning, when the membrane composition had not yet been affected by MβCD, the capsules attached to the cell membrane just as those without inhibitor (Figure 6.16A 5 min, note the perfect rounded shape of the capsule). However, only minutes later, signs of dislocation began to appear (Figure 6.16, note the distorted shape of the capsule) suggesting that the attachment became to weaken with time as MβCD started to deplete the cholesterol from the cell membrane. About 30 min after the adding of MβCD, some capsules started to lose the attachment and rolled away from the cell membrane. For those capsules still attached to the cell membrane, their attachments were also too weak to withstand the pushing the pipette during the scanning (Figure 6.16B-C). As the pipette hopped near them, the capsules rolled away because of the pushing effect

described before in previous chapter. One hour after applying 2 mM of MβCD, only few capsules still attached to the cell membrane. The images showed in Figure 6.16 were from one experiment on one cell culture and were representative of the results from three experiments.

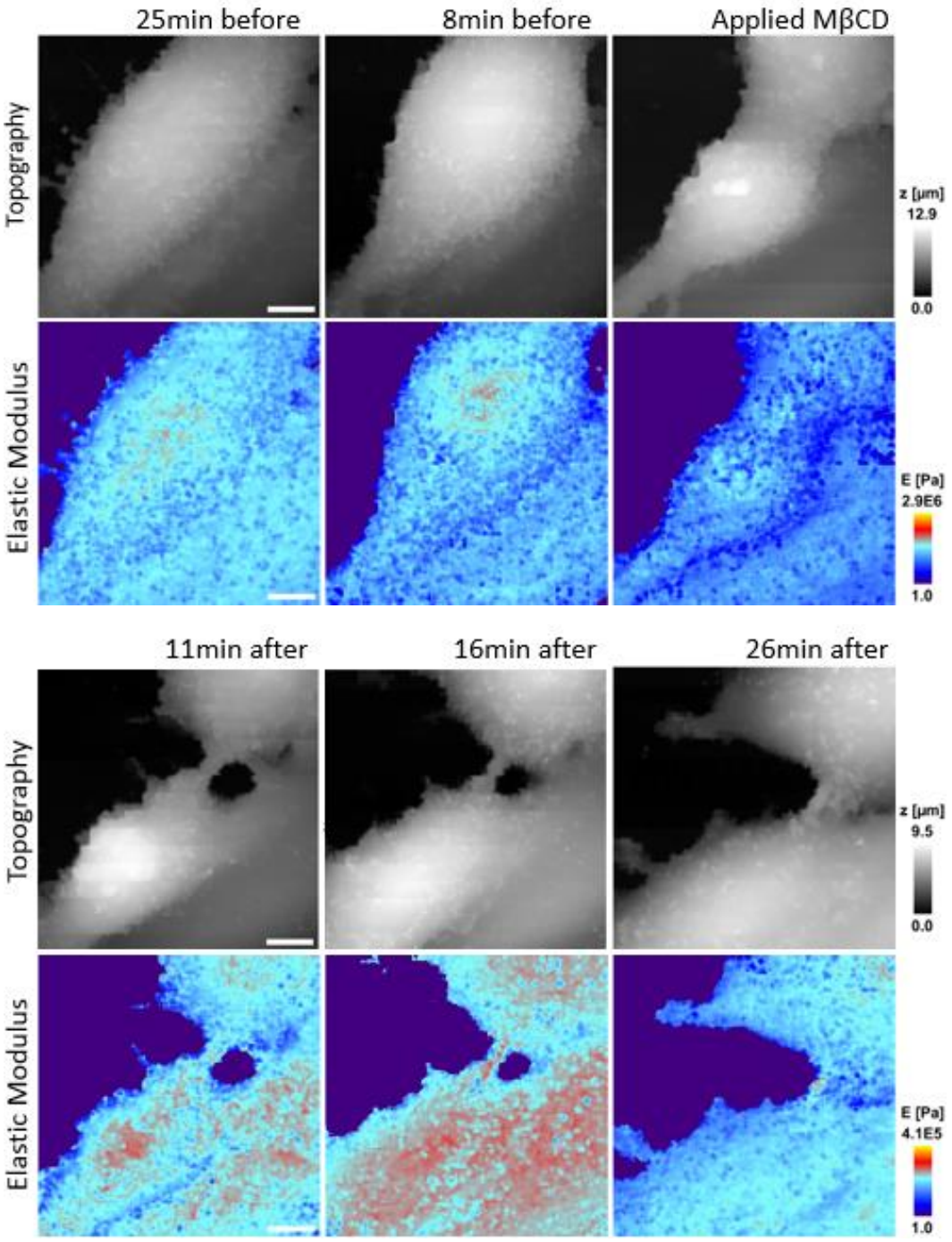

Figure 6.15 The effect of MβCD on A549 Cell. This particular cell divided into two during the time span of imaging, suggesting that neither the scanning of pipette nor the presence of 2 mM of MβCD interfered the process of cell division. (Scan area: 30 µm × 30 µm, scale bar: 5 µm)

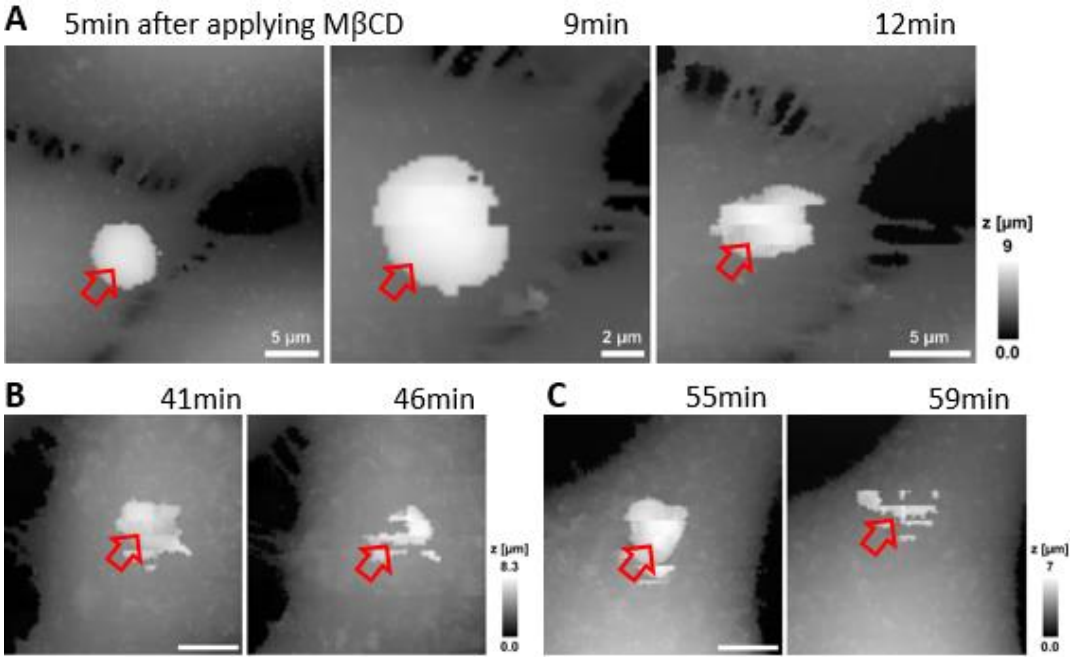

Figure 6.16 Capsule loose attachment as a result of MβCD. (A) Capsule dislocated shortly after the applying of MβCD. (B, C) Capsule rolled away after the cells were exposed in MβCD for over 30 minutes. (Scanning size: 30 µm×30 µm, scale bar: 5 µm×5 µm)

Despite the significant impact of MβCD on capsule attachment, there was no visible alternation to the morphology of cell membrane. Figure 6.17 showed three topography images of three cells, each had a capsule attached to them (observed from optical microscope), however, all three capsules rolled away half hour after adding the MβCD. The roughness R_{ms} (root mean square average of the profile height deviation) remained relatively unchanged half hour after the applying of 2 mM of MβCD, from 131.8 ± 24.6 (mean R_{ms} measured from 11 images) before applying MβCD to 134 ± 12.9 (mean R_{ms} measured from 11 images) after applying MβCD.

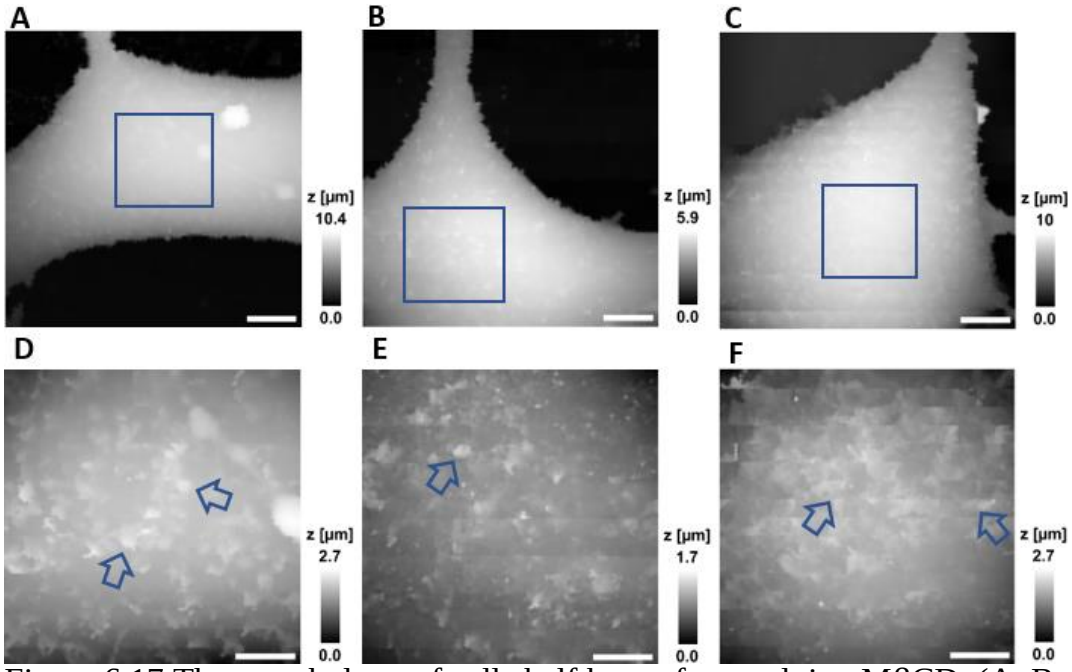

Figure 6.17 The morphology of cells half hour after applying MβCD. (A, B, C) the morphology of three different cells (Scanning size: 30 µm×30 µm, scale bar: 5 µm×5 µm). (D, E, F) close-up looks at the cell membranes from the area enclosed by the blue squares in A, B, C respectively. Note the presence of membrane protrusions over the cell membrane (blue arrows). (Scanning size: 10 µm×10 µm, scale bar: 2 µm×2 µm)

Though the capsules rolling was not restricted to MβCD as we described this also in previous chapter (Chapter 5.2). With those inhibitor-free samples we only observed capsule rolling occasionally shortly after the capsule attached to the cell membrane. The phenomenon of capsules rolled away simultaneously after attached to the cell membrane for a period of time was something never occurred before and could only be a result of the effect of MβCD. Previous research reported that cell membrane experienced a 31 % and 42 % decrease in cholesterol content after incubated with 5 mM MβCD for 30 min and 60 min respectively (Grimmer et al., 2002). No results on 2 mM MβCD could be found according to our knowledge. Nevertheless, we could expect that in our experiment, it was also the suppression in cholesterol level by 2 mM MβCD that disrupted the attachment of the capsule to the cell membrane and as a result, inhibited the entire internalisation process. This finding not only corresponded but also provided further information to the previous studies that cholesterol play an important role in micropinocytosis

by facilitating the formation of membrane ruffles (Grimmer et al., 2002, Ilangumaran and Hoessli, 1998, Lingwood and Simons, 2010, Lingwood et al., 2009).

7. Specific aspects of microcapsules internalisation observed using SICM

7.1 Targeting the initial stage of internalisation with capsule manipulation

In chapter 5.5 we described the procedure developed for imaging the internalisation of microcapsules. According to the procedure, we added the capsule to the cell culture by dipping drops of capsule suspension into the cell culture medium. One of the difficulties with suspension of capsules randomly landing on cells is that the exact moment of when the capsule made contact with the cell membrane is unknown unless it happened right in the area currently viewed by the microscope. To address this limitation, we utilized the possibility of using the glass nanopipette and x-y-z nano-positioning capability of the SICM to move capsules landed on coverslip onto the cell membrane, thus defining the moment of first contact between the two.

There were two possible ways to perform this manipulation. The first one involved grabbing and releasing the capsule by utilizing pressurized fluid flow at the tip opening. This was achieved by using pipette with large tip opening (200 nm in diameter) plugged into patch-clamp pipette holder and applying negative pressure to the pressure side-port of the pipette holder to capture nearby capsule and positive pressure to release it. It was proved possible to move capsule around with this method. However, the success rate was extremely low. We only managed to perform 3 capsule moving manipulations out of 10 trials. We also failed to capture the manipulation process as just the operation itself was already too manually demanding. The main difficulty with this method was that the capsule had a tendency to stick to the pipette tip upon application of suction and it proved difficult to be released afterwards using positive pressure. There were also great difficulties in its manual operations. The viewfinder of the optical microscope was dim

due to the use of 100x objective and also due to the fact that the light was blocked by the pipette holder. The pipette also needed to be changed frequently and a lot of manual operations were involved as the pipette used for moving capsule was not suitable for scanning images due to its large tip opening.

Due to the complexity of first above described method, later we developed an easier but less controllable alternative method. In this method, the side wall of the pipette was used to push the capsule that landed on the coverslip towards the cell. This method was proved to be highly reliable and repeatable. After few preliminary trials, we managed to successfully operate 6 consecutive capsule moving manipulations. For the purpose of demonstration, later we also dyed the cells with CellMask™ orange and recorded the whole manipulation process with time lapse images using epifluorescence microscope (Figure 7.1). First, the pipette tip was placed at a position where pipette tip, capsule and the aimed destination of the capsule form a straight line (Figure 7.1A). Then the feedback control was switched off to stop the pipette from hopping. Without feedback control, the pipette tip would maintain its height at approximately 2 μm away from the bottom of the petri dish even when it approached the capsule. After that, the pipette was moved manually towards the capsule until they made contacts (Figure 7.1B). Further horizontal movement of the pipette push the capsule towards the cell and later onto the cell (Figure 7.1C-E). As cell has a sloped membrane surface, the height of the pipette tip need to be adjusted in order to push the capsule onto the slope (Figure 7.1F-G). After the capsule was moved onto the cell, the pipette could be retracted without the adhesion of capsule (Figure 7.1H) for most of the time (4 out of 6). We also found that the adhesion force between the capsule and cell membrane was stronger than that of the capsule and pipette wall. Even if the capsule did attach to the pipette, we would still be able to retract the pipette without lifting the capsule by allowing the capsule to firmly attach to the cell membrane. This same pipette could later be used

for scanning the internalisation process that followed as this method did not required the using of large size pipettes. There was also no risk of pipette blockage after this operation as the pipette tip did not make direct contact with either the capsule or the cell.

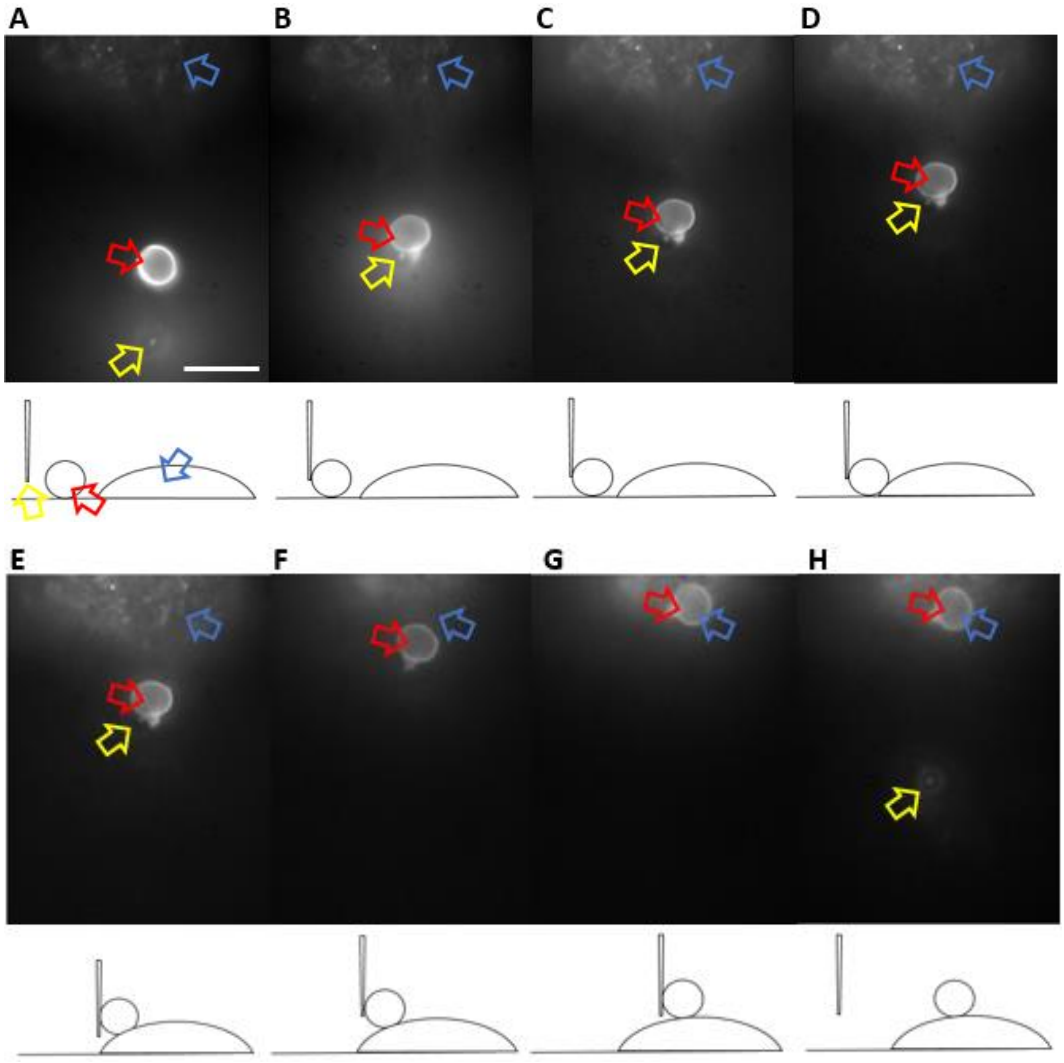

Figure 7.1 Epifluorescence time lapse images and their corresponding schematics demonstrating the procedure used for moving capsule by pushing the capsule (red arrows) with the side wall of the pipette (yellow arrows). The capsule was moved from its original position on the bottom of the petri dish (A, red arrow) to the final position on top of the cell (G, H, blue arrows). (Scale bar: 10 µm)

With the second method, we managed to precisely control and record the moment of first contact between the capsule and the cell. We did 5 successful manipulations with capsule moving followed by observing the interaction between the capsule and the cell with SICM imaging. Out of these 5

experiments, we observed 2 successful internalisations. In one of these 2 experiments (Figure 7.2), a single nanopipette was used throughout the whole experiment. Firstly, it was used to image a capsule that landed on the bottom of the petri dish (Figure 7.2A, top panel). Secondly, it was used to move that capsule onto the cell membrane. Finally, it was used for scanning both the topography and the elastic modulus of the following event and successfully recorded the internalisation process of that capsule entering the cell (Figure 7.2A, middle and bottom panel, Figure 7.2B). This was a perfect demonstration of nanopipette as a tool for both nano-imaging and nano-manipulation.

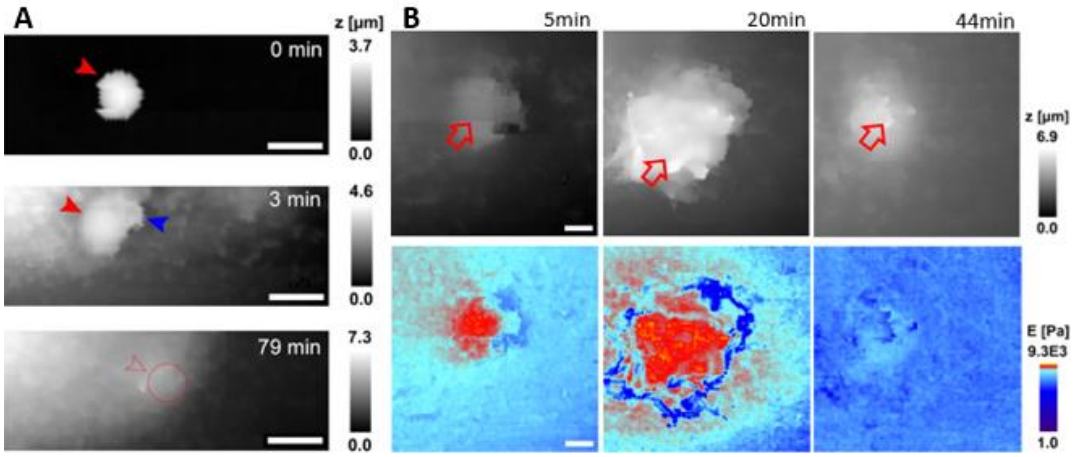

Figure 7.2 (A) Membrane protrusions start forming around the capsule within minutes from the first contact. Topographic images showing the stages Top panel, capsule landed on the coverslip. Middle panel, topography recording finished 3 minutes after the capsule was moved from substrate onto the cell membrane. Bottom panel, time lapse images showed the process of internalisation after it was moved onto the cell. (Scale bar: 5 µm) (B) Topography images and elastic modulus measurement recording the internalisation process of the capsule in A. (Scale bar: 2 µm)

In that experiment, the capsule was imaged right after we moved it onto the cell. The first image revealed that membrane protrusion started forming around the capsule surprisingly quickly – within the first 3 minutes of the first contact (Figure 7.2A, middle panel). The capsule has been internalised within 45 min, and after 80 minutes only a small remaining "bulge" gave away the location of the previous internalisation (Figure 7.2A, red dotted

circle). These times are comparable to the observations of randomly landing capsules where the time of first contact is uncertain.

7.2 Other notable behaviours observed during imaging the internalisation of microcapsules

In this section, less common but notable behaviour observed during imaging capsule internalisation is reported. Some of the behaviour might be related to the internalisation but exhibits some distinct features not present in the common behaviour described in detail in Chapter 6. So, these behaviours were not able to be easily confirmed as internalisation and worth additional attention in this section.

7.2.1 Movement of cells triggered by capsule

We observed the movement of 3T3 cell towards capsule from live time lapse confocal images. Later this behaviour was also observed with A549 cells twice from SICM time lapse images (Figure 7.3). In one experiment, we managed to capture this behaviour with 30 μm × 30 μm scan, detailed information of the cell movement was revealed, as illustrated in Figure 7.4.

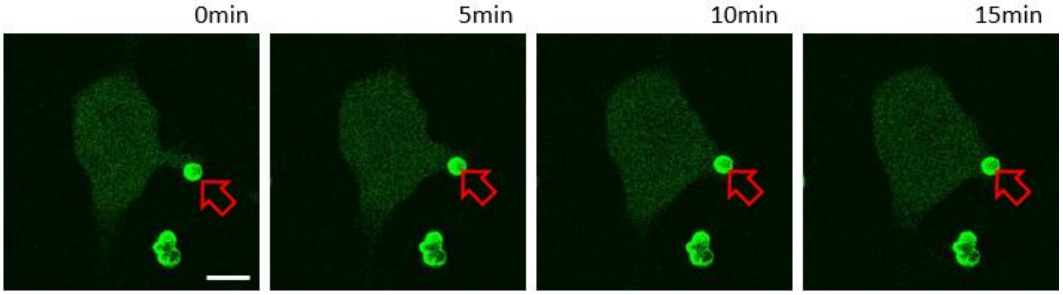

Figure 7.3 Live time lapse confocal images showing the movement of the cell towards the capsule. (Scale bar: 10 μm)

At the beginning of the recording, the capsule (red arrow) was not attached to the main body of the cell but on its periphery. This periphery was a thin layer of membrane (green arrow, Figure 7.4) that extended outside the main body of the cell (Figure 7.4C). This thin layer of membrane had a relative flat

appearance with a mean thickness of 1.31 ± 1.10 μm and extended about 12 μm outside the cell main body. This appearance was distinctively different from that of the main body, which had a mean thickness of 9.84 ± 2.56 μm and a shape that resembled an elongated water drop. The identity and function of this thin layer of membrane was unclear. However, it was likely to play a role in the motility of the cell as later the main body of the cell migrated towards this direction. The fact that the boundary of main body advanced 8 μm in 18 min (Figure 7.4B) and stopped advancing after reach the capsule suggested that it was not merely a coincident but a response of cell triggered by the presence of the capsule. Note the elastic modulus of the capsule at 0 min, which had only an average elastic modulus of 3075 Pa. The capsule that sits on the thin layer of membrane would be expected to have a much higher elastic modulus. However, here this capsule had an elastic modulus that close to that of the cell membrane (2259 Pa), suggesting that the capsule had already been covered by a certain amount of membrane at the beginning of the imaging. Membrane protrusions formed around the capsule (Figure 7.4 Slope images, 0 min and 8 min, cyan arrow) at the beginning of the imaging when the main body of the cell was still far away from the capsule. These protrusions formed in a way similar to those appeared in other internalisation events suggesting that this thin layer of membrane had already started to interact with the capsule before the main body of the cell joined in. This behaviour was also observed previously by us on 3T3 cells, as illustrated in Figure 7.5. In which the capsules outside the main body of the cells were covered by membrane from pseudopodia.

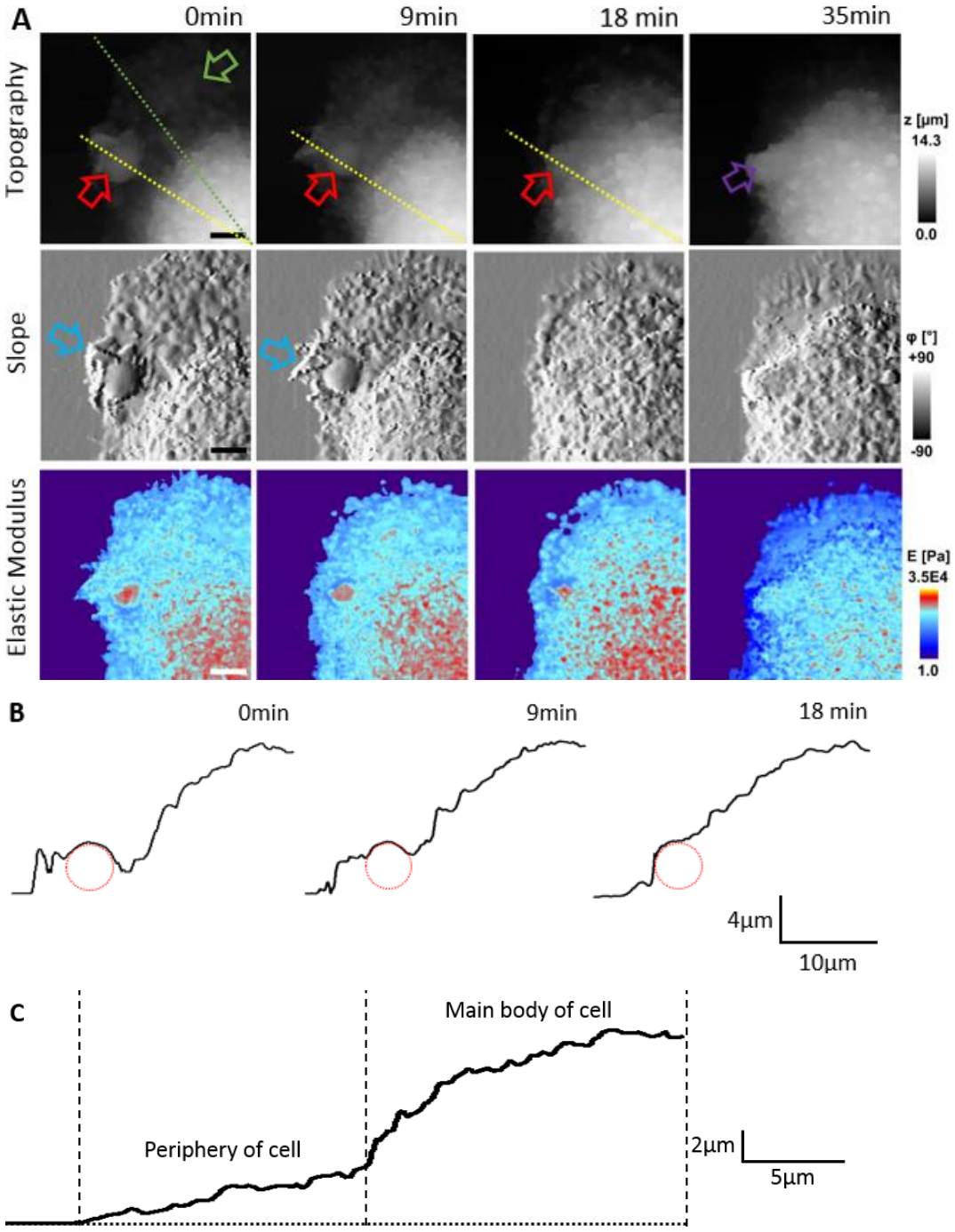

Figure 7.4 Movement of the cell towards capsule. (A) Time lapse topography images shown together with corresponding slop images and elastic modulus images. The time 0 min marks the beginning of the recording. Note the position of the capsule (red arrow) at 0 min, it was attached to a thin layer of membrane (green arrow) that extended outside the main body of the cell and the irregular protrusion (purple arrowhead) formed at the site where the capsule used to be at 35 min. (Scan area: 30 µm × 30 µm, scale bar: 5 µm) (B) The profile of the cross section subtracted from the yellow dotted line in the topography images at 0 min, 9 min and 18 min, showing the migration of the cell main body in this 18 minutes. (C) The profile of the cross section subtracted from the yellow dotted line in the topography images at 0min, the periphery of the cell and the main body of the cell could be distinguished from their different appearance.

What is also worth mentioning is the presence of an irregular shaped protrusion at the later stage of the recording (Figure 7.4A 35 min). The capsule was fully covered by the cell and almost disappear from topography at 18 min. However, there was this irregular part (purple arrow) began to stick out of the cell as the observation continue. The stiffness measurement revealed that the part that stick out of the cell main body had a much lower elastic modulus than the capsule, so it was unlikely to be the capsule itself or at least it was covered by a considerably thick layer of membrane.

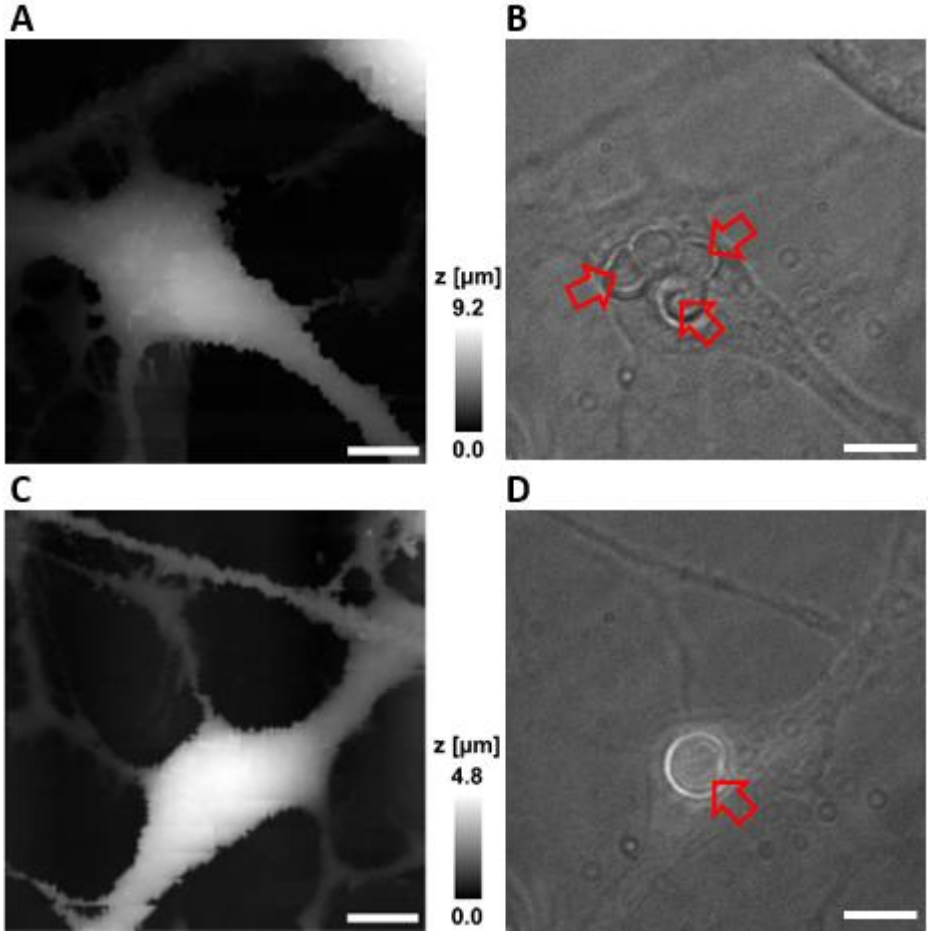

Figure 7.5 The membrane covering of the capsules on the pseudopodia of the 3T3 cells. (A, C) SICM images showed no sign of capsules (B, D) Optical microscopy images of the corresponding areas in A and C. Note the presence of capsules (red arrows). (Scale bar: 5 µm)

To conclude, this special recording (Figure 7.4) showed the response of the cell to the capsule that landed outside its main body. The results showed that

the thin layer of membrane outside the main body was capable of covering the capsule with membrane ruffles. It was also likely that signal was sent to the main body of the cell to trigger its migration towards the capsule.

7.3.2 Round-up of the cell

During the process of imaging, cells occasionally went through relatively large scale morphological changes. The most frequent large-scale morphological change observed was the round-up of the cell as illustrated in Figure 7.6. At the beginning of the recording, the cell was relatively flat and stretched out towards the bottom left corner (Figure 7.6A, 0 min) and the elastic modulus was relatively low (Figure 7.6B, 5 min). In the next one hour, the cell gradually shrank in its size as the periphery of the cell (the side that stretched towards the bottom of the image at 0 min) receded by 13 μm. By the end of the recording, the cell had shrunk into a rounded shape (Figure 7.6A, 85 min) and the elastic modulus of the cell had increased significantly (Figure 7.6B, 89 min). This rounded-up was also accompanied by the increase in the height of the cell, which could also be confirmed by SICM topography. As for this case, the cell almost doubled its height from 5.5 μm (0 min) to 9.5 μm (85 min). This rounded-up effect could also be viewed from the optical microscope.

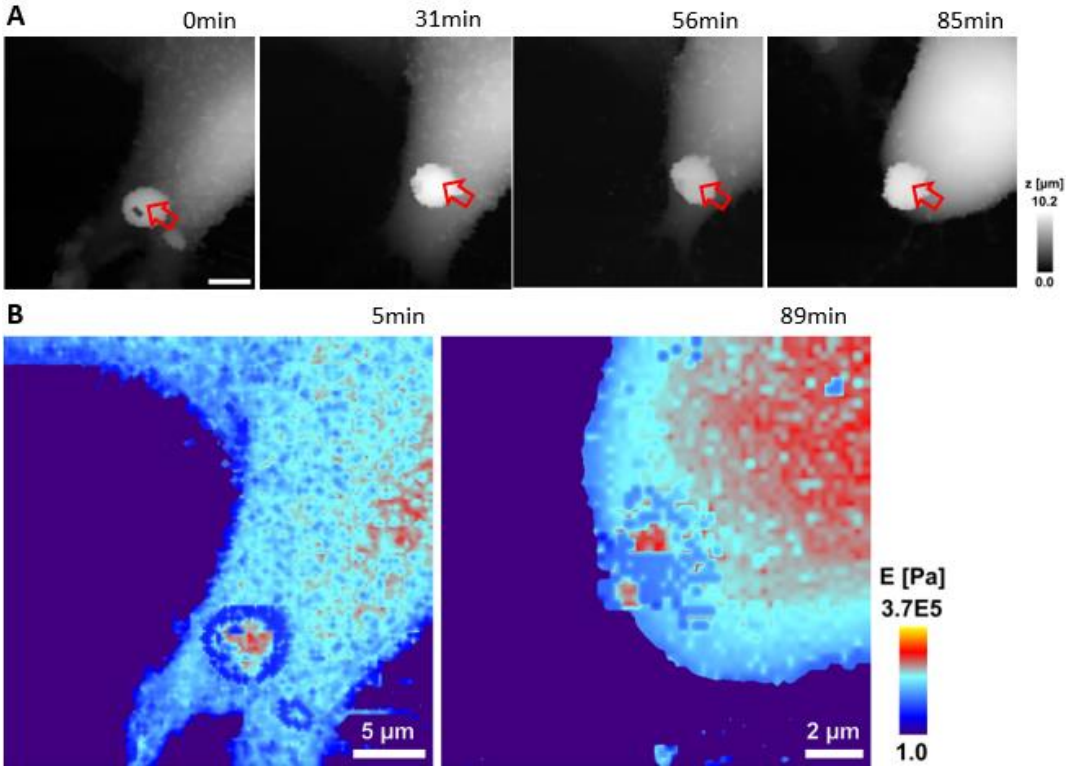

Figure 7.6 Round-up of the cell. (A) Time lapse topography images, note that the cell was spreading at 0 min and was rounded-up at 85 min. (Capsule pointed by red arrows, can size: 30 µm×30 µm, scale bar: 5 µm) (B) Elastic modulus images of the cell at 5min when it was spreading (left) and at 89 min when it had rounded-up (right). (scan size: 30 µm×30 µm (left), 15 µm×15 µm (right))

Sometimes (we imaged 2 of over 50 cases), the round-up of cell was accompanied by the successful internalisation of microcapsule, as illustrated in Figure 7.7. The cell immediately responded to the attachment of the capsule with membrane protrusions enormous in scale (Figure 7.7, 5 min). The whole internalisation finished within 19 minutes. Meanwhile, the height of the cell increased from 6.8 µm (0 min) to 15.7 µm (19 min), accompanied by the recession of the cell periphery. In both cases, the capsules were internalised by the cell regardless the large morphological change that occurred to the cell.

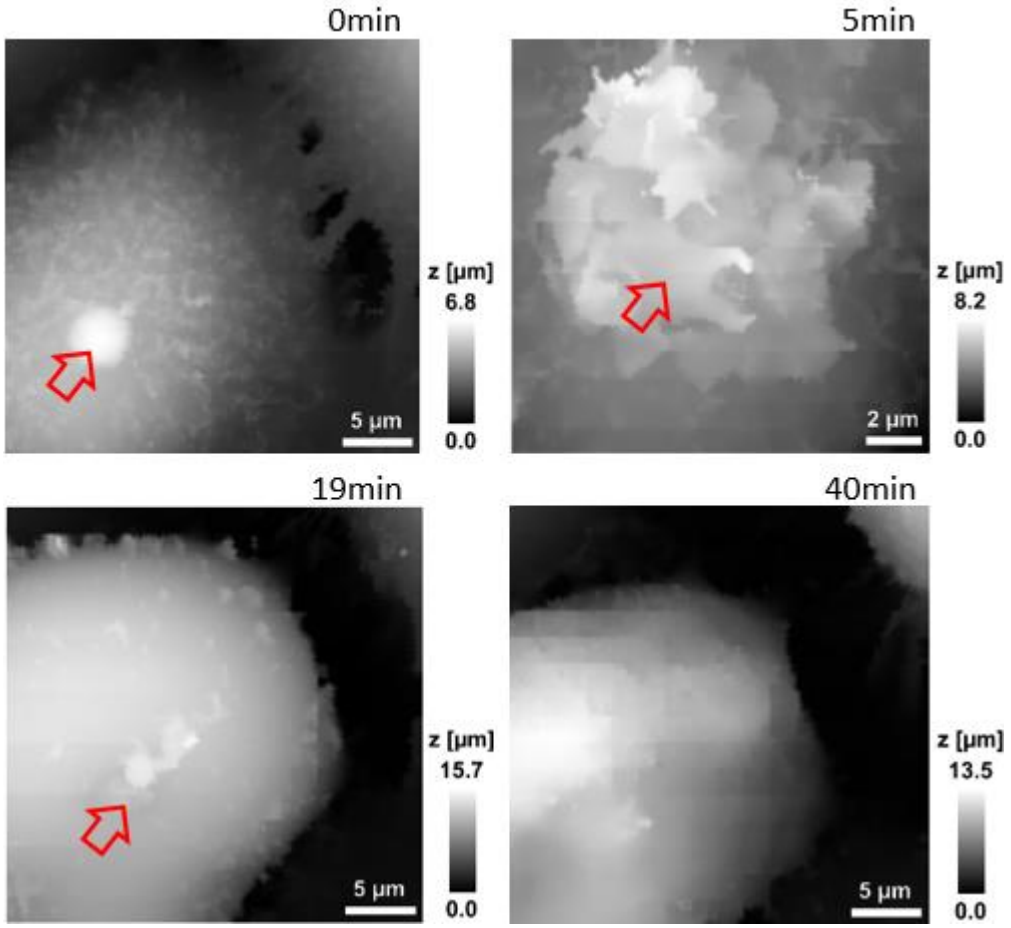

Figure 7.7 Round-up of the cell that happened accompanied by the internalisation of the capsule. The capsule and the site of capsule internalisation were pointed with red arrows.

The mechanism behind this round-up was complex, which could be programmed or unprogrammed cell death or cell division. It needs molecular biology means and knowledge to identify its exact mechanism, which is beyond the scope of this research. Therefore, we were not able to explain its mechanism and if this round-up of the cell was triggered by capsule or not. What was also unknown was the influence of this behaviour on cells' function of internalisation. Because of these uncertainties, in practice, we tried to avoid imaging those cells with increased height at the early stage of the imaging. In rare cases (around 10 %), in which round-up happened on the cells that was being time lapse imaged for their internalisation process, we considered those images sequences as neither internalised cases nor uninternalised cases.

8. Discussion

In this thesis, we established a procedure for SICM to image the live process of microcapsule internalisation. By using this procedure, we successfully visualised the whole internalisation process with time lapse topography images as well as elastic modulus mapping images.

Previously, the advantages of SICM were exploited in the study of nanoparticle internalisation (Shevchuk et al., 2012, Novak et al., 2014). The method we used shares many common traits with those methods used in previous research, including the use of SICM topography imaging combined with fluorescence microscopy and the recording of live cell process using time lapse images with optimized frame rate (Shevchuk et al., 2012, Novak et al., 2014). However, the height of the endocytic structures imaged previously using SICM was in the range of 0.2-1 μm (Shevchuk et al., 2012, Novak et al., 2014), which is substantially less than in our work here. While the previous work focused on overcoming the challenge of achieving nanoscale resolution of relatively small structures at sub-minute imaging speed, the challenge in our case was to achieve nanoscale resolution of processes where dynamic nanoscale membrane structures interact with foreign objects of microscale dimensions. It is of note that we were not able to find any previous work reporting similar achievement with any other scanning probe microscopy technique, including the well-established atomic force microscopy.

Other experimental details of our work, such as imaging microcapsules that attached to a certain region of the cell membrane to optimize the possibility of observing the internalisation, or examining the effect of elastic modulus mapping using the Clarke et al method (Clarke et al., 2016) on live membrane process have, to our best knowledge, never been reported before.

We found that capsules that attached to the edge of the cell or the boundary of two cells were less likely (or took longer) to be internalised by the cells. As far as we know, this factor has not been taken into consideration in previous researches on capsule internalisation. As a result, cell cultures with low confluency were used in our experiments in order to identify individual cells. The confluency used in previous researches were not specified, however, from the fluorescent images presented in some articles, we found low confluency has been used before in some of the previous researches (Sukhorukov et al., 2005, Javier et al., 2006).

Hopping mode SICM has been reported to be capable of imaging tall structures with sudden increase in height (Novak et al., 2009). Convoluted structures such as live hippocampal neurons and vertically protruding mechanosensitive stereocilia were successfully visualised without noticeable artefacts (Novak et al., 2009). However, in our experiment, when we imaged microcapsules shortly after they attached to cell membrane, significant artefacts were observed. In some extreme cases, the capsules were even pushed away by the scanning of the pipette, pointing to a limitation of the current implementation of the hopping mode SICM regarding imaging of the early stages of capsule-cell interaction. As explained in Chapter 5.2.2 this is mainly due to non-zero cone-angle of the nanopipette tip. Imaging artefacts due to non-zero cone angle have been previously reported when imaging similar overhanging structures using AFM cantilevers (see Figure 2.14 in Chapter 2.4.2) (Rheinlaender et al., 2011). Here we showed that a 5 minutes waiting time introduced between the applying of the capsules and the starting of imaging is enough to allow the capsule to attach firmly to the cell membrane and to virtually eliminate the artefacts.

The effect of elastic modulus mapping on the live internalisation process of microcapsule has not been previously investigated. In previous research that studied similar dynamic cellular process (Shevchuk et al., 2012, Novak et al.,

2014), only the topography of the sample was investigated and the imaging method for topography was considered as non-contact (Korchev et al., 1997a). However, for elastic modulus mapping, pipette exerts small, but non-zero force onto the sample surface at higher setpoints and causes deformation to the sample (Clarke et al., 2016). Although we were able to record whole process of internalisation while measuring elastic modulus, suggesting the deformation induced does not completely prevent capsule internalisation, we observed both pushing away of the capsule and the deformation of membrane underneath the capsule by the nanopipette.

With the procedure we established, we successfully recorded the interaction between the microcapsules and the cells. We recorded 27 cases, with 14 cases showing successful capsule internalisation. The overall internalisation rate, 51.9 % (14/27), corresponds to the results we got from cells incubated with capsule for one hour using confocal microscopy (55.7 %). This is lower than the ~70 % reported by Sukhorukov et al (5 μm capsules and MDA-MB-435s breast cancer cell, incubated for 1 hour, analysed using phase-contrast microscopy) (Sukhorukov et al., 2005). However, it is worth noting that the phase-contrast microscope used by Sukhorukov et al tend to overestimate the internalisation rate of the microcapsules as it is difficult to distinguish internalised capsules from those attach to the membrane surface (Javier et al., 2006). Generally speaking, it was difficult to directly compare the results on internalisation rate with previous reports as the capsules sizes, capsule compositions, cell lines, and analysis methods varied substantially across these studies.

In those cases in which the capsule got internalised, we observed the formation of membrane protrusion at the vicinity of the capsule, followed by the restructuring of these protrusions into membrane ruffles, these membrane ruffles then extended over the surface of the capsule and covered the whole surface of the capsule. The early stage of internalisation resembled the

filopodia-like structure reported by Kastl et al using SEM (Kastl et al., 2013). With SICM, we revealed these similar details with resolution that comparable to the SEM. However, the advantage of SICM over SEM is that these images were captured on live cell, so we could follow the whole process instead of providing random snapshot. Time lapse imaging allowed us to make a conclusion that the filopodia-like protrusions interacting with the microcapsules appear to be necessary but not sufficient for successful internalisation, a conclusion that could not be made based on static SEM imaging.

In those cases in which capsules did not get internalised within the time span of our recording, we observed the internalisation process stalled at its early stage where the membrane protrusion formed around the capsule failed to proceed by restructuring into membrane ruffles. This founding confirmed the previous concern suggested by Javier et al that the number of internalised capsules might be overestimated by using conventional optical microscopy as those capsules attached to the surface of the cell membrane might also be counted as internalised (Javier et al., 2006). The early stage interaction between capsule and cell membrane also suggests that the sample washing used before flow cytometry in previous research (Ai et al., 2005) might not be sufficient to remove the capsules from the membrane surface. As a result, the outcomes of the flow cytometry using this method may lead to overestimated numbers of internalised capsules. Additional clues, such as from the pH sensitive dye (Kreft et al., 2007, Semmling et al., 2008), should be used to properly analyse the internalisation rate using fluorescence and flow cytometry.

Lower elastic modulus of capsules observed in our experiments is likely due to the fact that the capsule is sitting on a soft cell with elastic modulus typically in the range of few kPa. This explanation is supported by the fact that measured values of elastic modulus of capsules are in a good agreement

with calculated equivalent elastic modulus of a model representing the capsule and the cell as two solid layers on top of each other exposed to the same stress. In two layers model, the capsule is represented by layer with elastic modulus E_{cap} and height h_{cap} which is equal to the diameter of the capsule. Cell is represented by layer with elastic modulus E_{cell} and the height h_{cell}. Compression induced by the nanopipette yields the measured elastic modulus E_{Meas}. If both layers are exposed to the same stress, then the two layers can be characterised by equivalent elastic modulus E_{Eq} calculated as:

$$E_{Eq} = \frac{h_{cell} + h_{cap}}{\frac{h_{cell}}{E_{cell}} + \frac{h_{cap}}{E_{cap}}}$$

If the elastic modulus of the capsule is substantially higher than the elastic modulus of the cell ($E_{cap} \gg E_{cell}$), the equation for equivalent elastic modulus simplifies to:

$$E_{Eq} \approx E_{cell} \times \frac{h_{cell} + h_{cap}}{h_{cell}}$$

Due to very low stress imposed by the nanopipette (typically in the range 1-100 Pa) (Clarke et al., 2016) the expected elastic modulus of capsules adhered to bare glass is beyond the measurement range of the method used here. Stress of 100 Pa would cause the capsule to compress by less than 5 pm (assuming capsule with diameter of 5 μm and equivalent elastic modulus of at least 100 MPa), three orders of magnitude below the practical resolution limit of SICM.

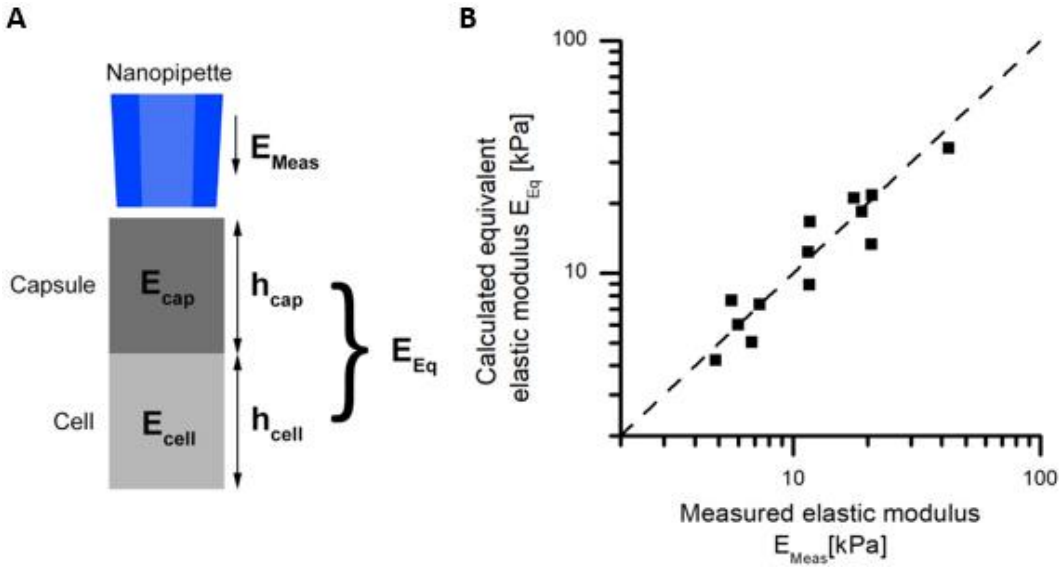

Figure 8.1 Measured values of elastic modulus of microcapsules on the cell membrane correspond to equivalent elastic modulus of a two-layer model. (A) Schematic of the two layers model. (B) Comparison of the calculated equivalent elastic modulus E_{Eq} assuming the model in (A) and elastic modulus of exposed capsules sitting on cell membrane E_{Meas} measured by SICM. The dashed line represents $E_{Eq} = E_{Meas}$.

With the elastic modulus mapping, we managed to investigate the fate of the microcapsules after they were internalised. In some cases, the capsules were buckled shortly after its internalisation. The buckling of microcapsule during internalisation under physiological conditions has been previously observed using fluorescence techniques (Sukhorukov et al., 2005), however the mechanical properties of the process have only been measured outside living cells (Palankar et al., 2013, Delcea et al., 2010, Dubreuil et al., 2003, Yu et al., 2016). Previously, it was suggested that this buckling was caused by the squeezing of the endocytotic vesicles (Sukhorukov et al., 2005, Delcea et al., 2010). However, our results on the elastic modulus of the capsule and cell showed the cell had a much lower elastic modulus compared to the polyelectrolyte microcapsules. This suggests the buckling of the capsule wall was caused by a combination of physico-chemical interactions inside the endocytotic vesicles rather than simple mechanical compression as suggested before (Delcea et al., 2010).

We also visualised the effect of two relevant chemical inhibitors on the

internalisation, cytochalasin D and MβCD. Cytochalasin D caused excessive changes in the morphology of cells in control conditions, which make its use as blocker of internalisation problematic. Our observations show that the location of initial capsule attachment seems to affect the success of internalisation, with the cytoplasmic region between the nucleus and edge of the cell being apparently one of the best areas. Collapse of the cytoskeleton and subsequent rounding up of cells caused by exposure to cytochalasin D as observed by others before (Rheinlaender and Schaffer, 2013) and confirmed by us in this project is likely to reduce chances of capsule internalisation not just because of negative effect on actin polymerisation but also due to the effect on overall cellular topography. It would be difficult to assess which of these two aspects of cytochalasin D effect is mainly responsible for reduction in the uptake rate. MβCD, on the other hand, did not appear to negatively affect cellular topography in control conditions to such extent as cytochalasin D. We found that 2 mM MβCD entirely inhibited the internalisation of microcapsules without affecting the morphology of the cell membrane. Previous reports suggested the cholesterol plays an important role in the forming of membrane ruffles (Grimmer et al., 2002) and lipid raft (Lingwood and Simons, 2010), both of which might involve in the process of the internalisation. The total inhibition of the internalisation was also reported before in many previous articles, not only on the internalisation of synthetic particles (Kastl et al., 2013), but also on the internalisation of biological samples, such as virus (Kumar et al., 2016, Mercer and Helenius, 2009), however the exact reason for the inhibition is not entirely clear. Our results suggest that exposure to MβCD negatively affects the binding between the capsules and the cell membranes. This suggests that the cholesterol facilitates the adhesion of polyelectrolyte capsules to the cell membrane, which is in contrast to the previous belief that the adhesion between cell membrane and foreign objects is caused just by simple electrostatic force (Javier et al., 2006).

9. Conclusion and future work

9.1 Conclusion

According to our knowledge the data presented in this work show the first live recordings of a complete internalisation cycle of single polyelectrolyte capsule from the viewpoint of 3D topography and mechanical properties. Previous studies using electron microscopy of fixed samples suggested involvement of membrane protrusions, however it was not clear to what extent are these protrusions important to the process of internalisation. The high resolution topographical imaging presented here revealed that these protrusions start forming within the first few minutes of the contact between capsule wall and cell membrane and appear to play a key role in engulfment of the capsule with membrane right until the final stage of the internalisation when the capsule is pulled into the intracellular space. The protrusions form predominantly in the vicinity of the capsules suggesting some form of local receptor signalling similar to phagocytosis rather than random formation of membrane ruffles in macropinocytosis. Crucially, the important step towards successful internalisation appeared to be nanoscale restructuring of the finger-like membrane protrusions into smooth sheets of membrane extending over the capsule surface. We were able to map the changes in elastic modulus of the membrane processes involved in the internalisation with resolution high enough to resolve the gradual extension of thin layer of membrane over the top of the capsule and demonstrated the possibility to use measurement of elastic modulus to follow capsule internalisation even after the capsule is fully covered by membrane. This opens possibilities for better understanding of the complex nature of membrane engulfment of wide range of nanostructured materials under physiological conditions and improved design of these materials which would take into account their interactions with the fine membrane processes.

9.2 Future work

In this thesis, we demonstrated the ability of SICM as a powerful characterisation technique to study the internalisation of microcapsules. We focused on testing and optimising the procedure for visualising the internalisation of microcapsule. Future work could be carried out to further investigate the mechanism behind the internalisation of microcapsules from a biological point of view, or to utilize SICM as a characterization method to study the interaction between capsules and cells from a biomedical engineering point of view. Some of the possible future work are:

- The topographical and elasticity mapping could be combined with fluorescence imaging to study the formation of endosome/lysosome using pH-sensitive dyes, such as SNARF (Kreft et al., 2007). This could help clarify the role of mechanical forces and pH changes in the observed buckling of capsules.

- The capability of the SICM to visualise the restructuring of membrane protrusions into sheets demonstrated in this thesis could be used for testing various surface modifications of the microcapsules aimed at "encouraging" the restructuring and thus increase the internalisation success.

- The observation of reduced attachment of capsules to cell membrane upon exposure to MβCD which depletes cholesterol opens new questions. Further investigation should determine whether capsules bind to cholesterol in the membrane or whether the depletion of cholesterol affect distribution of other membrane proteins facilitating capsule attachment.

- The attachment of capsules apparently triggers formation of finger-

like membrane protrusions in the vicinity of the capsule. Further experiments are needed to identify the receptors responsible for this process using known blockers. These protrusions would be very difficult to follow using available fluorescence techniques, therefore SICM would be very helpful for high-resolution inspection of the effects of blockers particularly on the formation of protrusions.

References

AI, H., PINK, J. J., SHUAI, X. T., BOOTHMAN, D. A. & GAO, J. M. 2005. Interactions between self-assembled polyelectrolyte shells and tumor cells. *Journal of Biomedical Materials Research Part A,* 73A**,** 303-312.

ALBANESE, A., TANG, P. S. & CHAN, W. C. W. 2012. The Effect of Nanoparticle Size, Shape, and Surface Chemistry on Biological Systems. *Annual Review of Biomedical Engineering, Vol 14,* 14**,** 1-16.

BANQUY, X., SUAREZ, F., ARGAW, A., RABANEL, J. M., GRUTTER, P., BOUCHARD, J. F., HILDGEN, P. & GIASSON, S. 2009. Effect of mechanical properties of hydrogel nanoparticles on macrophage cell uptake. *Soft Matter,* 5**,** 3984-3991.

BEHRENS, I., PENA, A. I. V., ALONSO, M. J. & KISSEL, T. 2002. Comparative uptake studies of bioadhesive and non-bioadhesive nanoparticles in human intestinal cell lines and rats: The effect of mucus on particle adsorption and transport. *Pharmaceutical Research,* 19**,** 1185-1193.

BENEY, L. & GERVAIS, P. 2001. Influence of the fluidity of the membrane on the response of microorganisms to environmental stresses. *Applied Microbiology and Biotechnology,* 57**,** 34-42.

BEST, J. P., YAN, Y. & CARUSO, F. 2012. The Role of Particle Geometry and Mechanics in the Biological Domain. *Advanced Healthcare Materials,* 1**,** 35-47.

BISCHOF, J. C. & HE, X. 2005. Thermal stability of proteins. *Ann N Y Acad Sci,* 1066**,** 12-33.

BYFIELD, F. J., KOWALSKI, M., CRUZ, K., LESZCZYNSKA, K., NAMIOT, A., SAVAGE, P. B., BUCKI, R. & JANMEY, P. A. 2011. Cathelicidin LL-37 Increases Lung Epithelial Cell Stiffness, Decreases Transepithelial Permeability, and Prevents Epithelial Invasion by Pseudomonas aeruginosa. *Journal of Immunology,* 187**,** 6402-6409.

CALDWELL, M., DEL LINZ, S. J. L., SMART, T. G. & MOSS, G. W. J. 2012. Method for Estimating the Tip Geometry of Scanning Ion Conductance Microscope Pipets. *Analytical Chemistry,* 84**,** 8980-8984.

CHAMPION, J. A., KATARE, Y. K. & MITRAGOTRI, S. 2007. Particle shape: A new design parameter for micro- and nanoscale drug delivery carriers. *Journal of Controlled Release,* 121**,** 3-9.

CHANG, Y. L., YANG, S. T., LIU, J. H., DONG, E., WANG, Y. W., CAO, A. N., LIU, Y. F. & WANG, H. F. 2011. In vitro toxicity evaluation of graphene oxide on A549 cells. *Toxicology Letters,* 200**,** 201-210.

CLARKE, R. W., NOVAK, P., ZHUKOV, A., TYLER, E. J., CANO-JAIMEZ, M., DREWS, A., RICHARDS, O., VOLYNSKI, K., BISHOP, C. & KLENERMAN, D. 2016. Low Stress Ion Conductance Microscopy of Sub-Cellular Stiffness. *Soft Matter,* 12**,** 7953-8.

CLARKE, R. W., ZHUKOV, A., RICHARDS, O., JOHNSON, N., OSTANIN, V. & KLENERMAN, D. 2013. Pipette-Surface Interaction: Current Enhancement and Intrinsic Force. *Journal of the American Chemical Society,* 135**,** 322-329.

CONNER, S. D. & SCHMID, S. L. 2003. Regulated portals of entry into the cell. *Nature,* 422**,** 37-44.

DAVOREN, M., HERZOG, E., CASEY, A., COTTINEAU, B., CHAMBERS, G., BYRNE, H. J. & LYNG, F. M. 2007. In vitro toxicity evaluation of single walled carbon nanotubes on human A549 lung cells. *Toxicology in Vitro,* 21**,** 438-448.

DE GEEST, B. G., DE KOKER, S., SUKHORUKOV, G. B., KREFT, O., PARAK, W. J., SKIRTACH, A. G., DEMEESTER, J., DE SMEDT, S. C. & HENNINK, W. E. 2009. Polyelectrolyte microcapsules for biomedical applications. *Soft Matter,* 5**,** 282-291.

DE GEEST, B. G., VANDENBROUCKE, R. E., GUENTHER, A. M., SUKHORUKOV, G. B., HENNINK, W. E., SANDERS, N. N., DEMEESTER, J. & DE SMEDT, S. C. 2006. Intracellularly degradable polyelectrolyte microcapsules. *Advanced Materials,* 18**,** 1005-+.

DE KOKER, S., DE GEEST, B. G., CUVELIER, C., FERDINANDE, L., DECKERS, W., HENNINK, W. E., DE SMEDT, S. & MERTENS, N. 2007. In vivo cellular uptake, degradation, and biocompatibility of polyelectrolyte microcapsules. *Advanced Functional Materials,* 17**,** 3754-3763.

DECHER, G. 1997. Fuzzy nanoassemblies: Toward layered polymeric multicomposites. *Science,* 277**,** 1232-1237.

DECHER, G., HONG, J. D. & SCHMITT, J. 1992. Buildup of Ultrathin Multilayer Films by a Self-Assembly Process .3. Consecutively Alternating Adsorption of Anionic and Cationic Polyelectrolytes on Charged Surfaces. *Thin Solid Films,* 210**,** 831-835.

DELCEA, M., SCHMIDT, S., PALANKAR, R., FERNANDES, P. A. L., FERY, A., MOHWALD, H. & SKIRTACH, A. G. 2010. Mechanobiology: Correlation Between Mechanical Stability of Microcapsules Studied by AFM and Impact of Cell-Induced Stresses. *Small,* 6**,** 2858-2862.

DIERENDONCK, M., DE KOKER, S., VERVAET, C., REMON, J. P. & DE GEEST, B. G. 2012. Interaction between polymeric multilayer capsules and immune cells. *Journal of Controlled Release,* 161**,** 592-599.

DONATH, E., SUKHORUKOV, G. B., CARUSO, F., DAVIS, S. A. & MOHWALD, H. 1998. Novel hollow polymer shells by colloid-templated assembly of polyelectrolytes. *Angewandte Chemie-International Edition,* 37**,** 2202-2205.

DUBREUIL, F., ELSNER, N. & FERY, A. 2003. Elastic properties of polyelectrolyte capsules studied by atomic-force microscopy and RICM. *European Physical Journal E,* 12**,** 215-221.

DUFRENE, Y. F., ANDO, T., GARCIA, R., ALSTEENS, D., MARTINEZ-MARTIN, D., ENGEL, A., GERBER, C. & MULLER, D. J. 2017. Imaging modes of atomic force microscopy for application in molecular and cell biology. *Nature Nanotechnology,* 12**,** 295-307.

EDIDIN, M. 2003. The state of lipid rafts: From model membranes to cells. *Annual Review of Biophysics and Biomolecular Structure,* 32**,** 257-283.

FOGED, C., BRODIN, B., FROKJAER, S. & SUNDBLAD, A. 2005. Particle size and surface charge affect particle uptake by human dendritic cells in an in vitro model. *International Journal of Pharmaceutics,* 298**,** 315-322.

FOSTER, K. A., YAZDANIAN, M. & AUDUS, K. L. 2001. Microparticulate uptake mechanisms of in-vitro cell culture models of the respiratory epithelium. *Journal of Pharmacy and Pharmacology,* 53**,** 57-66.

GAO, H., SAPELKIN, A. V., TITIRICI, M. M. & SUKHORUKOV, G. B. 2016. In Situ Synthesis of Fluorescent Carbon Dots/Polyelectrolyte Nanocomposite Microcapsules with Reduced Permeability and Ultrasound Sensitivity. *Acs Nano,* 10**,** 9608-9615.

GIARD, D. J., AARONSON, S. A., TODARO, G. J., ARNSTEIN, P., KERSEY, J. H., DOSIK, H. & PARKS, W. P. 1973. In-Vitro Cultivation of Human Tumors - Establishment of Cell Lines Derived from a Series of Solid Tumors. *Journal of the National Cancer Institute,* 51**,** 1417-1423.

GLINEL, K., SUKHORUKOV, G. B., MOHWALD, H., KHRENOV, V. & TAUER, K. 2003. Thermosensitive hollow capsules based on thermoresponsive polyelectrolytes. *Macromolecular Chemistry and Physics,* 204**,** 1784-1790.

GORELIK, J., SHEVCHUK, A., RAMALHO, M., ELLIOTT, M., LEI, C., HIGGINS, C. F., LAB, M. J., KLENERMAN, D., KRAUZEWICZ, N. & KORCHEV, Y. 2002. Scanning surface confocal microscopy for simultaneous topographical and fluorescence imaging: Application to single virus-like particle entry into a cell. *Proceedings of the National Academy of Sciences of the United States of America,* 99**,** 16018-16023.

GRIMMER, S., VAN DEURS, B. & SANDVIG, K. 2002. Membrane ruffling and macropinocytosis in A431 cells require cholesterol. *Journal of Cell Science,* 115**,** 2953-2962.

GUALTIERI, M., MANTECCA, P., CORVAJA, V., LONGHIN, E., PERRONE, M. G., BOLZACCHINI, E. & CAMATINI, M. 2009. Winter fine particulate matter from Milan induces morphological and functional alterations in human pulmonary epithelial cells (A549). *Toxicol Lett,* 188**,** 52-62.

HANSMA, P. K., DRAKE, B., MARTI, O., GOULD, S. A. C. & PRATER, C. B. 1989. The Scanning Ion-Conductance Microscope. *Science,* 243**,** 641-643.

HARTMANN, R., WEIDENBACH, M., NEUBAUER, M., FERY, A. & PARAK, W. J. 2015. Stiffness-Dependent In Vitro Uptake and Lysosomal Acidification of Colloidal Particles. *Angewandte Chemie-International Edition,* 54**,** 1365-1368.

HILLAIREAU, H. & COUVREUR, P. 2009. Nanocarriers' entry into the cell: relevance to drug delivery. *Cellular and Molecular Life Sciences,* 66**,** 2873-2896.

HUANG, M., MA, Z. S., KHOR, E. & LIM, L. Y. 2002. Uptake of FITC-chitosan nanoparticles by a549 cells. *Pharmaceutical Research,* 19**,** 1488-1494.

ILANGUMARAN, S. & HOESSLI, D. C. 1998. Effects of cholesterol depletion by cyclodextrin on the sphingolipid microdomains of the plasma membrane. *Biochemical Journal,* 335**,** 433-440.

JANMEY, P. A. 1998. The cytoskeleton and cell signaling: Component localization and mechanical coupling. *Physiological Reviews,* 78**,** 763-781.

JAVIER, A. M., KREFT, O., ALBEROLA, A. P., KIRCHNER, C., ZEBLI, B., SUSHA, A. S., HORN, E., KEMPTER, S., SKIRTACH, A. G., ROGACH, A. L., RADLER, J., SUKHORUKOV, G. B., BENOIT, M. & PARAK, W. J. 2006. Combined atomic force microscopy and optical microscopy measurements as a method to investigate particle uptake by cells. *Small,* 2**,** 394-400.

JAVIER, A. M., KREFT, O., SEMMLING, M., KEMPTER, S., SKIRTACH, A. G., BRUNS, O. T., DEL PINO, P., BEDARD, M. F., RAEDLER, J., KAES, J., PLANK, C., SUKHORUKOV, G. B. & PARAK, W. J. 2008. Uptake of Colloidal Polyelectrolyte-Coated Particles and Polyelectrolyte Multilayer Capsules by Living Cells. *Advanced Materials,* 20**,** 4281-4287.

JOHNSTON, A. P. R., CORTEZ, C., ANGELATOS, A. S. & CARUSO, F. 2006. Layer-by-layer engineered capsules and their applications. *Current Opinion in Colloid & Interface Science,* 11**,** 203-209.

KAM, N. W. S., JESSOP, T. C., WENDER, P. A. & DAI, H. J. 2004. Nanotube molecular transporters: Internalization of carbon nanotube-protein conjugates into mammalian cells. *Journal of the American Chemical Society,* 126**,** 6850-6851.

KASTL, L., SASSE, D., WULF, V., HARTMANN, R., MIRCHESKI, J., RANKE, C., CARREGAL-ROMERO, S., MARTINEZ-LOPEZ, J. A., FERNANDEZ-CHACON, R., PARAK, W. J., ELSASSER, H. P. & RIVERA GIL, P. 2013. Multiple Internalization Pathways of Polyelectrolyte Multilayer Capsules into Mammalian Cells. *Acs Nano,* 7**,** 6605-6618.

KORCHEV, Y. E., BASHFORD, C. L., MILOVANOVIC, M., VODYANOY, I. & LAB, M. J. 1997a. Scanning ion conductance microscopy of living cells. *Biophysical Journal,* 73**,** 653-658.

KORCHEV, Y. E., MILOVANOVIC, M., BASHFORD, C. L., BENNETT, D. C., SVIDERSKAYA, E. V., VODYANOY, I. & LAB, M. J. 1997b. Specialized scanning ion-conductance microscope for imaging of living cells. *Journal of Microscopy-Oxford,* 188**,** 17-23.

KREFT, O., JAVIER, A. M., SUKHORUKOV, G. B. & PARAK, W. J. 2007. Polymer microcapsules as mobile local pH-sensors. *Journal of Materials Chemistry,* 17**,** 4471-4476.

KRUTH, H. S., JONES, N. L., HUANG, W., ZHAO, B., ISHII, I., CHANG, J., COMBS, C. A., MALIDE, D. & ZHANG, W. Y. 2005. Macropinocytosis is the endocytic pathway that mediates macrophage foam cell formation with native low density lipoprotein. *J Biol Chem,* 280**,** 2352-60.

KUMAR, G. A., JAFURULLA, M. & CHATTOPADHYAY, A. 2016. The membrane as the gatekeeper of infection: Cholesterol in host pathogen interaction. *Chemistry and Physics of Lipids,* 199**,** 179-185.

LI, Y. C., PARK, M. J., YE, S. K., KIM, C. W. & KIM, Y. N. 2006. Elevated levels of cholesterol-rich lipid rafts in cancer cells are correlated with apoptosis sensitivity induced by cholesterol-depleting agents. *American Journal of Pathology,* 168**,** 1107-1118.

LINGWOOD, D., KAISER, H. J., LEVENTAL, I. & SIMONS, K. 2009. Lipid rafts as functional heterogeneity in cell membranes. *Biochemical Society Transactions,* 37**,** 955-960.

LINGWOOD, D. & SIMONS, K. 2010. Lipid Rafts As a Membrane-Organizing Principle. *Science,* 327**,** 46-50.

LIU, W. J., ZHOU, X. Y., MAO, Z. W., YU, D. H., WANG, B. & GAO, C. Y. 2012. Uptake of hydrogel particles with different stiffness and its influence on HepG2 cell functions. *Soft Matter,* 8**,** 9235-9245.

LIU, W. Z., WANG, X. C., BAI, K., LIN, M., SUKHORUKOV, G. & WANG, W. 2014. Microcapsules functionalized with neuraminidase can enter vascular endothelial cells in vitro. *Journal of the Royal Society Interface,* 11.

MANSOUR, H. M., RHEE, Y. S. & WU, X. A. 2009. Nanomedicine in pulmonary delivery. *International Journal of Nanomedicine,* 4**,** 299-319.

MAZUR, P., LEIBO, S. P. & CHU, E. H. Y. 1972. 2-Factor Hypothesis of Freezing Injury - Evidence from Chinese-Hamster Tissue-Culture Cells. *Experimental Cell Research,* 71**,** 345-&.

MERCER, J. & HELENIUS, A. 2009. Virus entry by macropinocytosis. *Nature Cell Biology,* 11**,** 510-520.

MIRAGOLI, M., MOSHKOV, A., NOVAK, P., SHEVCHUK, A., NIKOLAEV, V. O., EL-HAMAMSY, I., POTTER, C. M. F., WRIGHT, P., KADIR, S. H. S. A., LYON, A. R., MITCHELL, J. A., CHESTER, A. H., KLENERMAN, D., LAB, M. J., KORCHEV, Y. E., HARDING, S. E. & GORELIK, J. 2011. Scanning ion conductance microscopy: a convergent high-resolution technology for multi-parametric analysis of living cardiovascular cells. *Journal of the Royal Society Interface,* 8**,** 913-925.

MUHLFELD, C., ROTHEN-RUTISHAUSER, B., BLANK, F., VANHECKE, D., OCHS, M. & GEHR, P. 2008. Interactions of nanoparticles with pulmonary structures and cellular responses. *American Journal of Physiology-Lung Cellular and Molecular Physiology,* 294**,** L817-L829.

NAKASE, I., NIWA, M., TAKEUCHI, T., SONOMURA, K., KAWABATA, N., KOIKE, Y., TAKEHASHI, M., TANAKA, S., UEDA, K., SIMPSON, J. C., JONES, A. T., SUGIURA, Y. & FUTAKI, S. 2004. Cellular uptake of arginine-rich peptides: Roles for macropinocytosis and actin rearrangement. *Molecular Therapy,* 10**,** 1011-1022.

NAZARENUS, M., ZHANG, Q., SOLIMAN, M. G., DEL PINO, P., PELAZ, B., CARREGAL-ROMERO, S., REJMAN, J., ROTHEN-RUTISHAUSER, B., CLIFT, M. J. D., ZELLNER, R., NIENHAUS, G. U., DELEHANTY, J. B., MEDINTZ, I. L. & PARAK, W. J. 2014. In vitro interaction of colloidal nanoparticles with mammalian cells: What have we learned thus far? *Beilstein Journal of Nanotechnology,* 5**,** 1477-1490.

NOVAK, P., LI, C., SHEVCHUK, A. I., STEPANYAN, R., CALDWELL, M., HUGHES, S., SMART, T. G., GORELIK, J., OSTANIN, V. P., LAB, M. J., MOSS, G. W. J., FROLENKOV, G. I., KLENERMAN, D. & KORCHEV, Y. E. 2009. Nanoscale live-cell imaging using hopping probe ion conductance microscopy. *Nature Methods,* 6**,** 279-281.

NOVAK, P., SHEVCHUK, A., RUENRAROENGSAK, P., MIRAGOLI, M., THORLEY, A. J., KLENERMAN, D., LAB, M. J., TETLEY, T. D., GORELIK, J. & KORCHEV, Y. E. 2014. Imaging Single Nanoparticle Interactions with Human Lung Cells Using Fast Ion Conductance Microscopy. *Nano Letters,* 14**,** 1202-1207.

NOWAKOWSKI, R. & LUCKHAM, P. 2002. Imaging the surface details of red blood cells with atomic force microscopy. *Surface and Interface Analysis,* 33**,** 118-121.

NWANESHIUDU, A., KUSCHAL, C., SAKAMOTO, F. H., ANDERSON, R. R., SCHWARZENBERGER, K. & YOUNG, R. C. 2012. Introduction to Confocal Microscopy. *Journal of Investigative Dermatology,* 132**,** 1-5.

OSSOLA, D., DORWLING-CARTER, L., DERMUTZ, H., BEHR, P., VOROS, J. & ZAMBELLI, T. 2015. Simultaneous Scanning Ion Conductance Microscopy and Atomic Force Microscopy with Microchanneled Cantilevers. *Physical Review Letters,* 115.

PALANKAR, R., PINCHASIK, B. E., SCHMIDT, S., DE GEEST, B. G., FERY, A., MOHWALD, H., SKIRTACH, A. G. & DELCEA, M. 2013. Mechanical strength and intracellular uptake of CaCO3-templated LbL capsules composed of biodegradable polyelectrolytes: the influence of the number of layers. *Journal of Materials Chemistry B,* 1**,** 1175-1181.

PAVLOV, A. M., SAPELKIN, A. V., HUANG, X. Y., P'NG, K. M. Y., BUSHBY, A. J., SUKHORUKOV, G. B. & SKIRTACH, A. G. 2011. Neuron Cells Uptake of Polymeric Microcapsules and Subsequent Intracellular Release. *Macromolecular Bioscience,* 11**,** 848-854.

POLLARD, T. D. & BORISY, G. G. 2003. Cellular motility driven by assembly and disassembly of actin filaments. *Cell,* 112**,** 453-465.

REIBETANZ, U., HALOZAN, D., BRUMEN, M. & DONATH, E. 2007. Flow cytometry of HEK 293T cells interacting with polyelectrolyte multilayer capsules containing fluorescein-labeled poly(acrylic acid) as a pH sensor. *Biomacromolecules,* 8**,** 1927-1933.

REIBETANZ, U., LESSIG, J., HOYER, J. & NEUNDORF, I. 2010. Surface Functionalized Colloidal Microparticles for Fast Endocytotic Cell Uptake. *Advanced Engineering Materials,* 12**,** B488-B495.

REJMAN, J., BRAGONZI, A. & CONESE, M. 2005. Role of clathrin- and caveolae-mediated endocytosis in gene transfer mediated by lipo- and polyplexes. *Molecular Therapy,* 12**,** 468-474.

RHEINLAENDER, J., GEISSE, N. A., PROKSCH, R. & SCHAFFER, T. E. 2011. Comparison of Scanning Ion Conductance Microscopy with Atomic Force Microscopy for Cell Imaging. *Langmuir,* 27**,** 697-704.

RHEINLAENDER, J. & SCHAFFER, T. E. 2009. Image formation, resolution, and height measurement in scanning ion conductance microscopy. *Journal of Applied Physics,* 105.

RHEINLAENDER, J. & SCHAFFER, T. E. 2013. Mapping the mechanical stiffness of live cells with the scanning ion conductance microscope. *Soft Matter,* 9**,** 3230-3236.

RHEINLAENDER, J., VOGEL, S., SEIFERT, J., SCHACHTELE, M., BORST, O., LANG, F., GAWAZ, M. & SCHAFFER, T. E. 2015. Imaging the elastic modulus of human platelets during thrombin-induced activation using scanning ion conductance microscopy. *Thrombosis and Haemostasis,* 113**,** 305-311.

RUENRAROENGSAK, P., NOVAK, P., BERHANU, D., THORLEY, A. J., VALSAMI-JONES, E., GORELIK, J., KORCHEV, Y. E. & TETLEY, T. D. 2012. Respiratory epithelial cytotoxicity and membrane damage (holes) caused by amine-modified nanoparticles. *Nanotoxicology,* 6**,** 94-108.

SAHAY, G., ALAKHOVA, D. Y. & KABANOV, A. V. 2010. Endocytosis of nanomedicines. *Journal of Controlled Release,* 145**,** 182-195.

SANCHEZ, D., JOHNSON, N., LI, C., NOVAK, P., RHEINLAENDER, J., ZHANG, Y. J., ANAND, U., ANAND, P., GORELIK, J., FROLENKOV, G. I., BENHAM, C., LAB, M., OSTANIN, V. P., SCHAFFER, T. E., KLENERMAN, D. & KORCHEV, Y. E. 2008. Noncontact measurement of the local mechanical properties of living cells using pressure applied via a pipette. *Biophysical Journal,* 95**,** 3017-3027.

SATIR, P. 2017. CILIA: before and after. *Cilia,* 6**,** 1.

SCHAFFER, T. E. 2013. Nanomechanics of Molecules and Living Cells with Scanning Ion Conductance Microscopy. *Analytical Chemistry,* 85**,** 6988-6994.

SEMMLING, M., KREFT, O., JAVIER, A. M., SUKHORUKOV, G. B., KAS, J. & PARAK, W. J. 2008. A Novel Flow-Cytometry-Based Assay for Cellular Uptake Studies of Polyelectrolyte Microcapsules. *Small,* 4**,** 1763-1768.

SHCHUKIN, D., PATEL, A. A., SUKHORUKOV, G. B. & LVOV, Y. 2003. DNA encapsulation in biocompatible polyelectrolyte microcapsules. *Abstracts of Papers of the American Chemical Society,* 226**,** U492-U492.

SHENOY, D. B., ANTIPOV, A. A., SUKHORUKOV, G. B. & MOHWALD, H. 2003. Layer-by-layer engineering of biocompatible, decomposable core-shell structures. *Biomacromolecules,* 4**,** 265-272.

SHEVCHUK, A. I., HOBSON, P., LAB, M. J., KLENERMAN, D., KRAUZEWICZ, N. & KORCHEV, Y. E. 2008a. Endocytic pathways: combined scanning ion conductance and surface confocal microscopy study. *Pflugers Archiv-European Journal of Physiology,* 456**,** 227-235.

SHEVCHUK, A. I., HOBSON, P., LAB, M. J., KLENERMAN, D., KRAUZEWICZ, N. & KORCHEV, Y. E. 2008b. Imaging single virus particles on the surface of cell membranes by high-resolution scanning surface confocal microscopy. *Biophysical Journal,* 94**,** 4089-4094.

SHEVCHUK, A. I., NOVAK, P., TAYLOR, M., DIAKONOV, I. A., ZIYADEH-ISLEEM, A., BITOUN, M., GUICHENEY, P., LAB, M. J., GORELIK, J., MERRIFIELD, C. J., KLENERMAN, D. & KORCHEV, Y. E. 2012. An alternative mechanism of clathrin-coated pit closure revealed by ion conductance microscopy. *Journal of Cell Biology,* 197**,** 499-508.

SHUKLA, R., BANSAL, V., CHAUDHARY, M., BASU, A., BHONDE, R. R. & SASTRY, M. 2005. Biocompatibility of gold nanoparticles and their endocytotic fate inside the cellular compartment: A microscopic overview. *Langmuir,* 21**,** 10644-10654.

STUART, M. A. C., HUCK, W. T. S., GENZER, J., MULLER, M., OBER, C., STAMM, M., SUKHORUKOV, G. B., SZLEIFER, I., TSUKRUK, V. V., URBAN, M., WINNIK, F., ZAUSCHER, S., LUZINOV, I. & MINKO, S. 2010. Emerging applications of stimuli-responsive polymer materials. *Nature Materials,* 9**,** 101-113.

SUKHORUKOV, G. B., ANTIPOV, A. A., VOIGT, A., DONATH, E. & MOHWALD, H. 2001. pH-controlled macromolecule encapsulation in and release from polyelectrolyte multilayer nanocapsules. *Macromolecular Rapid Communications,* 22**,** 44-46.

SUKHORUKOV, G. B., DONATH, E., DAVIS, S., LICHTENFELD, H., CARUSO, F., POPOV, V. I. & MOHWALD, H. 1998a. Stepwise polyelectrolyte assembly on particle surfaces: a novel approach to colloid design. *Polymers for Advanced Technologies,* 9**,** 759-767.

SUKHORUKOV, G. B., DONATH, E., LICHTENFELD, H., KNIPPEL, E., KNIPPEL, M., BUDDE, A. & MOHWALD, H. 1998b. Layer-by-layer self assembly of polyelectrolytes on colloidal particles. *Colloids and Surfaces a-Physicochemical and Engineering Aspects,* 137**,** 253-266.

SUKHORUKOV, G. B., DONATH, E., MOYA, S., SUSHA, A. S., VOIGT, A., HARTMANN, J. & MOHWALD, H. 2000. Microencapsulation by means of step-wise adsorption of polyelectrolytes. *Journal of Microencapsulation,* 17**,** 177-185.

SUKHORUKOV, G. B., ROGACH, A. L., GARSTKA, M., SPRINGER, S., PARAK, W. J., MUNOZ-JAVIER, A., KREFT, O., SKIRTACH, A. G., SUSHA, A. S., RAMAYE, Y., PALANKAR, R. & WINTERHALTER, M. 2007. Multifunctionalized polymer microcapsules: Novel tools for biological and pharmacological applications. *Small,* 3**,** 944-955.

SUKHORUKOV, G. B., ROGACH, A. L., ZEBLI, B., LIEDL, T., SKIRTACH, A. G., KOHLER, K., ANTIPOV, A. A., GAPONIK, N., SUSHA, A. S., WINTERHALTER, M. & PARAK, W. J. 2005. Nanoengineered polymer capsules: Tools for detection, controlled delivery, and site-specific manipulation. *Small,* 1**,** 194-200.

SUN, H. L., WONG, E. H. H., YAN, Y., CUI, J. W., DAI, Q., GUO, J. L., QIAO, G. G. & CARUSO, F. 2015. The role of capsule stiffness on cellular processing. *Chemical Science,* 6**,** 3505-3514.

SWANSON, J. A. 2008. Shaping cups into phagosomes and macropinosomes. *Nature Reviews Molecular Cell Biology,* 9**,** 639.

TAKAHASHI, Y., SHEVCHUK, A. I., NOVAK, P., BABAKINEJAD, B., MACPHERSON, J., UNWIN, P. R., SHIKU, H., GORELIK, J., KLENERMAN, D., KORCHEV, Y. E. & MATSUE, T. 2012. Topographical and electrochemical nanoscale imaging of living cells using voltage-switching mode scanning electrochemical microscopy. *Proceedings of the National Academy of Sciences of the United States of America,* 109**,** 11540-11545.

TAKAHASHI, Y., SHEVCHUK, A. I., NOVAK, P., ZHANG, Y. J., EBEJER, N., MACPHERSON, J. V., UNWIN, P. R., POLLARD, A. J., ROY, D., CLIFFORD, C. A., SHIKU, H., MATSUE, T., KLENERMAN, D. & KORCHEV, Y. E. 2011. Multifunctional Nanoprobes for Nanoscale Chemical Imaging and Localized Chemical Delivery at Surfaces and Interfaces. *Angewandte Chemie-International Edition,* 50**,** 9638-9642.

TAKEUCHI, K., SATO, N., KASAHARA, H., FUNAYAMA, N., NAGAFUCHI, A., YONEMURA, S., TSUKITA, S. & TSUKITA, S. 1994. PERTURBATION OF CELL-ADHESION AND MICROVILLI FORMATION BY ANTISENSE OLIGONUCLEOTIDES TO ERM FAMILY MEMBERS. *Journal of Cell Biology,* 125**,** 1371-1384.

USHIKI, T., YAMAMOTO, S., HITOMI, J., OGURA, S., UMEMOTO, T. & SHIGENO, M. 2000. Atomic force microscopy of living cells. *Japanese Journal of Applied Physics Part 1-Regular Papers Short Notes & Review Papers,* 39**,** 3761-3764.

VELEZ-ORTEGA, A. C., BELOV, O., NOVAK, P., RAWASHDEH, S. A., SINHA, G. P., KORCHEV, Y. E. & FROLENKOV, G. I. 2014. High-Speed Hopping Probe Scanning Ion Conductance Microscopy. *Biophysical Journal,* 106**,** 797a-798a.

VIEIRA, O. V., BOTELHO, R. J. & GRINSTEIN, S. 2002. Phagosome maturation: aging gracefully. *Biochemical Journal,* 366**,** 689-704.

VOLODKIN, D. V., LARIONOVA, N. I. & SUKHORUKOV, G. B. 2004a. Protein encapsulation via porous CaCO3 microparticles templating. *Biomacromolecules,* 5**,** 1962-1972.

VOLODKIN, D. V., PETROV, A. I., PREVOT, M. & SUKHORUKOV, G. B. 2004b. Matrix polyelectrolyte microcapsules: New system for macromolecule encapsulation. *Langmuir,* 20**,** 3398-3406.

YANG, X., LIU, X., LU, H. J., ZHANG, X. F., MA, L. Y., GAO, R. L. & ZHANG, Y. J. 2012. Real-Time Investigation of Acute Toxicity of ZnO Nanoparticles on Human Lung Epithelia with Hopping Probe Ion Conductance Microscopy. *Chemical Research in Toxicology,* 25**,** 297-304.

YI, Q. Y. & SUKHORUKOV, G. B. 2013. Externally Triggered Dual Function of Complex Microcapsules. *Acs Nano,* 7**,** 8693-8705.

YU, A. M., WANG, Y. J., BARLOW, E. & CARUSO, F. 2005. Mesoporous silica particles as templates for preparing enzyme-loaded biocompatible microcapsules. *Advanced Materials,* 17**,** 1737-+.

YU, W., ZHANG, W. B., CHEN, Y., SONG, X. X., TONG, W. J., MAO, Z. W. & GAO, C. Y. 2016. Cellular uptake of poly(allylamine hydrochloride) microcapsules with different deformability and its influence on cell functions. *Journal of Colloid and Interface Science,* 465**,** 149-157.